

**A VENTRAL ROOT INTERFACE FOR NEUROPROSTHETIC CONTROL OF  
LOCOMOTION**

by

**Matthew Joel Stoesz Bauman**

B.A., Goshen College, 2006

Submitted to the Graduate Faculty of  
Swanson School of Engineering in partial fulfillment  
of the requirements for the degree of  
Doctor of Philosophy

University of Pittsburgh

2018

UNIVERSITY OF PITTSBURGH  
SWANSON SCHOOL OF ENGINEERING

This dissertation was presented

by

Matthew Joel Stoesz Bauman

It was defended on

November 20, 2017

and approved by

Lee Fisher, Ph.D., Assistant Professor  
Department of Physical Medicine and Rehabilitation

Robert Gaunt, Ph.D., Assistant Professor  
Department of Physical Medicine and Rehabilitation

Gelsy Torres-Oviedo, Ph.D., Assistant Professor  
Department of BioEngineering

Sergiy Yakovenko, Ph.D., Assistant Professor  
West Virginia University Blanchette Rockefeller Neurosciences Institute

Advisor: Douglas Weber, Ph.D., Associate Professor  
Department of BioEngineering

Copyright © by Matthew Joel Stoesz Bauman

2018

# **A VENTRAL ROOT INTERFACE FOR NEUROPROSTHETIC CONTROL OF LOCOMOTION**

Matthew Joel Stoesz Bauman, Ph.D.

University of Pittsburgh, 2018

Recent advances in state of the art prosthetic limbs have demonstrated unprecedented levels of dexterity and control within the constraints of an anthropomorphic structure. Unfortunately, patients still struggle to naturally control and rely upon relatively simpler lower limb devices with just one or two joints. For patients living with the loss of a limb, functional motor circuitry is still intact through the spinal cord and into the peripheral nerves, transforming higher level control signals into discrete muscle activations. An interface at the spinal roots can take advantage of this final output of the nervous system to control the device, completely avoiding some of the context sensitivity issues in higher level structures. Further, the anatomical separation of motor and sensory signals into distinct ventral and dorsal components and the relative stability of the spinal column provide a path towards a targeted neuroprosthetic interface.

This dissertation develops and validates methods to target motor axons in the ventral roots with multielectrode arrays. We demonstrate the ability to chronically record well-isolated signals from diverse populations of motor axons and develop techniques to identify the muscles they innervate. We then use these motor signals to estimate kinematics during locomotion as accurately as estimations from simultaneously recorded muscle activity in the intact limb, demonstrating that a ventral root prosthetic interface is possible for patients living with loss of limb.

## TABLE OF CONTENTS

<b>PREFACE.....</b>	<b>XII</b>
<b>1.0 INTRODUCTION.....</b>	<b>1</b>
<b>1.1 THE NEED FOR A PERIPHERAL MOTOR INTERFACE.....</b>	<b>1</b>
<b>1.2 RESTORING MOTOR CONTROL.....</b>	<b>3</b>
<b>1.2.1 Actuating movements.....</b>	<b>3</b>
<b>1.2.2 Peripheral neural interfaces.....</b>	<b>5</b>
<b>1.2.3 Interfaces at the ventral roots.....</b>	<b>10</b>
<b>1.3 PERIPHERAL MOTOR ANATOMY.....</b>	<b>11</b>
<b>1.3.1 The motor neuron.....</b>	<b>12</b>
<b>1.3.2 Structure of the spinal roots.....</b>	<b>14</b>
<b>1.4 RESEARCH OBJECTIVES.....</b>	<b>15</b>
<b>1.4.1 Chapter Summaries.....</b>	<b>17</b>
<b>2.0 ACCESSING AND IDENTIFYING MOTOR AXONS AT THE VENTRAL ROOT.....</b>	<b>18</b>
<b>2.1 INTRODUCTION.....</b>	<b>18</b>
<b>2.1.1 Previous work.....</b>	<b>19</b>
<b>2.2 DEVELOPMENT OF METHODS.....</b>	<b>21</b>

2.2.1	Implant surgery .....	21
2.2.1.1	Insertion of multielectrode arrays into the spinal roots .....	21
2.2.1.2	Protective connector housing and circuitry .....	26
2.3	DISCUSSION.....	32
2.3.1	Implant procedure .....	32
2.3.2	Circuitry configurations: Lessons learned .....	34
2.4	CONCLUSION .....	36
3.0	RECORDING NEURAL ACTIVITY FROM THE VENTRAL ROOTS.....	37
3.1	INTRODUCTION .....	37
3.2	METHODS.....	39
3.2.1	Chronic recordings .....	39
3.2.2	Motor axon identification .....	42
3.2.3	Effects of electrode location .....	43
3.3	RESULTS .....	44
3.3.1	Ventral root identification .....	44
3.3.2	Location effects .....	49
3.4	DISCUSSION.....	51
3.5	CONCLUSION .....	54
4.0	MOTOR UNIT POPULATION RECORDINGS FOR NEUROPROSTHETIC CONTROL OF LOCOMOTION.....	55
4.1	INTRODUCTION .....	55
4.2	METHODS.....	56
4.2.1	Experimental protocol.....	57
4.2.2	Estimation of muscle activity and kinematic state .....	58

<b>4.3</b>	<b>RESULTS .....</b>	<b>61</b>
<b>4.3.1</b>	<b>Muscle target identification and estimation .....</b>	<b>61</b>
<b>4.3.2</b>	<b>Kinematic estimation.....</b>	<b>64</b>
<b>4.4</b>	<b>DISCUSSION.....</b>	<b>66</b>
<b>4.5</b>	<b>CONCLUSION .....</b>	<b>69</b>
<b>5.0</b>	<b>THE BEHAVIOR OF MOTOR UNITS AND FUTURE EXPERIMENTS.....</b>	<b>71</b>
<b>5.1</b>	<b>INTRODUCTION .....</b>	<b>71</b>
<b>5.2</b>	<b>METHODS.....</b>	<b>73</b>
<b>5.2.1</b>	<b>Identifying innervated muscles by spike-triggered averages .....</b>	<b>73</b>
<b>5.3</b>	<b>RESULTS .....</b>	<b>78</b>
<b>5.3.1</b>	<b>Detected muscle responses by spike-triggered averaging .....</b>	<b>78</b>
<b>5.4</b>	<b>DISCUSSION.....</b>	<b>81</b>
<b>6.0</b>	<b>SUMMARY OF RESULTS AND CONCLUSION.....</b>	<b>84</b>
<b>6.1</b>	<b>SUMMARY OF RESULTS .....</b>	<b>84</b>
<b>6.2</b>	<b>CONCLUSION .....</b>	<b>85</b>
<b>APPENDIX A</b>	<b>.....</b>	<b>87</b>
<b>A.1</b>	<b>INTRODUCTION .....</b>	<b>88</b>
<b>A.2</b>	<b>METHODS.....</b>	<b>90</b>
<b>A.2.1</b>	<b>Electrode design and pre-operative testing .....</b>	<b>90</b>
<b>A.2.2</b>	<b>Surgery and electrode placement.....</b>	<b>92</b>
<b>A.2.3</b>	<b>Neural signal recording.....</b>	<b>94</b>
<b>A.2.4</b>	<b>Electrode impedance measurements.....</b>	<b>95</b>
<b>A.2.5</b>	<b>Neural signal processing and analysis .....</b>	<b>96</b>

<b>A.3</b>	<b>RESULTS .....</b>	<b>98</b>
<b>A.3.1</b>	<b>SNR and unit yield over time.....</b>	<b>99</b>
<b>A.3.2</b>	<b>Effects of nearest neighbor electrodes .....</b>	<b>102</b>
<b>A.3.3</b>	<b>Effect of site size on SNR and unit yield .....</b>	<b>103</b>
<b>A.3.4</b>	<b>Effect of site size on chronic electrode impedances .....</b>	<b>108</b>
<b>A.4</b>	<b>DISCUSSION.....</b>	<b>110</b>
<b>A.5</b>	<b>ACKNOWLEDGEMENTS .....</b>	<b>115</b>
	<b>BIBLIOGRAPHY.....</b>	<b>116</b>

## LIST OF TABLES

Table 1. Summary of all 15 subjects implanted.....	45
Table 2. Summary of subjects included in this study .....	60
Table 3. Summary of data, initial yield description, and reasons for terminating experiments .	102

## LIST OF FIGURES

Figure 1. Relative selectivity and invasiveness of various peripheral nerve interfaces.....	7
Figure 2. Anatomy of the spinal roots. ....	15
Figure 3. Implantation of arrays into spinal roots.....	22
Figure 4. Intra-operative procedure for optimizing array placement.....	24
Figure 5. Summary of implanted hardware .....	26
Figure 6. Protective backpack and circuitry .....	28
Figure 7. Typical setup of the adapter board and its revision.....	31
Figure 8. Dissection photograph of a poorly placed array.....	33
Figure 9. Example recordings from the ventral root interface.....	41
Figure 10. Classifying neurons as ventral root axons.....	46
Figure 11. Overall VR identification summary .....	48
Figure 12. Location effects on neuron identification.....	50
Figure 13. Summary of identified target muscles.....	62
Figure 14. Accuracy of EMG estimations, example and summary .....	63
Figure 15. Example decoding of kinematic state.....	65
Figure 16. State prediction accuracy and relative timing of the estimated stance onset .....	66
Figure 17. Example spike-triggered average of a spike and its response in EMG.....	76
Figure 18. Example randomized spike-triggered average of a spike and its EMG response .....	77

Figure 19. Example spike-triggered averages of unit with multiple significant EMG responses	79
Figure 20. Number of units with statistically significant STA results.....	79
Figure 21. Most frequently co-occurring pairs of significant STA results.....	80
Figure 22. Floating microelectrode array geometry .....	91
Figure 23. Example recordings .....	100
Figure 24. Summary of recording quality and quantity for the duration of all implants .....	101
Figure 25. Signal to noise ratio by site size .....	104
Figure 26. Signal to noise ratio over time.....	105
Figure 27. Percentage of electrodes recording at least one unit by site size.....	107
Figure 28. Electrode impedances and fraction functional over time .....	109

## **PREFACE**

I am both humbled and honored to provide you with an examination into my research and efforts in this dissertation. This has been a long journey, but I have not been alone. The experiments and analyses herein wouldn't have been possible without all the support of my colleagues and mentors in Doug Weber's lab.

Most importantly, this dissertation exists because of the unwavering encouragement and steadfast patience from my wife, Charity.

Thank you, love.

## **1.0 INTRODUCTION**

### **1.1 THE NEED FOR A PERIPHERAL MOTOR INTERFACE**

In 2007, there were an estimated 1.7 million persons in the United States living with the loss of at least one limb (McFarland et al. 2010). That population is projected to grow significantly over the next 35 years, increasing to 3.6 million by 2050 (Ziegler-Graham et al. 2008). Lower limb loss is much more prevalent, at 80% of all cases. Approximately 45 percent of amputations are a result of a traumatic injury; from 2001 to 2006 over 5 percent of all severe military casualties resulted in the amputation of a limb (Ziegler-Graham et al. 2008; Stansbury et al. 2008). All-told, US hospital costs associated with amputation totaled 1.8 billion dollars in 2009 (Amputee Coalition 2015), and each amputee is burdened with a projected lifetime healthcare cost exceeding \$500,000 (MacKenzie et al. 2007).

In an effort to improve quality of life for amputees, state of the art prosthetic limbs have been developed with unprecedented levels of dexterity and control within the constraints of an anthropomorphic structure for both upper and lower limbs (Johannes et al. 2011; Wodlinger et al. 2014). In contrast to the one or two degrees of freedom (DOF) in conventional passive prostheses, these new devices have up to 22 individually controlled DOF for the upper limb and up to seven in the lower limb. Controlling these multifunctional devices is difficult, requiring richer and higher bandwidth command interfaces to make full use of the prosthesis. Indeed, adding volitional state

control to powered lower limb prostheses has been shown to decrease error rates in movement mode classification (Hargrove et al. 2013). The nervous system contains all the information required to control an anthropomorphic prosthetic limb in a natural and intuitive manner, but interfaces must be developed to access and use that information as part of a neuroprosthetic device.

Work in the peripheral nervous system (PNS) pioneered the use of electrophysiological signals to control external devices, initially using surface electromyography (EMG) and shortly thereafter with electrodes implanted directly into a peripheral nerve. These initial devices were relatively limited in their accuracy and degrees of freedom due to the distance and amount of tissue between the electrophysiological source and the recording electrode.

This was extended and continued with interfaces in the central nervous system (CNS), initially using visually evoked responses in electroencephalogram (EEG) signals to control a cursor through a two-dimensional maze (Vidal 1977), and gradually progressing to more intuitive control of paralyzed limbs and robotic prostheses with single-unit recordings from the motor cortex (Ethier et al. 2012; Collinger et al. 2013). To facilitate these procedures, high density electrode arrays and high bandwidth recording systems were developed to record from hundreds of neurons at once (Normann, Campbell, and Jones 1991; Liu et al. 1999). Recording from central structures like the motor cortex has some significant disadvantages, however. The neurons in these higher-level structures are generally not the direct output layer and represent a small sampling of the intermediate processing stages. Although neural decoders have been improving, there remains a significant challenge with context-sensitivity in generalizing performance to novel untrained tasks (Wodlinger et al. 2014). Further, the implant surgeries are extremely invasive procedures that require craniotomies and expose the surface of the brain.

For patients living with the loss of a limb, there remains functional motor circuitry through the spinal cord and into the peripheral nerves and proximal muscles up to the point of amputation (Di Pino, Guglielmelli, and Rossini 2009). By moving the neural interface into the periphery, we are able to take advantage of existing spinal circuitry that computes the final output to individual muscles. While there remain challenges in accessing and decoding peripheral nerve activity, this approach has the potential to avoid the context-sensitivity problems and invasiveness of CNS interfaces.

## **1.2 RESTORING MOTOR CONTROL**

### **1.2.1 Actuating movements**

The ideal prosthesis for patients living with limb loss would transparently restore motor control in a biomimetic manner. Fully achieving this goal requires accurate and precise control of many independent degrees of freedom. The upper limb naturally controls 23 degrees of freedom in the hand and another six in the arm (Sturman 1992). Simultaneously modulating so many independent motions reliably requires a high bandwidth interface with a minimal conscious cognitive load. The bandwidth of the interface is a direct factor in determining the number of independent degrees of freedom that it modulates, whereas the cognitive load is a practical concern in the ability of the user to fully exercise the device. Even if the interface itself allows for many independent movements with a theoretically high bandwidth, the cognitive effort required may be prohibitive to allow for effective simultaneous control. Previous work has demonstrated that this is not just a theoretical concern. Simultaneous control of multiple movements has only been demonstrated in

limited situations that use recordings from physiologically relevant signals and exploit increased signal fidelity by intentionally choosing distant recording sites or even artificially increasing the distance through advanced surgical techniques (Birdwell et al. 2015; Kuiken et al. 2009; Smith, Kuiken, and Hargrove 2014).

The situation is simpler with the more stereotyped behaviors of the lower limb. Each lower limb can generally be described with seven degrees of freedom (Dollar and Herr 2007), and while locomotion requires simultaneous activation of each joint with varying intensities, the patterns of activation are highly stereotyped and consistent. This has led to a wide range of control strategies for the actuation of active prosthetic legs, progressing from completely pre-determined trajectories and ensemble movements towards the direct volitional control of each articulated joint as interface bandwidths have increased.

Clever mechanical systems have demonstrated that locomotion can be a completely passive process, requiring no active control systems or higher level input (Collins and Ruina 2005). Indeed, passive prosthetic devices have long performed moderately well in assisting patients in accomplishing activities of daily living. However, these passive prostheses require the patient to control the device with residual motions in a biomechanically deficient manner. They become particularly challenging to control over unstable terrain or situations like stair climbing where the activities require much higher energy output than can be easily achieved with the residual structures alone.

Powered prostheses seek to address these deficiencies. Initial systems focused on adding simple state-based behaviors to single joints like the knee (Fite et al. 2007), enabling the patient to rely upon the prosthesis in energetically demanding situations. These powered knee prostheses generally select between several patterns of activation including rest, level walking, and stair

climbing and descent. The accuracy of this state selection is crucially important; the patient is only able to rely upon the prosthesis if the error rate in selecting these states is sufficiently low to garner trust. Reductions in error rates from 2.2 to 1.8% have been reported as being clinically relevant (Hargrove et al. 2013), but even one mistake every hundred steps is still far too frequent for a patient to walk confidently. An ideal lower limb prosthesis would go beyond a finite set of pre-programmed patterns and instead would enable the user to dynamically and proportionally respond to changing environments, stimuli, and obstacles. This not only allows more natural recovery from trips and stumbles, but also decreases the impact of errors—rather than incorrectly selecting a completely inappropriate modality, errors become proportional and far less disruptive.

The mechanism through which the patient communicates intention to these powered devices is crucially important in reducing this error rate and enabling the completion of activities of daily living. A variety of peripheral neural interfaces have been proposed to accomplish this task.

### **1.2.2 Peripheral neural interfaces**

A wide variety of electrode designs have been developed and used to record activity from the peripheral nervous system at a variety of anatomical locations. Implanted peripheral interfaces are generally divided into three categories, ranging from least invasive to most invasive: extraneural electrodes on the surface of the nerves, penetrating intraneural electrodes, and regenerative interfaces (Figure 1) (Navarro et al. 2005). Each category has its own set of advantages and challenges in achieving the required signal quality and bandwidth with an effective and feasible surgical technique. In general, the more invasive methods are able to achieve higher selectivity across more degrees of freedom. Conversely, less invasive methods are highly desirable as they

tend to have fewer of surgical complications—or avoid surgery altogether—and may have longer stability over time, but their electrodes are also generally farther away from individual neurons, which decreases their signal to noise ratio, limiting the information available to the interface.

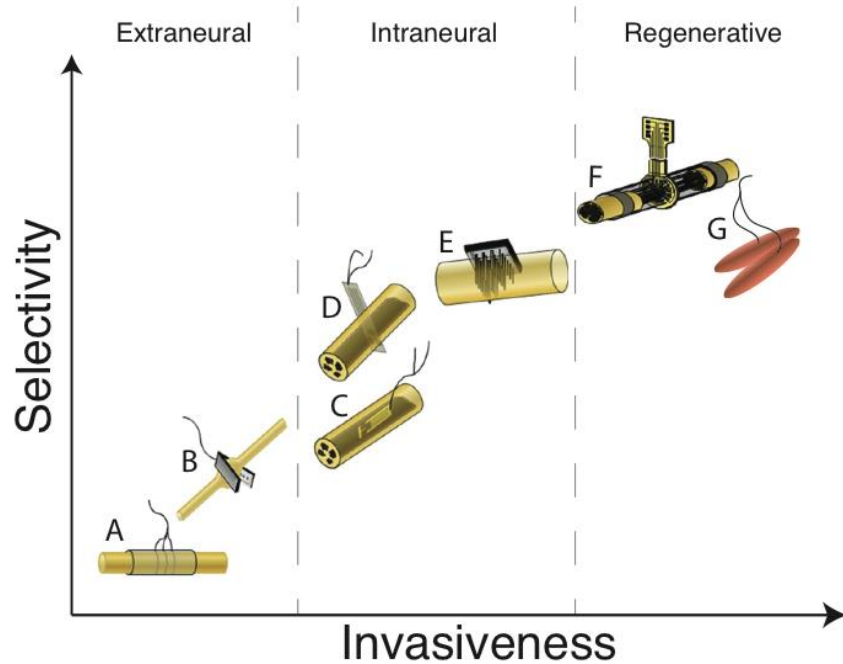


**Figure 1.** Relative selectivity and invasiveness of various peripheral nerve interfaces. Extraneural interfaces have their recording sites on the outside of the nerve, with cuff electrodes (A) and the flat interface nerve electrode (B) displayed as examples. Their selectivity is limited by their distance from the axons from which they record, but they have the advantage of being less invasive. Intraneural interfaces, on the other hand, use penetrating electrodes to place the recording sites inside the nerve, increasing both selectivity and invasiveness. Displayed as examples are the longitudinal intrafascicular electrode (C), the transverse intrafascicular multichannel electrode (D) and the Utah slanted multielectrode array (E). Finally, regenerative interfaces transect live nerves and encourage regeneration through electrodes or into denervated muscle. Depicted are the regenerative sieve electrode (F) and recorded muscle tissue following targeted muscle reinnervation (G). Figure adapted from del Valle and Navarro (del Valle and Navarro 2013).

Extraneural interfaces record whole nerve activity rather than individual action potentials, limiting the total number of accessible degrees of freedom. The recorded signals are representative of larger populations of neurons, and these populations may not necessarily be homogenous in function or even modality. Some selectivity in the recordings can be obtained by reshaping the nerve such that individual fascicles are spread out; for example the flat interface nerve electrode (FINE) flattens the nerve to increase the circumference and bring individual fascicles closer to the surface electrodes in a manner that aims to restrict the recorded population for a single electrode to just axons within a subset of fascicles (Durand, Wodlinger, and Park 2013). The interface is theoretically able to recover both fascicular and even some sub-fascicular activity, and has demonstrated real-time control of a rabbit ankle joint and simulated control of the human ankle joint (Park and Durand 2015). Advanced beamforming algorithms could potentially further improve the ability to separate and recover activity from individual fascicles, with modeling suggesting an upper bound of 80% accuracy when trying to recover 10 independent signals (Wodlinger and Durand 2009).

Penetrating intraneural electrodes have increased their recording density over recent years, progressing from longitudinal intra-fascicular electrodes (LIFE) with just two recording contacts placed into the peripheral nerve (Lefurge et al. 1991) and a dozen individually placed small “hatpin” electrodes in the ventral roots (Hoffer and Loeb 1980) to microelectrode arrays with many dozens of recording sites. For example, the Utah slanted electrode array (USEA) has 96 electrodes and has demonstrated success decoding movements when implanted in the median or ulnar nerve. Two patients have demonstrated control of two different movements online, with another thirteen movements decoded offline to various degrees of accuracy, but crosstalk between the modalities

made independent control a challenge (Davis et al. 2016). Further, the proximity to large muscles in the distal periphery has made isolating the relatively smaller signals from axons within the nerve a challenge for some subjects (Clark et al. 2014).

Regenerative interfaces where the transected nerve grows into an electrode array were some of the first to be developed (A. F. Marks 1969), but axons have not reliably regenerated close enough to the electrodes to allow recording of single-unit activity until recent work with the 18-channel regenerative multielectrode interface (Garde et al. 2009). In theory, it may be possible to use neural growth factors to selectively guide regenerating axons of different modalities towards different arrays, but so far these interfaces are not modality-selective (Lotfi et al. 2011). Another approach towards regenerative motor interfaces is to use the neuromuscular junction as a biological amplifier. By coaxing the transected nerve to regenerate into either transplanted muscle grafts (Woo et al. 2014) or denervated skeletal muscles with targeted muscle reinnervation (Kuiken et al. 2009), a purely motor interface can be reconstructed with the resulting EMG signals. While the interface is somewhat limited by their low spatial resolution (recent studies have only used up to 12 electrodes), movement classifications have successfully been performed in human patients (Kuiken et al. 2009). While the technique can be extended to provide more degrees of freedom with higher-resolution intramuscular electrodes and more re-targeted tissues, it comes at a cost of more denervation of healthy tissue and a more traumatic surgery. Furthermore, this approach is unavailable to patients with nerve injuries to more proximal peripheral structures like the brachial plexus.

These existing interfaces have drawbacks in their stability, selectivity, and bandwidth. Recording from nerves in the periphery is, in general, a challenge due to the large electrical activity

from nearby muscles and large movements (Novak, Mehdian, and Schroeder 2012; Patel, Heidenreich, and Bindra 1998), which can cause artifacts in the recordings (Goodall, Lefurge, and Horch 1991) and may damage the device or axons (Edell 1986).

### **1.2.3 Interfaces at the ventral roots**

Previous studies have demonstrated the feasibility of recording from individually placed electrodes in the ventral roots (Hoffer, Loeb, Marks, et al. 1987). Hoffer and colleagues have shown that penetrating electrodes within the ventral roots allow for isolated single-unit recordings with potentially large signal amplitudes ( $10\mu\text{V}$  to  $128\mu\text{V}$ ), allowing for very high signal-to-noise ratios (SNR) (Hoffer, Loeb, Marks, et al. 1987). As people can learn to control individual motor units in isolation through feedback training, each recorded axon could theoretically correspond to an independent degree of freedom (Basmajian 1963). Intuitive and naturalistic control, however, will likely require recordings from a large number of units associated with a diverse set of functional behaviors.

While these previous studies have shown promise for ventral root recordings as a source for neuroprosthetic control, little work has been done in recording and decoding large populations of motor axons in awake behaving animals. There is a substantial engineering challenge in developing the required infrastructure to record from dozens of electrodes chronically implanted in the ventral roots. The development and validation of a ventral root neural interface will be an important step towards restoring mobility to amputees through intuitive control of prosthetic limbs.

### 1.3 PERIPHERAL MOTOR ANATOMY

Neural interfaces in the periphery have a significant advantage over the more central structures due to the relatively simpler and more accessible anatomy. Work in the periphery dates back to some of the first neuroscientists like Sherrington, who identified the motor neuron as the “final common path” to muscle in 1906 and then later as the “smallest quantum of excitation” (Sherrington 1906; Eccles and Sherrington 1930). Indeed, all of the nervous system converges upon motor neurons to form the final synthesis of the output, with each motor neuron terminating upon tens to hundreds of muscle fibers within a single muscle to evoke a very specific movement. The neuron and the muscle fibers it innervates are considered jointly as a motor unit<sup>1</sup>.

The simpler and well-known physiology of the motor axons at the ventral roots greatly simplifies the interpretability of the recorded signals. Each action potential represents a direct muscle twitch or an indirect increase of force through the potentiation of afferent feedback in a specific muscle (Gandevia et al. 1990). This is contrasted against recordings from higher level structures in the central nervous system like the primary motor cortex (M1). Many of the output cells from M1 are still two or more synapses away from this “final pathway” to the muscle and represent just part of the intermediate computation. Only in phylogenetically newer species have there been found corticomotoneuronal cells that are just one synapse removed from muscle (Rathelot and Strick 2009). Unlike their multi-synaptic counterparts, these “New M1” cells largely demonstrate muscle-like tuning and yet they still demonstrate significant disparities between their

---

<sup>1</sup> Note that established conventions in literature also refer to well-isolated neurons within electro-physiological recordings as single units. Unless specifically qualified as a motor unit, the term ‘unit’ within this dissertation will refer to a single, well-isolated neuron.

activity and the evoked muscle activity—for example, one such neuron was found to facilitate as many as eight different muscles in a macaque forearm (Griffin, Hoffman, and Strick 2015).

Recording from the final motor neuron yields a much higher level of granularity than is possible in the cortical structures. At the same time, however, this means that each degree of freedom requires an ensemble of signals for precise control. The orderly recruitment pattern in force generation by axon size (Henneman and Somjen 1965; Milner-Brown, Stein, and Yemm 1973) further requires a diversity of axon sizes within each ensemble in order to represent movements across a wide range of forces. Therefore, the interface must sample from a sufficient number of neurons that are both diverse in the action they evoke and the magnitude of the evoked action.

### **1.3.1 The motor neuron**

Motor neurons are typically classified into three broad groups based upon their innervated target: alpha motor neurons innervate extrafusal muscle fibers that are directly responsible for generating muscle twitches, whereas gamma motor neurons innervate intrafusal muscle fibers that control the gain of proprioceptive afferent feedback from the muscle spindle, and beta motor neurons innervate both. The orderly recruitment by size as described by Henneman has been found to not only apply across the three classes (as the classes themselves generally vary in size), but within them, as well.

Alpha motor neurons are the largest and most easily studied of the three groups as their large axons yield themselves easily to both intra- and extra-cellular recordings. There are mainly three types of alpha motor neurons, each of which innervates a specific class of extrafusal muscle fiber. There are two different types of fast-twitch muscle fibers; those motor neurons that innervate

the more fatigable fibers are termed FF (fast-twitch fatigable), while those that innervate fatigue resistant fibers are dubbed FR or FFR (fast-twitch fatigue resistant). These neurons were initially distinguished by pH sensitivity of the ATPase reaction and more recently correlated with protein expression (Brooke and Kaiser 1970; Scott, Stevens, and Binder-Macleod 2001). The slow-twitch muscle fibers are innervated by type S (slow-twitch) motor neurons. They have smaller cell bodies, slower conduction velocities and innervate relatively fewer slow-twitch muscle fibers (Burke, Rymer, and Walsh 1973; Bessou, Emonet-Dénand, and Laporte 1965). While some classification schemes include finer gradations between these types, it's important to note that there is plasticity within the motor unit itself (Gordon and Pattullo 1993).

The gamma motor neuron, on the other hand, is the smallest of the three and does not directly evoke muscle twitches. Instead, it innervates intrafusal fibers of the muscle spindle to modulate afferent feedback from muscle spindles, increasing or decreasing the sensitivity of the spindle as required (Hunt 1951; Granit 1975). Divided into static and dynamic sub-classes, gamma motor neurons either affect the steady-state or dynamic responses of muscle spindles to change in muscle length, respectively. Static gamma motor neurons innervate nuclear chain and/or static nuclear bag fibers, whereas axons of dynamic gamma motor neurons innervate dynamic nuclear bag fibers. This division is, in turn, tied to the type of muscle spindle that is affected. Gamma motor neurons are the smallest of the three types of motor neurons.

Finally, the beta motor neuron innervates both intra- and extra-fusal fibers and accordingly demonstrates behaviors like both alpha and gamma motor neurons, but they are far less common and less studied. Just like the gamma motor neurons, they are divided into two sub-classes depending upon the type of intrafusal fibers that they innervate. Dynamic beta motor neurons innervate both the slow-twitch muscle that is innervated by type S alpha motor neurons as well as

the intrafusal dynamic bag fibers that are also innervated by dynamic gamma motor neurons. Likewise, static beta motor neurons innervate the same static bag fibers as static gammas, and they also innervate the fatigue resistant fast-twitch fibers (Emonet-Dénand and Laporte 1975).

### **1.3.2 Structure of the spinal roots**

The specific anatomy at the spinal roots is precisely what makes a ventral root neural interface both attractive and feasible. A structural separation between the dorsal root ganglia, containing sensory cell bodies and axons, and the ventral roots, with motor axons, allows for specific targeting of the two distinct modalities (Figure 2) (Coggeshall 1980). This is in contrast to both the peripheral nerve, where motor and sensory axons are commingled, even within single fascicles. It also stands in contrast with the spinal cord itself, where synapses and higher-level processing with sensory cells, interneurons, and their dendrites mean that well-isolated action potentials generally no longer represent single motor units, even within the motor neuron layers of the ventral horn.

The location within the spinal column affords some distinct advantages in addition to the structural separation of sensory and motor modalities. Protected by the surrounding vertebrae, recordings are more isolated from both movement and contaminating electrical activity from the surrounding muscles than more distal placements.

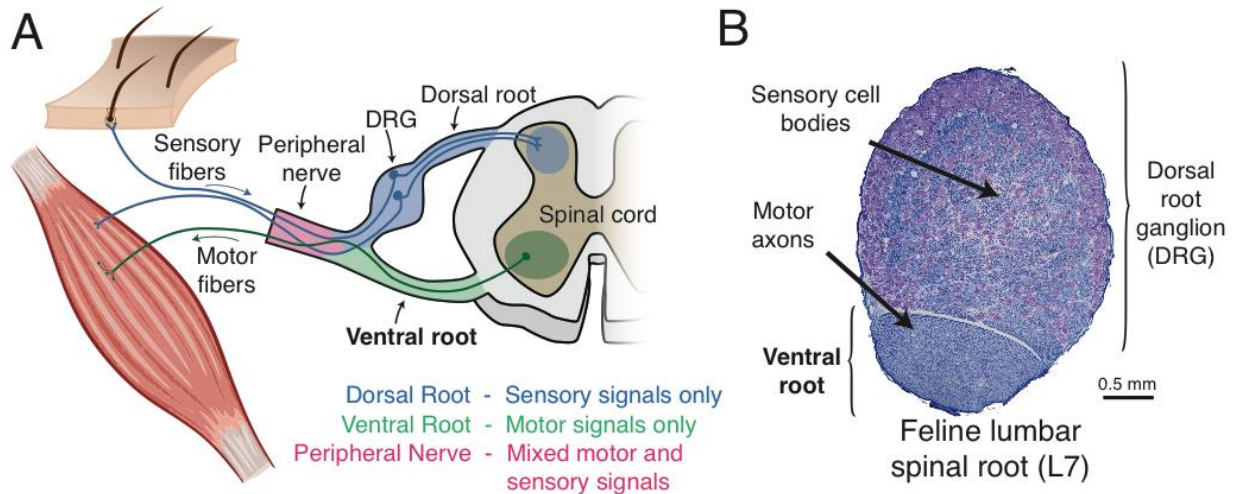


**Figure 2.** Anatomy of the spinal roots. The separation of sensory and motor neurons at the spinal roots enables specific targeting of each modality. A) The peripheral nervous system as represented by a schematic diagram. B) A histological transverse cross-section of feline spinal root demonstrating the compartmentalization of axons in the ventral root (with myelin stained by Luxor fast blue) and sensory cell bodies in the dorsal root ganglion (in purple Nissl stain).

## 1.4 RESEARCH OBJECTIVES

The goal of this work is to develop and validate methods for using motor neuron axons in the ventral root as a source for neuroprosthetic control. In doing so, we demonstrate the ability to record signals from diverse populations of ventral root neurons (Aim 1) and decode intended limb movements using those signals (Aim 2).

**Aim 1: Record from, identify, and characterize populations of ventral root axons in behaving animals.** While previous studies (Hoffer, Loeb, Marks, et al. 1987; Hoffer, Sugano, et al. 1987) have demonstrated the potential for ventral root recordings to serve as a source for

neuroprosthetic control, little work has been done in recording and decoding large populations of motor unit axons in awake behaving animals. A major engineering effort is required to develop and optimize a stable recording interface of many electrodes, both in electrode design and in the supporting hardware. Secondly, recordings from motor neurons in the ventral root must be specifically targeted by the recording arrays and conclusively identified as motor efferents. Finally, to allow for a wide range of independent and finely graded control signals, these populations of motor neurons must be diverse in both their recruitment thresholds and innervation targets. The goal of this aim was to chronically record from and identify ventral root axons with recordings lasting up to three months. The innervated target muscles and recruitment thresholds of these axons was characterized, with the hypothesis that they would provide a representative sampling of the total population with slight biases towards larger axons with higher recruitment thresholds and more distal muscles in the caudal roots (Cullheim 1978; Towe and Harding 1970).

**Aim 2: Use neural recordings from populations of ventral root axons to decode hindlimb muscle activity and joint kinematics.** Current strategies for decoding motor intent from central nervous system (CNS) structures such as primary motor cortex are highly dependent upon context and training (Shenoy and Carmena 2014; Wodlinger et al. 2014). By moving to the periphery and using motor neurons as the source for a decoder, we avoid many of these higher order complexities, since each recorded motor neuron innervates just one functional subset of muscle fibers (Hunt and Kuffler 1954; Feindel, Hinshaw, and Weddell 1952).

This work demonstrates that the recorded motor neurons in the L6 and L7 ventral roots provide sufficient diversity to estimate the limb kinematics as well as or better than estimations from recorded EMG across locomotion and bipedal standing.

### 1.4.1 Chapter Summaries

This thesis describes and develops 1) the methods necessary for recording of motor axons in the ventral roots, 2) examines their usefulness in driving prosthetic control, and 3) looks further at the ability to precisely identify innervated muscles of the ventral root axons.

**Chapter 2** describes the methods and techniques that were developed in order to access and record from the ventral roots in an experimental setting. **Chapter 3** examines the recording quality from the neural interface in over a dozen subjects and develops an algorithm that identifies ventral root units. **Chapter 4** then uses these identified units to estimate evoked muscle activity as a proof-of-concept for neural control of locomotion. **Chapter 5** goes on to further examine the behaviors of the motor units and proposes additional experiments. Finally, **Appendix A** describes some of the iterative development done on the recording electrodes themselves in optimizing the recording quality and the chronic stability of first two-thirds of the subjects.

## **2.0 ACCESSING AND IDENTIFYING MOTOR AXONS AT THE VENTRAL ROOT**

### **2.1 INTRODUCTION**

In the development of a high density ventral root interface, novel engineering solutions are required to overcome the challenges of implanting multielectrode arrays into the spinal roots. This multi-faceted problem includes inserting the arrays, accurately targeting the ventral roots, creating percutaneous routing that is both durable and easy to optimize for peak recording quality, and finally achieving chronic recordings of many motor axons. Alongside the VR microelectrode arrays, the research prototype additionally requires supporting up to ten intramuscular bipolar EMG pairs and a nerve cuff with five contacts. These additional physiological signals are crucially important in order to test the interface for functional usefulness (as required in Chapter 4), but they would not be needed in a clinical or production setting.

While others have previously recorded from ventral root axons (Hoffer, Loeb, Marks, et al. 1987; Hoffer, Sugano, et al. 1987; Hoffer, Loeb, Sugano, et al. 1987), their efforts were limited to a few individually placed electrodes at any given time. Recent advances in electrode arrays enable the possibility of large scale simultaneous recordings from very focused locations within the neural anatomy. Recording from many independent neural signals is an essential pre-requisite

for a functional interface that controls multiple degrees of freedom, as each additional degree requires an ensemble of relevant neural recordings for effective modeling and inference of the movements across a wide range of movement intensities.

The interface must additionally be well-placed in the ventral compartment of the spinal root in order to record action potentials from motor axons. There are sensory afferents that pass through the roots on the dorsal side. Even a very well-placed electrode array may record from sensory afferents on some of its outlying electrodes. These sensory afferents do contain relevant and useful information that can be used to augment the interface with state-based contextual information, as demonstrated by their use in closed-loop control of stepping (Bruns et al. 2013) or locomotion (Holinski et al. 2013). These neurons, however, are only indirect representations of the patient's volitional intent. It is the axons in the ventral root that are directly responsible for motor control. In fact, human subjects have been able to directly modulate individual motor units under closed loop control (Kudina and Andreeva 2010). This sort of volitional control is crucial in the creation of an intuitive and naturalistic motor interface.

### **2.1.1 Previous work**

In the 1980s, Hoffer, Loeb, and colleagues conducted a set of experiments, where they recorded simultaneously from up to 12 penetrating “hatpin” microelectrodes implanted chronically in the L5 ventral roots of cats (Hoffer, Loeb, Marks, et al. 1987; Hoffer, Sugano, et al. 1987; Hoffer, Loeb, Sugano, et al. 1987). These studies were performed to study motor unit recruitment physiology in locomoting cats and demonstrated initial feasibility for chronic ventral root recordings. While allowing the cats to move freely, individual units could be recorded for a whole day or longer, allowing recording to occur during a range of activities and over long periods of

time. The studies found that the modulation of firing frequency closely resembled modulation in EMG amplitude recorded in individual leg muscles. Motor unit recordings were made in ventral root axons over several months, but their chronic stability was not characterized. While they looked at the activity and innervation patterns of these axons, the possibility of neuroprosthetic control was not evaluated.

Since that foundational series of papers, little work has been done with regards to recordings from the ventral roots. Instead, most of the work at the ventral root has been focused on stimulation and not recording, with techniques like sacral root stimulation aimed at restoring renal functionality (Ren et al. 2015) or experiments to evoke movements (Bourbeau 2011). Largely, though, researchers have moved proximally into the ventral horn of the spinal column or out into the distal nerve where the motor axons are commingled with sensory afferents.

These previous studies have shown promise for ventral root recordings as a source for neuroprosthetic control, but there remains a substantial engineering challenge in developing chronic interfaces to simultaneously record from dozens of electrodes in the VR. The development and validation of a ventral root neural interface will be an important step towards restoring mobility to amputees through intuitive control of prosthetic limbs, especially in cases where myoelectric control from proximal structures is not a possibility. This chapter focuses on the development of the required surgical techniques, hardware, and analysis algorithms that are required to record from populations of axons within the ventral root.

## **2.2 DEVELOPMENT OF METHODS**

All procedures were approved by the University of Pittsburgh Institutional Animal Care and Use Committee and the US Army Medical Department Animal Care and Use Review Office.

### **2.2.1 Implant surgery**

Surgeries to implant two or three 32-channel floating micro-electrode arrays (FMAs, Microprobes, Inc.) were performed on 15 adult male cats (3-6 kg) as described in Appendix A (Debnath et al. 2014). The subjects were anesthetized with isoflurane and atropine sulfate (0.15 mg/kg IV) was administered to reduce airway secretions. Vitals including blood pressure, ECG, body temperature, oxygen saturation, and end tidal CO<sub>2</sub> were monitored continuously throughout the procedure. An electric heat pad was used to maintain body temperature near 37° C.

#### **2.2.1.1 Insertion of multielectrode arrays into the spinal roots**

Laminectomies were performed to expose the L6 and L7 spinal roots, and the FMAs were inserted rapidly through the epineurium and dorsal root into the ventral root with a pneumatically-actuated inserter (Blackrock Microsystems, Salt Lake City, UT) (Rousche and Normann 1992). The FMAs were configured with electrode lengths ranging from 1.5-3.5mm, electrode spacings of either 400µm or 250µm, and exposed tip lengths spanning 25-160µm. The higher density arrays had shorter electrode lengths (1.5-2.5mm) and were inserted proximal to the dorsal root ganglia, whereas the arrays with 400µm electrode spacing were inserted through the dorsal root ganglia (Figure 3). The selection and performance of these design characteristics were evaluated in a companion study (Appendix A).

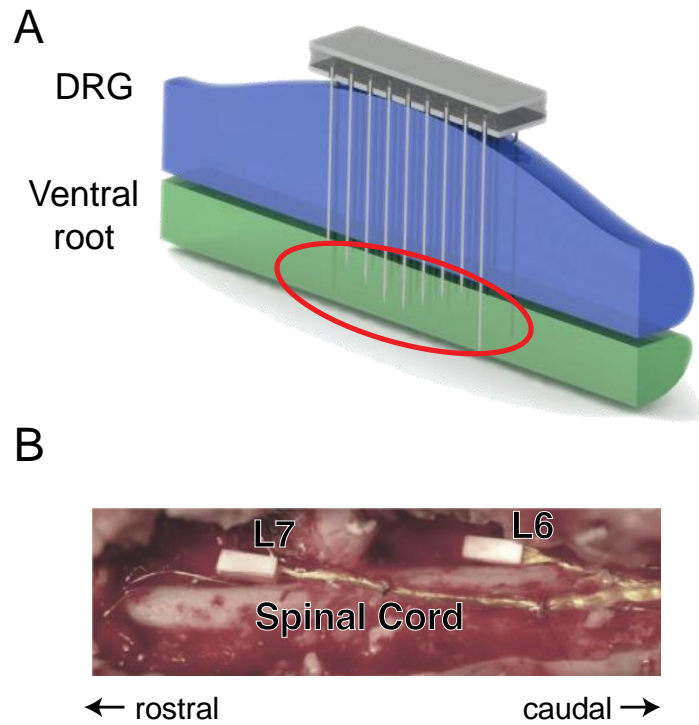


**Figure 3.** Implantation of arrays into spinal roots. A) A cartoon depicts a longitudinal slice of a spinal root, with an implanted floating microelectrode array and the ventral root and dorsal root ganglion (DRG) identified. The ideal location of electrode tips in the ventral root is circled in red. B) A surgical photo of the dorsal side of the spinal column as viewed through the laminectomy. Two floating microelectrode arrays are implanted in the left spinal roots at the lumbar L6 and L7 segments. Their substrates are visible in white with the gold wire bundles exiting the caudal side of the image.

The arrays were held by vacuum pressure to a custom-built spring-loaded housing designed to transfer the impact of the pneumatic inserter while maintaining their orientation. This allowed for precise positioning of each array above the dorsal root ganglia with a multi-axis micromanipulator such that the electrode tips were nearly touching the surface prior to the first impact with the pneumatic inserter.

In order to target the ventral root compartment lying underneath the dorsal root or DRG, the arrays were impacted repeatedly to drive the arrays to a depth of 2-3.5 mm into the spinal nerve complex. The pneumatic inserter was configured with a travel of 1.0-1.5 mm, and the arrays were impacted once or twice through the holder assembly until the electrode tips were inserted sufficiently far for the array to maintain its orientation without the support of the holder assembly. The arrays were then impacted by the inserter directly.

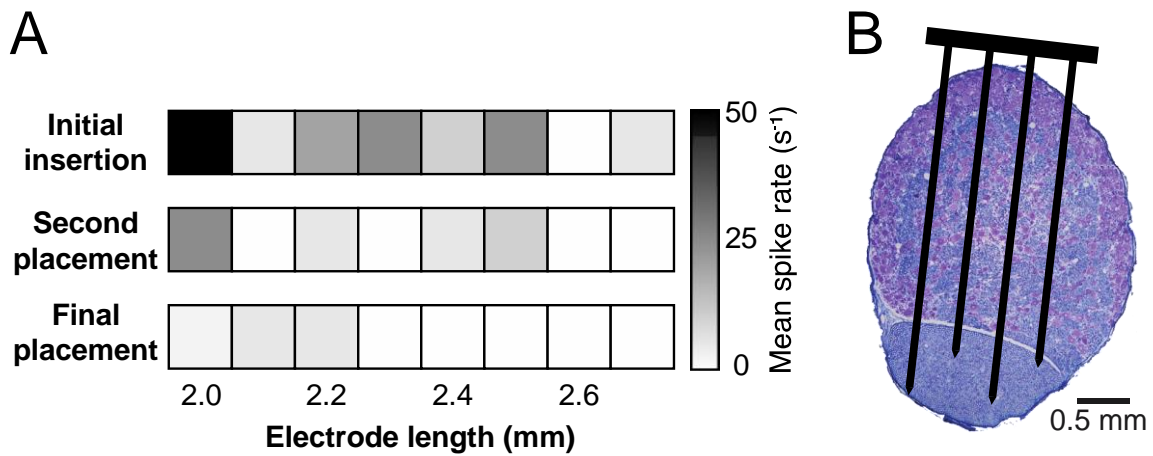


**Figure 4.** Intra-operative procedure for optimizing array placement. Panel A demonstrates the mean spike rate for electrodes of the same length on an example array during manual palpation of the leg under anesthesia. Three different stages of the array’s insertion are depicted, with each successive test following an impact by the pneumatic inserter driving the array deeper. The mean spike rate decreased as the electrodes progressed past the active sensory cells in the dorsal root. Panel B is a cartoon demonstrating the dimensions of an array implanted through a histological cross-section of the spinal roots with a superimposed scale model of an array with 3.0 and 3.4 mm electrode lengths and 80  $\mu\text{m}$  exposed tips. The larger dorsal root ganglion contains cell bodies (purple with Nissl stain), whereas the smaller ventral root is almost entirely axons (stained with Fast Blue).

Following each impact, neural recordings were performed intra-operatively while passively manipulating the hindlimb to activate sensory fibers in the dorsal roots and DRG. As the subject remained sedated under anesthesia, motor activity in the ventral roots was largely suppressed while evoked and spontaneous activity remained in the dorsal structures. Therefore, if a large proportion of the electrodes recorded spiking activity, then the pneumatic impactor was applied again to advance the array deeper into the spinal nerves. This procedure was repeated until activity was found only on the shortest electrodes (Figure 4). After array placement, the wire bundles were sutured to the spinal cord dura mater approximately 1-2 cm away from the array. The deinsulated end of an approximately 20cm long stainless steel wire (AS636, Cooner Wire, Chatsworth, CA) was placed between the dura and vertebra at the caudal end of the laminectomy to optionally serve as an external reference signal. The arrays, reference wire, and exposed spinal cord were protected with a silicone elastomer (Kwik-Cast, World Precision Instruments, Sarasota, FL) or thin plastic film. A 10cm stainless steel wire (Cooner Wire AS632) was anchored to the iliac crest with a titanium bone screw to serve as a ground for the EMG recording system and an optional ground for the multielectrode arrays in the spinal roots. The incision was closed in layers with sutures on both the fascia and skin.

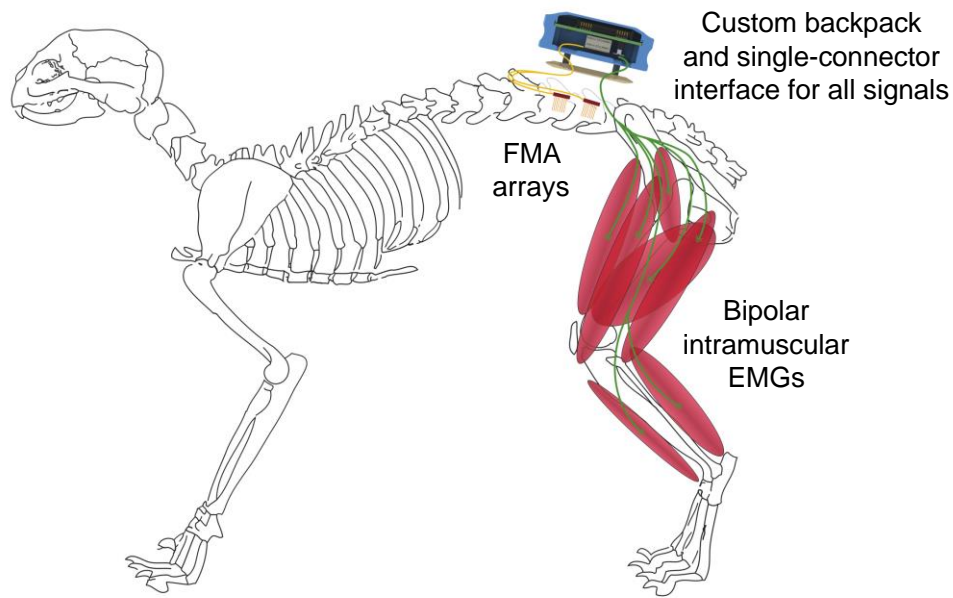


**Figure 5.** Summary of implanted hardware. This cartoon displays the floating microelectrode arrays (FMAs) and their gold wire bundles in the spinal column as well as the muscles targeted by intramuscular electromyography (EMG) electrodes and their leads in green. These wires were routed percutaneously to the custom backpack, which was mounted to the fascia above the dorsal laminectomy.

### **2.2.1.2 Protective connector housing and circuitry**

The wire bundles were routed percutaneously through the surgical incision into a protective custom-printed plastic backpack (Figure 6). The backpack mounted to a plastic or titanium baseplate that attached to the fascia and iliac crest with large gauge suture. Four standoffs from this baseplate penetrated through the skin and provided mounting points for a protective backpack. The array connectors and wire bundles were mounted and protected within this custom-printed plastic backpack.

The current standard for connecting multielectrode arrays like the FMA is the Omnetics Nano Strip connector, but this connector has significant limitations for performing recordings in unrestrained behaving animals. While its small size is advantageous in some circumstances, it is difficult to align and mate quickly on an awake animal. Its 36 contacts are fragile and unpolarized, meaning it is possible to physically mate the connectors in the reverse orientation. Even worse, it is often not possible to detect that connectors mated the wrong way by the recorded signals alone, leading to erroneous results and conclusions. Since the ground and reference electrodes are symmetric with respect to rotation, this mistake is both easy to make and hard to detect. Lastly, it is quite fragile and breakable, rated for only 200 insertion cycles.

Using these devices directly as manufactured requires independently connecting the two or three electrode arrays, each with its own Omnetics connector. Furthermore, support for recording from additional physiological signals like those from muscles and nerves requires an entirely custom fourth connector with up to 28 contacts. All told, this amounts to four independent connections with over 120 individual contacts. Connecting all of these in an awake behaving animal has proven very difficult. In response, a pair of custom circuit boards were developed to alleviate these issues by routing all signals through a single, more robust connector (Figure 6).

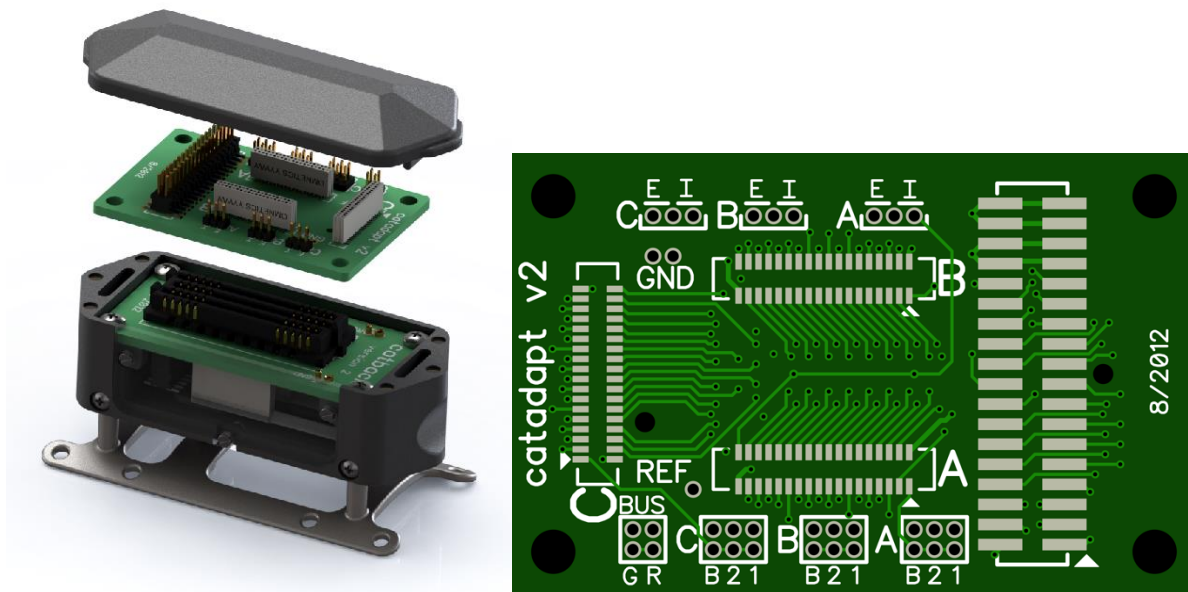


**Figure 6.** Protective backpack and circuitry. The printed titanium standoffs provided a stable attachment to the fascia and secure percutaneous attachment points for a plastic housing that protected the connectors and presented a single interface for all the physiological recording signals. The lid attached magnetically when not in use. The top-side adapter board allowed for configuration of the ground and reference signals while at the same time allowing the headstages to be connected in advance. Once the subject was ready for a recording session, the adapter boards coupled together with one easy-to-mate connector. See Figure 7 for typical jumper configurations and how they were revised.

To support the high number of physiological recording signals and improve upon the Omnetics Nano Strip Connectors, a pair of custom-printed circuit boards were created to collect the three Omnetics array leads into just one mating connector (SEAM/SEAF SEARAY array, Samtec), and then split back out again on the other board to connect to the recording headstages. In addition to carrying up to 102 neural signals, these custom boards also supported up to 10 pairs of bipolar EMG wires, and 5 leads from a nerve cuff for a total of 125 independent physiological signals through just one connection. Using the polarized SEAM and SEAF connectors as the single primary interconnect was a vast improvement over individually connecting each array for every session. They were easier to quickly align and connect and proved far more robust than the Omnetics connectors, with five times the rated durability (1000 insertion cycles instead of 200). Their large and stable housing anchored very securely to the board and completely eliminated failures at the solder joints, which was by far the most common failure mode of the Omnetics connectors. In addition to signal routing, the top board exposed hardware selection of ground and references with jumpers for each array, allowing for custom, optimized recording configurations for each subject.

A series of jumpers on the top breakout board enabled configurable selection of the ground and neural reference electrode for each recording headstage. Enabling the configurability of these signals proved to be critically important in achieving good recording quality as their characteristics directly impacted all other signals. Neural recordings demand both a stable ground and a nearby reference recording to ensure that the potentials accurately reflect local phenomena. Each FMA had two long reference electrodes as well as two completely deinsulated electrodes shunted together to be used as an internal ground. The two stainless steel wires placed during the laminectomy provided extra options for reference and ground. This amounted to a theoretical total

of 3-4 ground options and 5-7 reference options for each headstage. Only a subset of the possible configurations was supported, however, to limit the interface complexity and maintain a low profile on the adapter board.

On the top (system) side adapter board, each headstage had a reference channel routed to a 2x3 male header strip. A jumper placed on this header strip enabled independent selection of one of three different possible reference sources for each array. Two of these three selectable signals directly connected to the reference electrodes on the given array. The third signal was different; it was a shared bus that wasn't permanently connected to any of the signals within the subject. Instead, it was shared across the three array reference header strips, allowing a single array to both select its own reference electrode with one jumper and then additionally share this reference source to the other two headstages. A fourth 2x2 header strip allowed this bus to be connected to either the reference or ground Cooner wires. Each headstage had its other reference channel routed directly to the internal ground electrodes on the connected array. The Plexon recording system exposed this option as a dynamically configurable software setting.

A simpler structure was used to configure the ground; the ground for each headstage was routed to the middle pin of a 1x3 header strip, with the outside pins connected to the array's ground electrodes and the implanted Cooner wire ground. A jumper connected this middle pin to either ground source for each array.

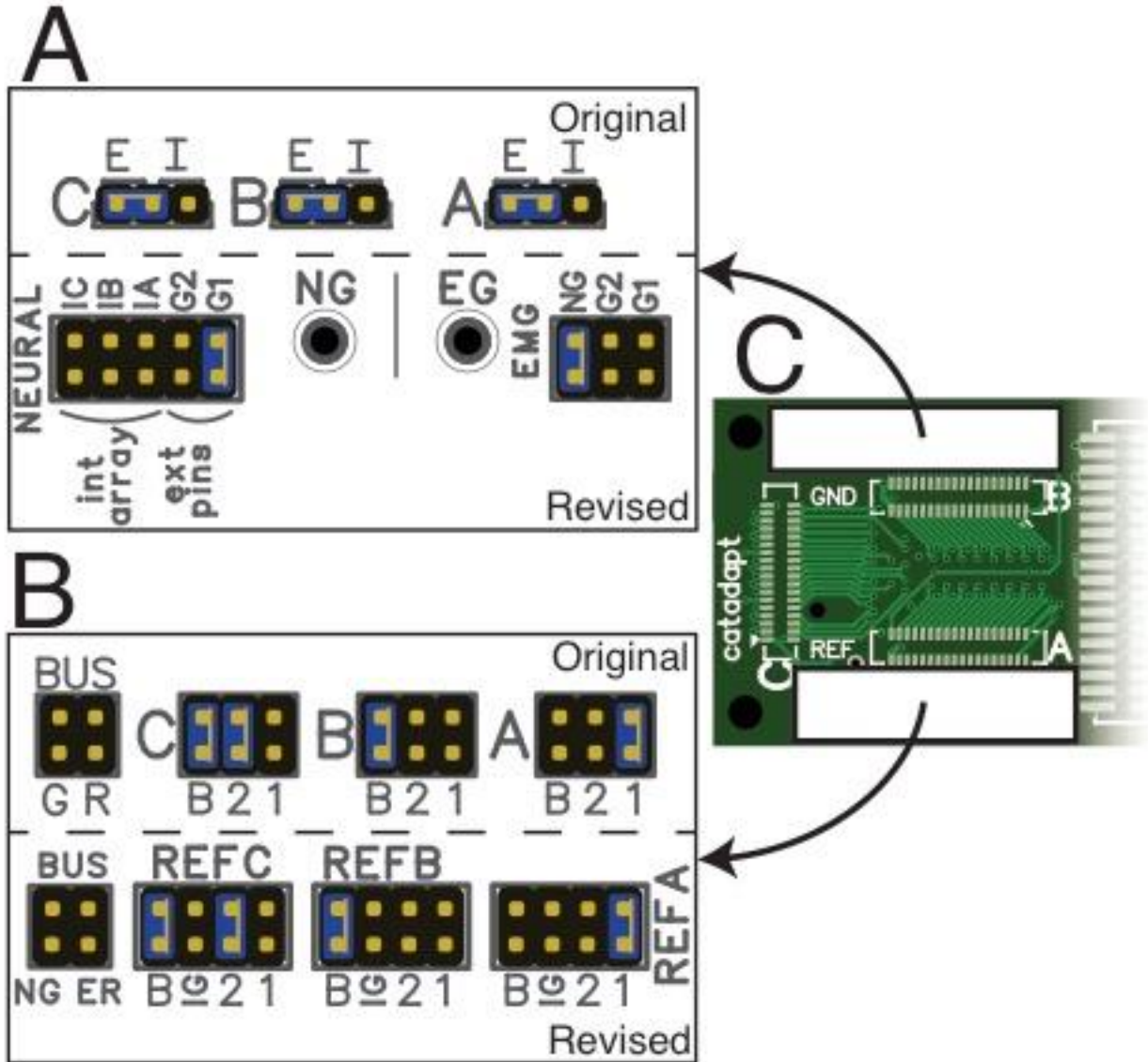


**Figure 7.** Typical setup of the adapter board and its revision. Panel C shows the entire board, with panels A and B highlighting the original and revised headers in the same configuration as enlarged detail views. In general, the arrays are identified as ‘A’, ‘B’, or ‘C’. **Panel A)** The grounds of both EMG and neural recording systems connect to the Cooner wire (‘E’ or ‘G1’). The revision consolidated all three array grounds into one neural ground (‘NG’), which could connect to any ground source including internal array grounds (‘I’ or ‘IA’, ‘IB’, ‘IC’), and it enabled custom configurations for the EMG ground (‘EG’). It also added test points for debugging. **B)** The reference for array A connects to one of its own reference electrodes, and array B connects to the signal bus (‘B’). Array C connects to one of its own reference electrodes, and it additionally shares that to the signal bus. The revision simply added the ability to select the internal ground (‘IG’) for each array and clarified some of the labels. **C)** The unpopulated board itself.

## 2.3 DISCUSSION

### 2.3.1 Implant procedure

Implanting FMAs through intact epineurium proved to be difficult and required the use of high-speed pneumatic impact insertion methods. The size of the dorsal root ganglia at the L6 and L7 roots required long electrodes to penetrate from the dorsal epineurium down into the ventral root — approximately 2-3 mm. While the maximum travel distance of the pneumatic inserter was 1 or 1.5 mm, the arrays rarely penetrated the full travel distance into the neural substrate. Thus, insertions frequently required 3-5 repeated hits, with varying travel distance each time. The variability in travel distance was a challenge in ensuring proper placement, but in general the slow insertion was advantageous in determining the final placement. The repeated hits and electrode travel of less than 1 mm turned out to be essential in properly targeting the ventral root — a structure that was typically ~1 mm or less in total length along the axis of the electrodes.

This procedure stands in contrast to multi-electrode array insertion techniques used in the cortical structures of the brain. The six layers of the neocortex, and more importantly, the distances from the surface to each layer tend to be highly regular within specific areas and are generally preserved across individuals (Creutzfeldt 1977). This allows for very specific targeting of certain layers simply by designing electrodes with appropriate length shanks and simply inserting them fully. While there are still challenges with “dimpling” and compression of neural tissue and the subsequent expansion which shifts the array out of place, arrays inserted into cortical structures

typically perform quite well. On the other hand, we found the size of the spinal roots (and specifically the dorsal root ganglia) to be much more variable between individuals, consistent with the identification of “pre- or post-fixation” of vertebral alignments with respect to the lumbosacral plexus (Romanes 1951; VanderHorst and Holstege 1997). While we attempted to successively refine the electrode lengths (as described in Appendix A), it was never the case that complete insertions meant that arrays were properly targeting the ventral roots. Improvements here could be possible through more incremental insertions by vibration (Shoffstall et al. 2018), allowing more precise and less damaging positioning of the array. Further, pre-operative or intra-operative imaging techniques may enable better visualization of location of the ventral root, and, accordingly, better trajectory planning for the array.



**Figure 8.** Dissection photograph of a poorly placed array. The electrodes tips were driven completely through the root and presumably contacted against the wall of the spinal column during insertion, causing them to bend and break.

A major factor in the difficulty was in targeting the ventral root from a dorsal approach. The ventral root is a small structure obscured below the dorsal root and ganglion. While we developed an intra-operative protocol aimed at maximizing proper electrode depths, this was not sufficient in order to ensure that the recording sites on the electrode tips ended up in the ventral root. By design, at least some of the shorter electrodes remained in the dorsal compartment and recorded sensory activity. Conversely, there was evidence of some longer electrodes exiting the ventral border (Figure 8).

The ideal array would be implanted percutaneously and tunneled through the foramen under image guidance. Visual guidance through imaging promises to improve array placement and a percutaneous approach would reduce the invasiveness. Further, using an array with multisite electrodes along each shank could allow for increased yields by sampling the region at a greater density than is possible with FMAs. These further developments into the electrode design and surgical approach would greatly improve the interface and chances for clinical success.

Consistent electrode targeting was difficult to achieve throughout the experiments. Observations of perfused spinal nerve tissue have shown that electrodes can pass through the ventral surface of the ventral root and that these electrode shafts can bend, presumably as a result of mechanical contact with the spinal canal (Figure 8). These results suggest that other approaches to implantation, such as targeting the ventral root from the lateral or ventral side, may be more appropriate for accessing the ventral root.

### **2.3.2 Circuitry configurations: Lessons learned**

In practice, the hardware configuration options afforded by the custom circuitry proved invaluable by enabling quick and reliable changes that optimized the recording quality for each subject and

each recording session. Without this board, a direct connection from the headstage to the array would have provided no configuration options for the ground and only the two reference electrodes on the connected array would have been options as a software setting. In practice, the software selection of these references was easy to overlook and difficult to ensure consistent settings across multiple subjects and over time. With hardware jumpers, however, it was quick and easy to visually validate the settings and each subject could have a dedicated configuration board to ensure consistent recordings.

Informed by these experiments, several improvements to the boards were made for future use. While the improved board was not used for the subjects in this thesis, the changes are informative and worth documenting. The structure of both the ground and reference jumper banks were modified. The changes to the references were motivated only to improve their ease of use. It proved confusing to have the reference configuration split between the hardware jumpers and a software switch (which selected either the hardware jumpers or the array's internal ground as the reference source). Users of the configuration board overwhelmingly favored the hardware selections, so the internal ground was added as a fourth hardware jumper setting. This hardware reference was connected to both of the headstage reference channels, obviating the software switch; the references were always chosen in hardware regardless of the software setting.

The modifications to the ground jumpers were much more substantial. In practice, it wasn't beneficial to select different ground sources for the different headstages. Optimal recordings always shared a common ground across all headstages. At the same time, the most effective ground choice was typically the Cooner wire, but this ground source was also permanently connected to the EMG connector ground. There were situations when it would have been advantageous to decouple these two systems, particularly in other projects that used electrical stimulation. In

response, the three array ground jumper banks were unified into one larger bank of jumpers that selected the ground for all three arrays at once. This also exposed the option for a secondary Cooner ground wire to be implanted and selected as a backup. A second jumper bank was added to enable customization of the ground channel for the EMG system, allowing the two grounds to be optionally disconnected. Finally, test points were added to both the neural and EMG ground networks to simplify testing and add a final ground option—they can be used as the ground source when no jumpers are mounted on the header strips.

## **2.4 CONCLUSION**

This work established a chronically implantable system that supported up to 96 electrodes simultaneously recording from the spinal roots. Without any one of the components listed here, the subsequent work on validating the interface for neuroprosthetic control would have been much more challenging or impossible.

## **3.0 RECORDING NEURAL ACTIVITY FROM THE VENTRAL ROOTS**

### **3.1 INTRODUCTION**

Highly important in the development of any neural interface is the ability to record from relevant neurons with sufficient quality and quantity for the device to have enough information to perform tasks of daily living in a useful manner. High quality recordings—well-isolated recordings of single axons—enable the identification of discrete output signals, whereas the sheer number of such signals provide a rough upper bound on the theoretical degrees of freedom available to the interface. While these two characteristics are both necessary, the existence of both is not sufficient. The recorded signals must further modulate in a manner that is relevant to the task at hand. Finally, for a neural interface to be clinically translatable, it must consistently maintain recording stability over an adequate period of time. For the purposes of this chapter, we'll focus on simply the quantity and quality of the recorded signals. For more in-depth examination of longevity and recording quality over time, see Appendix A.

Previous studies in the ventral roots have successfully recorded single-unit activity with individually placed hatpin electrodes in the ventral roots (Hoffer, Loeb, Marks, et al. 1987). They showed that penetrating electrodes within the ventral roots allow for isolated single-unit recordings with varying signal amplitudes (10 $\mu$ V to 128 $\mu$ V reported), representing a large range of signal-to-noise ratios (Hoffer, Loeb, Marks, et al. 1987). Beyond the demonstration of quality of the

recording, Hoffer and colleagues were able to demonstrate relevance by examining instantaneous “frequencygrams” of the correlation between evoked muscle activity and the activity in the recorded signal from the ventral root. The individual nature of the hatpin electrodes, however, meant that recording from a large quantity of neurons simultaneously was a challenge. In most of their experiments they only recorded from a handful of neurons at any given time from as many as 12 implanted electrodes. As such, their focus was on the basic physiology of the ventral root axons and not neuroprosthetic control.

The high density multielectrode arrays that have developed since allow these studies to be revisited for the purposes of neuroprosthetic control. While arrays enable rapid implantation of many electrodes at once, the individual electrodes are not independently positioned and thus instead must be individually analyzed to ensure they record from the expected structures. In this case, the target is the relatively smaller ventral roots immediately adjacent to the larger dorsal structures. These sensory afferents in an intact model animal would likely not exist or be significantly reduced in the target patient population of individuals living with amputation. Distinguishing the motor efferents from accidentally recorded sensory afferents from misplaced electrodes is an important first step to enable a fairer—if slightly pessimistic—proxy for potential performance in the actual patient population based upon the results from the intact model animal.

This chapter examines our ability to record from chronically implanted multielectrode arrays targeting the ventral roots in fifteen intact cats during locomotion. An algorithm is developed to distinguish and discard sensory afferents, and our ability to specifically target ventral roots is quantified. This important first step is required to subsequently use these recordings as input for limb state decoders in the following chapters.

## 3.2 METHODS

As described in Chapter 2, 15 cats were implanted with two or three floating microelectrode arrays. All procedures were approved by the University of Pittsburgh Institutional Animal Care and Use Committee and the US Army Medical Department Animal Care and Use Review Office.

### 3.2.1 Chronic recordings

After the implant surgery, awake recording sessions were performed on each subject at least three times a week, with an anesthetized recording session under dexmedetomidine once a week. The neural and EMG signals were recorded with a high channel count data acquisition system (Omniplex D, Plexon Inc., Dallas Texas) at 40kHz and 10-20kHz, respectively. The neural data was band-pass filtered (300-3000 Hz). Action potentials (spikes) were detected by threshold crossing technique, using a threshold level set to three standard deviations of the neural signals on each channel measured during a 10 second period with the animal at rest. The threshold spikes were sorted manually using OfflineSorter (Plexon Inc.). The EMG data were bandpass filtered (80-500Hz) with a zero-lag fourth order Butterworth filter and amplitude normalized by z-score transformation.

During the awake sessions, the animals walked freely on a treadmill (Bertec Corporation, Columbus Ohio) at belt speeds ranging from 0.4 m/s to 1.2 m/s. Example neural signals from such a session are displayed in Figure 9, highlighting the ability to record from many channels with modulating spiking activity and individually isolated units with varying isolation from the background activity.

While the ventral and dorsal spinal roots are separated into distinct compartments of the spinal nerve, targeting the ventral root compartment is challenging, particularly given its small diameter relative to the dorsal ganglion. The shortest and thus shallowest electrodes were often located in the dorsal roots, requiring further testing to identify neural signals as motor or sensory. Once per week, subjects were anesthetized with intramuscular injections of a reversible anesthetic (dexmedetomidine, 0.4 mg/kg, and reversed with imidazole, 0.4mg/kg) and neural recordings were made during passive leg movements and manual palpation. The anesthesia suppresses motor activity (Farber, Poterack, and Schmeling 1997), while preserving sensory responses from muscle and cutaneous afferent neurons. Each anesthetized session consisted of four 30 second recordings, one without any external manipulations, and three where the limb was manually moved or palpated (repeated whole-leg flexion and extension, sequential isolated joint movements, and cutaneous palpations).

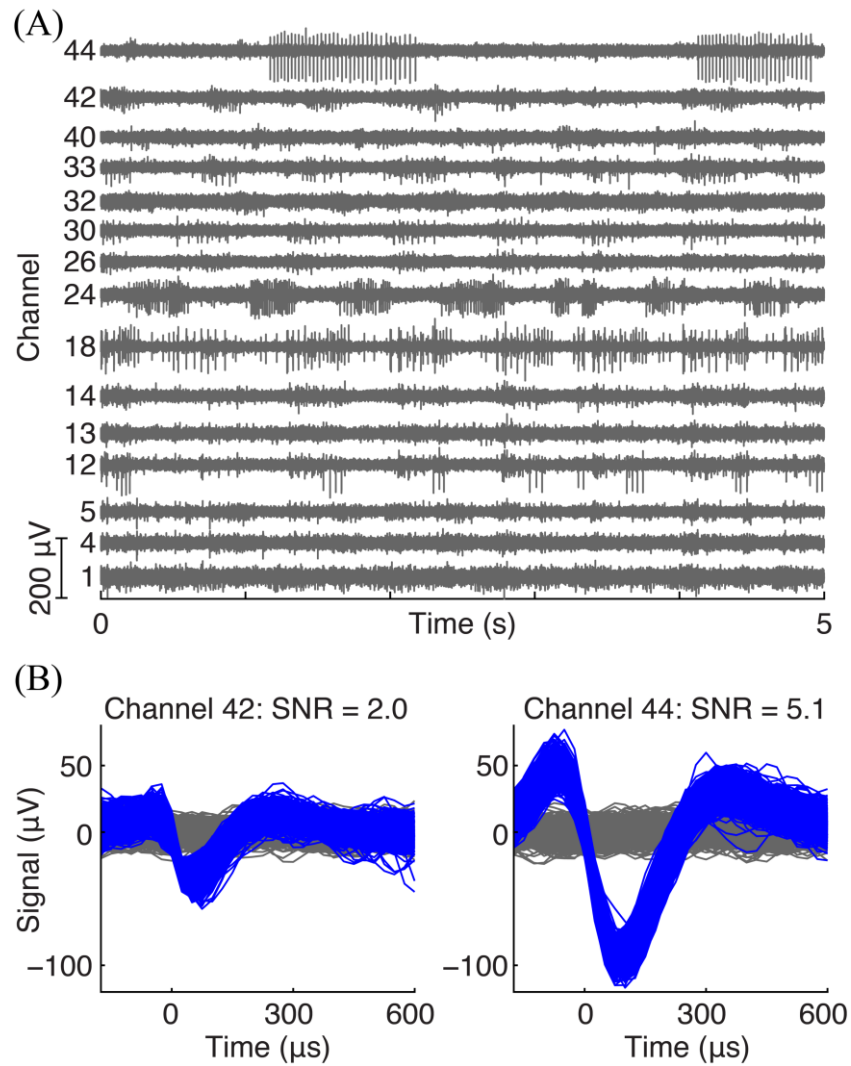


**Figure 9.** Example recordings from the ventral root interface, adapted from Appendix A. Panel A) Five seconds of recordings from fifteen channels during treadmill locomotion. This is representative of the phasically modulated spiking activity that occurred throughout the trial. Panel B) Two example units with their threshold-aligned action potential waveforms overlaid against their channels typical background activity as concrete examples for low and high signal to noise ratios (SNRs).

### 3.2.2 Motor axon identification

Results from the anesthetized testing sessions were used to identify motor and sensory neurons across the array of microelectrodes. A neuron was identified as a motor unit if it and any other neuron on the same electrode did not respond to manual manipulation of the leg under anesthesia. A neuron was deemed responsive if its firing rate exceeded one spike per second during manipulations. Neurons identified as motor units by this criterion were further analyzed to verify that their firing rate properties were consistent with those of motor neurons. Exceptions to this secondary criterion were made for motor units that exhibited doublet activity — those with rapid pairs of action potentials separated by less than 10ms. Typically, motor efferents have a mean firing rate of 20-40 spikes per second, but quickly generating large responses from a muscle requires this secondary firing rate regime (Denslow 1948; Erim et al. 1996; Mrówczyński et al. 2015). Accordingly, to be confirmed as a motor neuron, fewer than 10% of the inter-spike intervals could be less than 20 ms unless those faster ISIs were consistent with doublet activity. In those cases where more than 10% of ISIs were under 20 ms, motor units were distinguished by ensuring that their inter-spike interval distributions were characteristic of a neuron that had two distinct firing rate regimes. Each unit's ISI distribution was fit to a two-component logarithmic Gaussian mixture model. The distribution was motor-like if the two components were well-separated ( $d' > 1$ ), with the mode of the smaller component under 10 ms and with less than 10% of the larger component occurring under 20 ms (Figure 10).

### 3.2.3 Effects of electrode location

In order to further evaluate the importance of array positioning, a nearest-neighbor analysis was also conducted to examine the importance of relative electrode location in its ability to record ventral root activity. Given the significantly smaller size of the ventral roots (~1 mm diameter) with respect to the overlying dorsal roots and DRG (~3 mm diameter), a successful implant requires a successful intra-operative targeting. This procedure, detailed above, assumes that the electrodes recording motor units are spatially clustered together and distinctly separated from electrodes recording non-motor activity.

To validate this assumption and reinforce the importance of successful targeting, a nearest-neighbor analysis was conducted over all electrodes across all recordings sessions of each subject. Each electrode had up to six immediately adjacent neighboring electrodes, with electrodes in the center of the array having all six neighbors (arranged hexagonally) and those on the edges and corners having two to five neighbors. A manufacturing defect in a small number of arrays (7/35) where the ground and reference electrodes were misplaced such that they were inset into the array by one position meant that the four electrodes on the narrow edges only had one nearest neighbor. Due to the varying number of recording sessions per cat, this only affected 248 of the 20960 (1.1%) of the sessions and electrode locations analyzed. The proportion of neighboring electrodes that recorded ventral root activity was analyzed for each electrode and grouped into three categories based upon the recording activity of the central electrode in question (had VR activity, had non-VR activity, or had no recorded units). An analysis of variance (ANOVA) was used to statistically compare these groups with a significance level of  $p=0.01$ .

### **3.3 RESULTS**

The primary aim of this study was to evaluate and quantify the ability to record specifically from motor axons in the ventral compartment of the spinal roots. Table 1 summarizes the animals included in this study and their overall recording summaries.

#### **3.3.1 Ventral root identification**

Across the 15 subjects, 2277 individually sorted units with at least 300 spikes recorded during two or more minutes of treadmill walking were recorded and examined. This excluded 717 units that did not have the required 300 spikes; this cutoff simply ensured sufficient data to fit distributions against the inter-spike intervals and compare against anesthetized recordings. The chronic recordings spanned implants lasting from 1-12 weeks, so it's important to note that some of these units may have been duplicated across sessions and days. While no attempt was made to concretely identify the stability of individual units over time, we anecdotally identified units with stable and consistent waveforms and spiking patterns across multiple days while performing the experiments.

**Table 1.** Summary of all 15 subjects implanted. The total number of units was highly variable, dependent upon both array placement and recording quality. The first ten subjects were implanted with two arrays penetrating through the L6 and L7 dorsal root ganglia. The final five subjects were implanted with three arrays; one array was implanted through the L7 dorsal root ganglion like the first cohort, and the other two arrays were higher density and implanted through the L6 and L7 roots proximal to the ganglia.

	Implant duration	Number of testing days	Number of implanted FMA arrays	Number of recorded VR units	Number of total units recorded	Average number of VR units per day	Average number of total units per day
W	83 days	14	2	15	39	4.9	13.5
V	20	2	2	39	63	36.0	53.0
U	34	6	2	14	34	9.5	17.2
T	17	6	2	21	54	13.0	27.7
S	34	16	2	13	39	6.3	17.8
R	59	23	2	8	71	2.9	21.4
Q	9	3	2	16	77	11.0	49.0
P	78	43	2	24	46	6.7	15.6
O	22	3	2	4	35	3.0	26.7
N	7	0	2	-	-	-	-
M	12	14	3	58	135	30.0	81.9
L	62	13	3	100	150	32.0	51.2
K	14	4	3	48	105	45.0	92.3
J	6	2	3	22	44	19.5	39.5
I	9	1	3	3	9	3	9

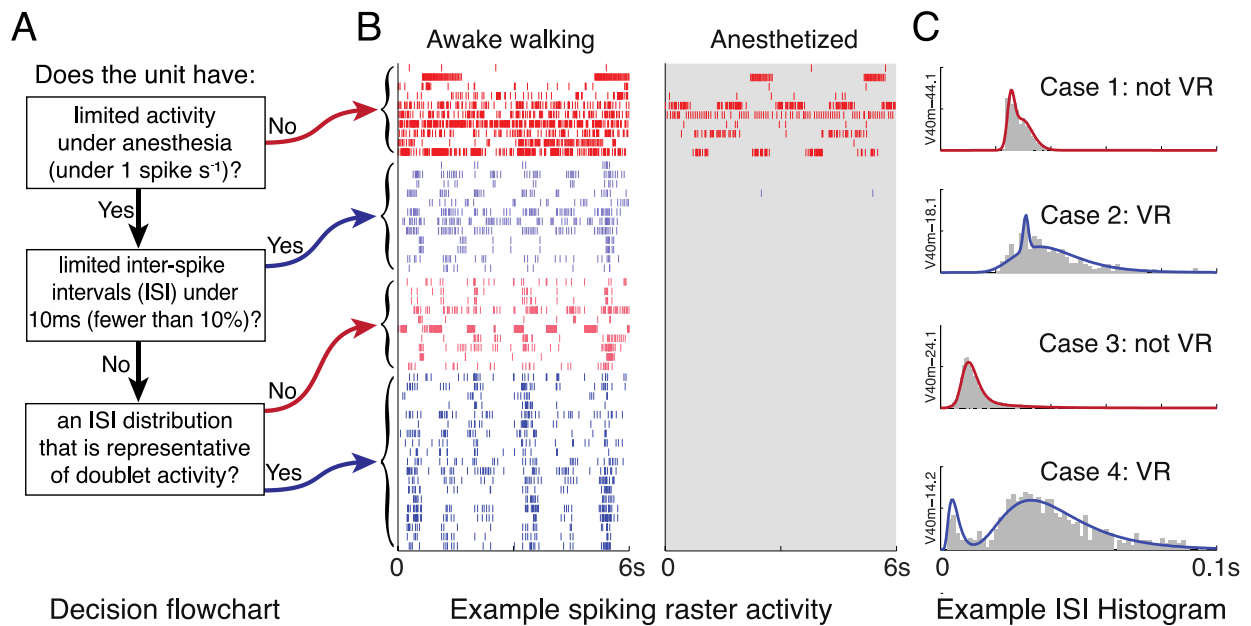


**Figure 10.** Classifying neurons as ventral root axons. A) The decision flowchart for determining if a given neuron is motor-like based upon its behavior. B) Example rasters during awake walking and under anesthesia. Each row represents the spiking behavior of one isolated neuron and is consistent across the two panels. The neurons are arranged into groups and colored based upon the decision flowchart outcome, with red representing those that were discarded and blue representing identified motor units. C) Example inter-spike interval (ISI) histograms for each category of neuron.

Of these 2277 units, 749 units (32.9%) were classified as motor efferents by the algorithm described above (example in Figure 10, overall results in Figure 11). Spiking activity while under anesthesia disqualified 913 of the units from consideration as motor efferents. The manipulations performed under anesthesia attempted to span a wide range of movements and perturbations in order to activate as many different sensory modalities as possible. By design, therefore, very few afferents were active during the entire duration of the anesthetized session, leading to relatively low overall firing rates. The mean firing rate for these disqualified units (across the entire duration of the anesthetized session) was 7.5pps, with an interquartile range from 1.2 to 9.6 pps.

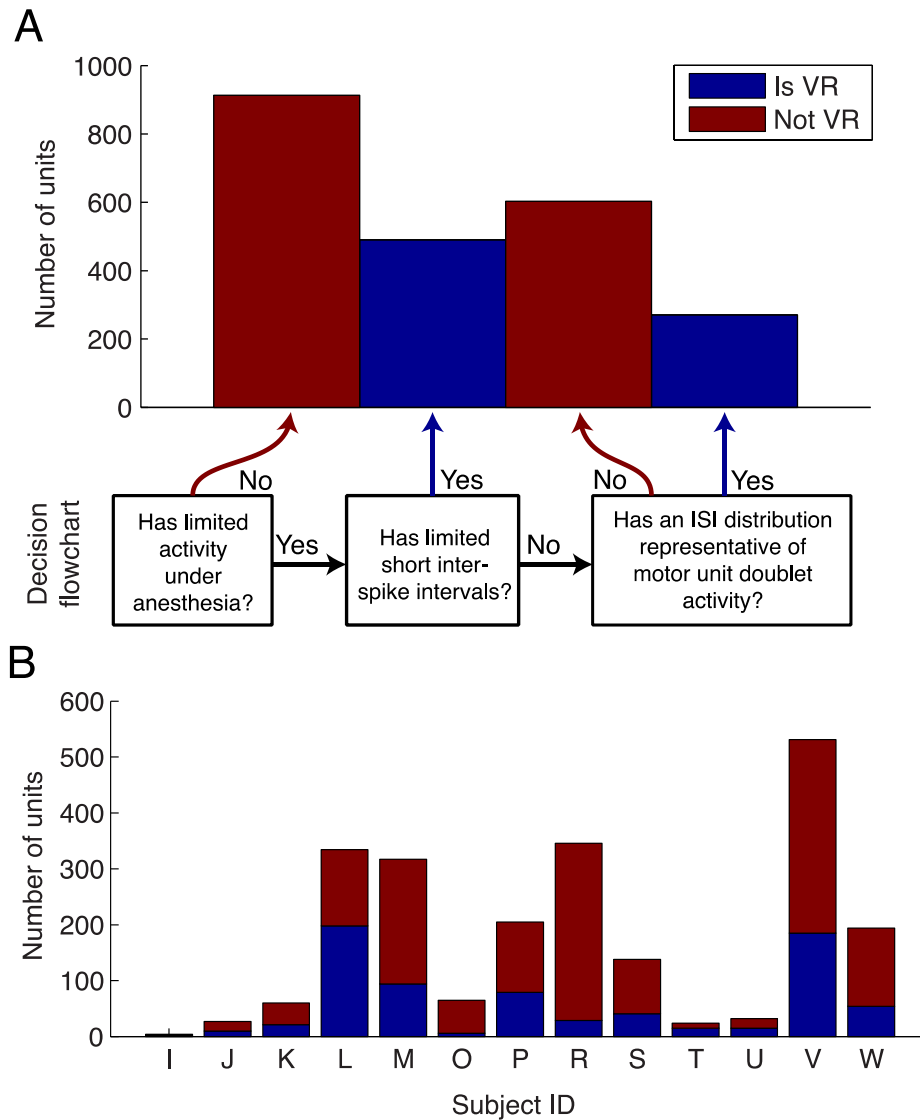


**Figure 11.** Overall VR identification summary. Panel A) Breakdown of the number of units that were identified as VR or not, using the same decision flowchart as Figure 10. B) Total number of units grouped by subject ID and colored by VR identification. The total number of units recorded was most dependent upon the total number of trials recorded for the subject, whereas the proportion VR depended upon the placement and stability of the array.

The firing rate behaviors eliminated another 603 units, leaving a total of 749 identified motor units. 490 of these motor units were identified as motor-like simply because they had few (less than 10%) of their spikes occurring within 20 ms of the previous spike. The remaining 271 identified motor units had inter-spike intervals that fit a two-component logarithmic Gaussian mixed model with doublet-like heuristics: well-separated components ( $d' > 1$ ) and a fast component with a mode faster than 10 ms.

### **3.3.2 Location effects**

The ability to successfully target the ventral root and the importance of the relative location of individual electrodes with respect to one another was determined using a nearest neighbor analysis. The identifications of units recorded by electrodes with respect to their layout on three example arrays is shown in Figure 12, demonstrating different classes of spatial orientations within the spinal roots. These examples not only demonstrate the importance of electrode length, with the array in panel C demonstrating motor efferents on the deeper electrodes, but also the insertion angles. The array in panel B has all its motor units located on electrodes along the lateral edge of the array, suggesting that the array was inserted with an incorrect angle of rotation with respect to the axis of the root. Finally, the array in panel A demonstrates a cluster of identified motor units on the rostral tip of the array, indicating that the dominant effect in this case was the rostral-caudal angle of the array with respect to the ventral root.

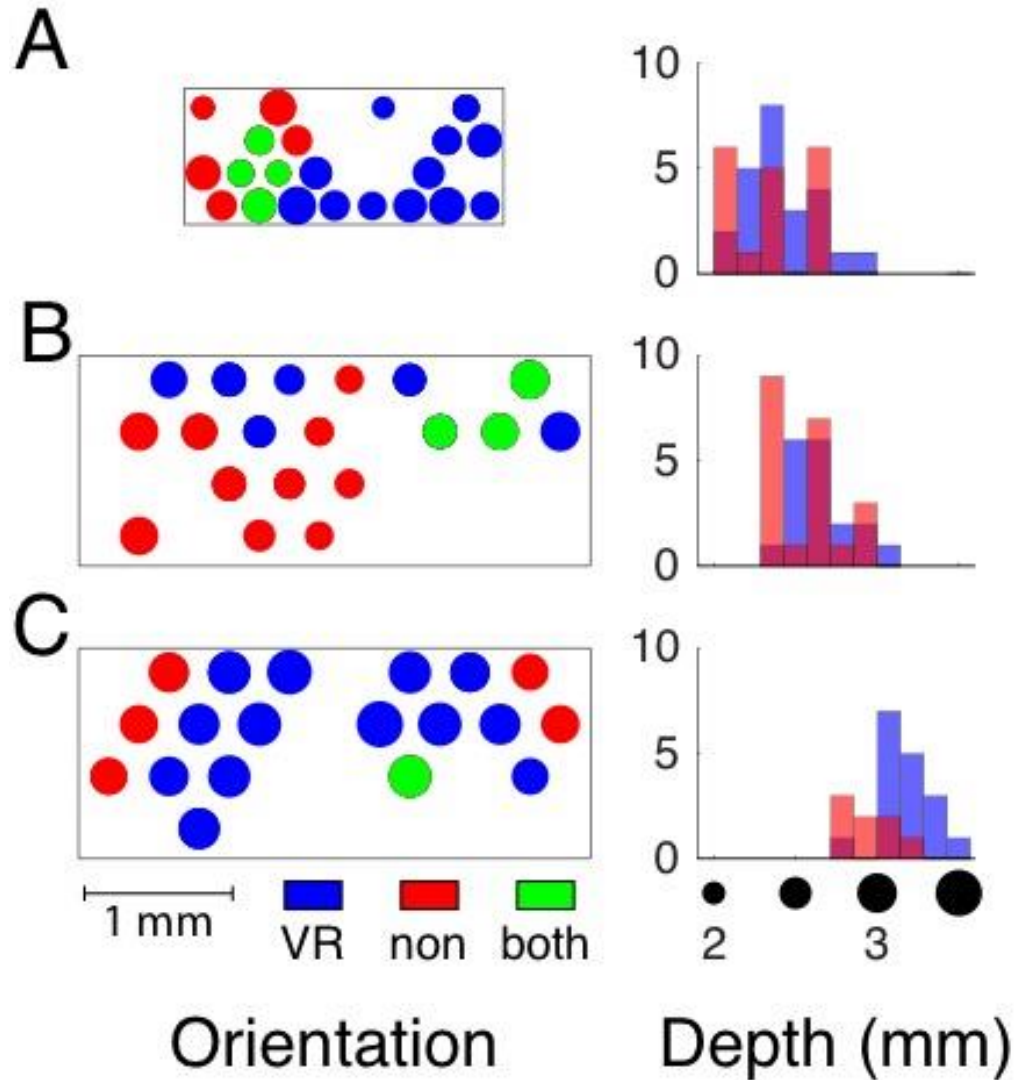


**Figure 12.** Location effects on neuron identification. Three example arrays are shown. The left side displays the spatial locations of electrodes that recorded activity within the outline of each array's substrate. The electrodes are shown as circles, with size proportional to length and colored by identification. The wire bundles exited to the left, proximally towards the spinal cord. On the right side are the corresponding histograms of the number of units by depth. A) At the top is a high-density array in the proximal L6 spinal roots from subject J demonstrates spatial separation between unit types along the long axis of the array. It is likely that the distal end of the array ended up being implanted further into the spinal roots, enabling it to reach the motor axons in the ventral root. B) An L7 array from subject Q demonstrates spatial clustering on a lateral side of the array. C) An L7 array from subject T exhibits clustering by electrode depth.

Averaged across all implanted electrodes and sessions, 12% of an arbitrary electrode's neighbors recorded motor activity during awake treadmill walking trials. However, given that an electrode itself recorded motor activity, 46% of its neighboring electrodes recorded motor activity, which was a significantly higher percentage ( $p < 0.01$ ). For electrodes that only recorded non-motor activity, the percentage of neighboring electrodes recording motor activity was 15%, again significantly different than both of the previous two groups ( $p < 0.01$ ). These results suggest that if an electrode was successfully positioned in the ventral root and recorded motor activity, its neighbors also frequently recorded motor activity. Furthermore, if we restrict the set of nearest neighbors to those that are the same length or longer than the electrode in question, then the proportion of neighbors for electrodes recording ventral root activity increases to 51%, and for electrodes recording non-motor activity it decreases to 12%.

Even more dramatically, 74% of electrodes that recorded motor activity had at least one neighboring electrode that also recorded motor activity. This is in stark contrast to the 21% of electrodes recording non-motor activity with at least one neighboring electrode with motor activity. When averaging across all electrodes, this proportion drops to 18%, but that is unsurprising given that some arrays had very few active electrodes, especially towards the end of the implant period.

### **3.4 DISCUSSION**

The primary goal of this work was to assess the ability to record extracellular action potentials from populations of motor axons in the ventral roots using penetrating microelectrode arrays implanted chronically in lumbar spinal roots of adult cats. We developed a set of criteria to identify

motor axons and validate the placement and potential usefulness of the recorded signals. These criteria formed an algorithm that identified those units representing volitional control and eliminated the passive sensory afferents. Finally, an evaluation of the physical location of the electrodes was performed to examine and validate the locations of electrodes with motor activity.

The motor axon identification algorithm eliminated 39% of the recorded units based upon their activity under anesthesia and another 19% based upon their firing rate properties. It is important to note that while anesthetized activity is the most direct form of evidence that a unit is sensory, it is not sufficient to eliminate all sensory afferents from the dataset. It's possible some afferents with limited receptive fields or sufficiently high thresholds were not activated by the perturbations. The additional checks for motor-like firing rates (condition 2) and consistency across multiple units on the same electrode (condition 1) were designed to eliminate these afferents.

A limitation to this approach is that the firing rate distribution heuristics required by condition 2 are not necessarily unique to motor efferents. It is very possible for a sensory afferent to have a firing rate distribution that conforms to the requirements. If that unit was not eliminated by condition 1 with activity under anesthesia, then it would falsely be classified as a motor efferent. We estimated an upper bound on the number of false-positive identifications by artificially removing all anesthetized activity and only using firing rate heuristics; this resulted in an additional 52 (18%) motor identifications.

While this work is focused on recordings from the ventral roots and thus discards sensory afferents, a functional neuroprosthetic interface could make great use of both signals. State estimation alone—with no volitional input—is sufficient to establish rudimentary walking behaviors, but it requires an intact limb (Wagenaar 2011; Bauman et al. 2011). In the case of

amputation, only incomplete sensory information is available, but those electrodes that recorded sensory afferents may still be exploited with electrical stimulation to provide feedback to the patient (Fisher et al. 2014).

A necessary condition for the successful recording of units from the ventral roots was, of course, a successful placement of the electrode tips. The target location, however, was small and obscured by the larger dorsal root ganglion immediately adjacent. Accurate placement of electrodes in the ventral root was challenging to achieve, even with carefully chosen electrode shank lengths the guided placement through intraoperative recordings. While the intraoperative procedure helped identify the boundary of the dorsal root ganglion, it did not inform the mediolateral position of the ventral root. Poor targeting is hypothesized to be one of the major factors responsible for the poor yield, with 7 of the 35 implanted arrays never recording a single motor unit. As expected, however, the well-targeted electrodes that did record identified motor activity were found to be clustered together. On those arrays that recorded at least one identified motor unit, however, an average of 14 other units were also recorded. In addition, electrodes recording identified motor units tended to be clustered together; those that recorded motor activity were statistically more likely to be neighbors of other electrodes that also recorded motor activity than those that did not.

The clustering behaviors observed here are highly suggestive that the major limiting factor was indeed the placement of the array. Improvements in array targeting—perhaps with either intraoperative ultrasound imaging or pre-operative mapping—have great promise to increase the yield of recordings in the ventral root with more accurate electrode placement. Further improvements to array geometries—like multisite electrodes with multiple recording sites on each shank—may also help reduce the importance of precise positioning by oversampling the region.

### 3.5 CONCLUSION

A functional neuroprosthetic interface in the ventral roots aims to record from motor axons to extract volitional control, but the close proximity to the dorsal root and ganglion likely results in a mixture of both efferents and afferents. While limb state information from afferents would likely beneficially augment efferent data in the controller, patients living with amputation will only have a limited subset of the sensory information that an intact subject would, only arising from the residual proximal structures. Even if these limited efferent data are included as inputs, it still may be beneficial to explicitly differentiate between the two modalities in the controller. This chapter demonstrates our ability to not only record from the spinal roots, but also to identify and classify each unit as either sensory or motor, specifically demonstrating recording from clusters of motor axons in the ventral roots. Further improvements in array geometries and targeting hold promise to further increase the ability to specifically record from large numbers of ventral root axons.

## **4.0 MOTOR UNIT POPULATION RECORDINGS FOR NEUROPROSTHETIC CONTROL OF LOCOMOTION**

### **4.1 INTRODUCTION**

Prosthetic devices for patients living with loss of limb require input from the patient for their use and control. Even passive devices implicitly use the posture and behavior of the residual limb for their response and positioning. Recent improvements in powered prostheses have dramatically improved on their anthropomorphism, and in doing so, have similarly increased the number of controllable degrees of freedom. While these new devices could theoretically be extremely beneficial in helping patients complete activities of daily living, developing accurate and biomimetic control strategies and inputs for such devices has remained a challenge.

With the developed methods from Chapters 2 and 3, we are now in a position to examine the use of those neural signals for neuroprosthetic control for locomotion. The ventral root's proximal location stands in contrast to some existing approaches like myoelectric devices that are farther distal into the periphery and capitalize on the residual muscle structures to operate the prosthesis. Patients with more proximal amputations, however, are much more limited in the number of muscles available to provide control sources as compared to those with more distal

transections. By placing a neural interface at the ventral roots, we are able to take advantage of existing spinal circuitry that maps control signals to individual muscles, even if those muscles have been amputated.

This study works towards this goal by demonstrating that the ventral root may be specifically targeted by multielectrode arrays to record from individually identified motor efferents. A rudimentary target identification is performed to find the muscle innervated by each motor efferent, and the EMG activity during locomotion is estimated. Further, we use the ventral root activity to classify the gait phase with an accuracy comparable to an EMG classifier in four of the nine subjects.

## **4.2 METHODS**

All procedures were approved by the University of Pittsburgh Institutional Animal Care and Use Committee and the US Army Medical Department Animal Care and Use Review Office. Surgeries to implant two or three 32-channel micro-electrode arrays in fifteen adult male cats (FMAs, Microprobes, Inc.) were performed as described in Chapter 3. Nine subjects were selected for inclusion in this work. Two subjects were excluded due to aphysiological gait. Three subjects were excluded due to corrupted kinematic recordings. One subject was excluded due to a total lack of identified ventral root units.

### 4.2.1 Experimental protocol

After the implant surgery, awake recording sessions were performed on each subject at least three times a week, with an anesthetized recording session under dexmedetomidine sedation once per week. The signals from the ventral roots (FMA electrodes) and muscles (EMG electrodes) were simultaneously recorded with a high channel count data acquisition system (Omniplex D, Plexon Inc., Dallas Texas) at 40kHz and 20kHz, respectively. The ventral root recordings were band-pass filtered (300-3000 Hz). Action potentials (spikes) were detected by threshold crossings, using a threshold level set to three standard deviations of the neural signals on each channel measured during a 10 second period with the animal at rest. The threshold spikes were manually sorted to identify well-isolated units using OfflineSorter (Plexon Inc.).

During the awake sessions, the animals walked freely on a treadmill (Bertec) at belt speeds ranging from 0.4 m/s to 1.2 m/s. Kinematics of the joint positions, (hip, knee, ankle, and metatarsophalangeal (MTP)), were recorded with either OptiTrak (NaturalPoint, Inc., Corvallis, OR) or Cineplex (Plexon, Inc.) motion capture systems at 80 or 70 Hz, respectively.

While the ventral and dorsal spinal roots are separated into distinct compartments of the spinal nerve, targeting the ventral root compartment is challenging, particularly given its small diameter (~1 mm). The shortest and thus shallowest electrodes were often located in the dorsal roots, requiring further testing to identify neural signals as motor or sensory. Once per week, subjects were anesthetized with dexmedetomidine (0.04mg/kg) and neural recordings were made during passive leg movements and manual palpation. The anesthesia suppresses motor activity (Farber, Poterack, and Schmeling 1997), while preserving sensory responses from muscle and

cutaneous afferent neurons. The anesthetized sessions consisted of four 30 second recordings, one without any perturbations, and three with perturbations: repeated whole-leg flexion and extension, sequential isolated joint movements, and cutaneous palpations.

These anesthetized recordings were used in conjunction with the ventral root identification algorithm developed in Chapter 3 in order to limit the analyses to only ventral root axons.

#### **4.2.2 Estimation of muscle activity and kinematic state**

Firing rates from ensembles of simultaneously recorded motor units were used to estimate both muscle activity and gait phase during 100 seconds of locomotion for each subject. Smoothed firing rates were computed by convolving the spike times with a 100ms one-sided causal triangular kernel. The EMG signals were bandpass filtered (fourth order Butterworth filter from 80-500Hz), normalized with a z-score transformation, rectified, and low pass filtered (fourth order Butterworth filter at 10Hz) to form envelopes. Correlation coefficients were computed between each smoothed firing rate and the EMG envelopes. Rudimentary target muscle assignments were computed for each unit based upon the EMG envelope that had the greatest correlation with its smoothed firing rate. Units without any correlating envelopes ( $r > 0.2$ ) were not assigned to any target muscle.

Multivariate linear regression models were used to estimate EMG envelopes from only the firing rates of motor neurons assigned to each muscle. Regression coefficients were found using a least-squares fit of 50 seconds of walking data, with the remainder of the data held out for 2-fold cross validation. Model accuracy was measured with cross-sectional mean absolute scaled error

(MASE), a unitless metric that allows for robust comparisons between muscles and across subjects (Hyndman and Koehler 2006). The mean absolute error of the estimated EMG in the test set is scaled by the mean absolute error of the mean of the training set:

$$MASE = \frac{\text{mean}(|y_{test} - \hat{y}_{test}|)}{\text{mean}(|y_{train} - \bar{y}_{train}|)}$$

This procedure was repeated 100 times with randomly selected training and testing segments in order to compute the mean and standard deviation in decoder performance.

The relative position and motion of the hip and MTP markers were used to divide the step cycle into four phases of the gait cycle. The stance phase was identified by regions of near zero vertical velocity of the MTP marker while the leg was moving backwards, indicating that the foot was planted on the floor. The stance phase was further divided into two regions based upon the relative horizontal position of the MTP with respect to the hip marker; Stance 1 when MTP leads the hip and Stance 2 when MTP trails the hip. The swing phase was the remaining time of the cycle, and similarly divided into two subsections: Swing 1 when MTP trails the hip and Swing 2 when MTP leads the hip (Figure 15).

Both the EMG envelopes and smoothed firing rates were used to train two separate multinomial logistic regression models to estimate the gait phase. Just like the EMG envelope estimation, 50 seconds of locomotion was used to train the models, and they were tested against separate 50 seconds from the same session, repeated 100 times. The performance of the logistic models was evaluated by their overall classification accuracy on the test set.

**Table 2.** Summary of subjects included in this study. For each subject an exemplar day was chosen within three weeks of the implant surgery such that the subject exhibited good walking behavior and sufficiently high-quality recordings across all physiological and kinematic signals. This table summarizes key metrics on that exemplar day, including how long post-implant the trial was conducted, the number of arrays and EMGs implanted, the total number of units recorded, and the range of walking speeds exhibited during the trial. Of particular note are the number of units identified as ventral root activity and the total number of EMGs identified as being targeted by at least one or two of those VR units.

Id	Days post implant	Number of FMA arrays implanted	Number of VR units recorded	Number of total units recorded	Number of EMG electrodes implanted	Number of EMGs targeted by 1+ VR units	Number of EMGs targeted by 2+ VR units	Walking speeds during trial (m/s)
V	20	2	32	51	8	7	4	0.4 - 0.8
U	6	2	11	17	7	2	2	0.6
T	8	2	15	24	9	6	5	0.4 - 0.8
S	8	2	8	31	9	2	2	0.4 - 1.0
R	7	2	7	57	9	2	1	0.4 - 0.8
M	12	3	20	55	10	7	4	0.6 - 1.0
L	13	3	18	31	9	6	4	0.4 - 1.0
J	6	3	11	27	10	4	1	0.4 - 0.6
I	9	3	2	4	7	2	0	0.2 - 0.6

## 4.3 RESULTS

### 4.3.1 Muscle target identification and estimation

Target muscles were identified for 106 of the 128 ventral root units, with an average of 4.2 muscles innervated per subject. Of the 78 muscles included in this study, 38 were identified as targets of at least one unit. 23 muscles had more than one unit identified and 13 had more than two. The EMGs were divided into three functional groups based upon their activity during walking; one group represented extensor muscles active during the stance phase (typically including LG and MG, BF and VL, and GM), another the retractors active during swing onset (typically ST and SM), and a third group for flexors active immediately preceding stance onset (often TA and sartorius) (Yakovenko et al. 2002). The stance phase muscles were most commonly identified as targets of the VR units, but this was largely due to the fact that more stance phase muscles were instrumented. Across all three functional groups, approximately half of the muscles were represented by VR units (49%, 39%, and 56%, respectively). All three functional groups were represented in four of the subjects, and all but the two subjects with the fewest units (I and R) had both swing and stance phase groups represented.

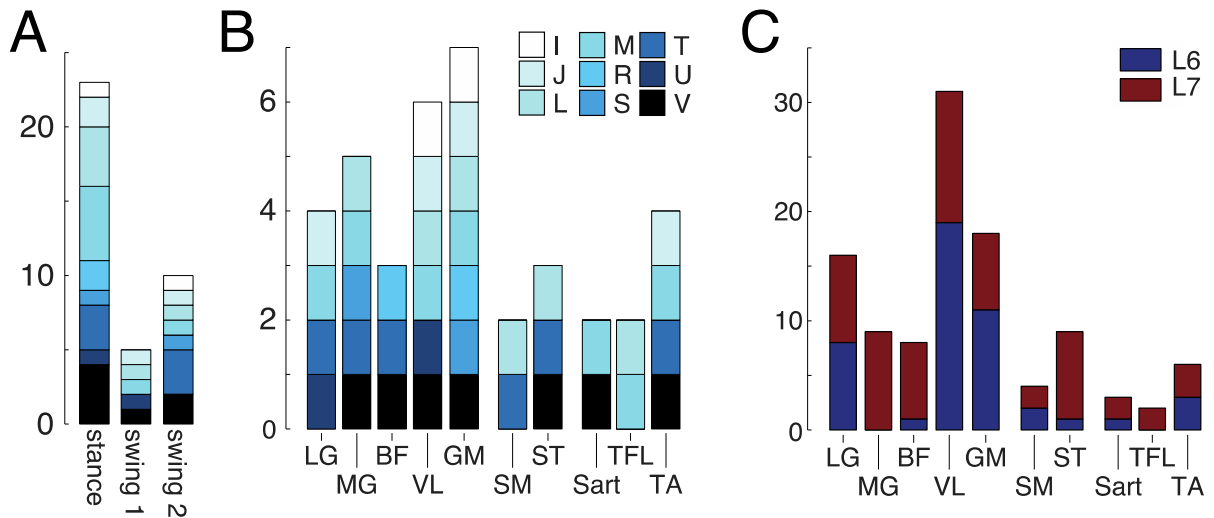


**Figure 13.** Summary of identified target muscles. A) Number of identified target muscles, arranged by functional group, with each bar divided into colors by subject. In general, more stance phase muscles were instrumented in each subject, leading to a bias in the number of units found to be innervating them. B) Number of identified target muscles arranged by specific EMG electrode location. C) Spinal root locations of units that innervated each muscle. The histogram is colored by the spinal root location of the electrode that recorded each unit.

The ability of the spiking activity to estimate the smoothed and rectified EMG envelope was significantly dependent upon the number of motor units available for estimating the EMG (Figure 14). Scaled error values near or greater than one represented models that failed to describe the behavior in a meaningful way. All models with at least two units performed better than chance (defined as the constant-choice model for the most common state) with mean average squared error lower than 0.9. Qualitatively, errors lower than 0.7 estimated the EMG envelopes fairly well. In 11 instances across four subjects, the EMGs were predicted with errors lower than 0.7. While including more units increased overall accuracy, there were cases where just one or two units were sufficient to provide very good estimations of the EMG envelope.

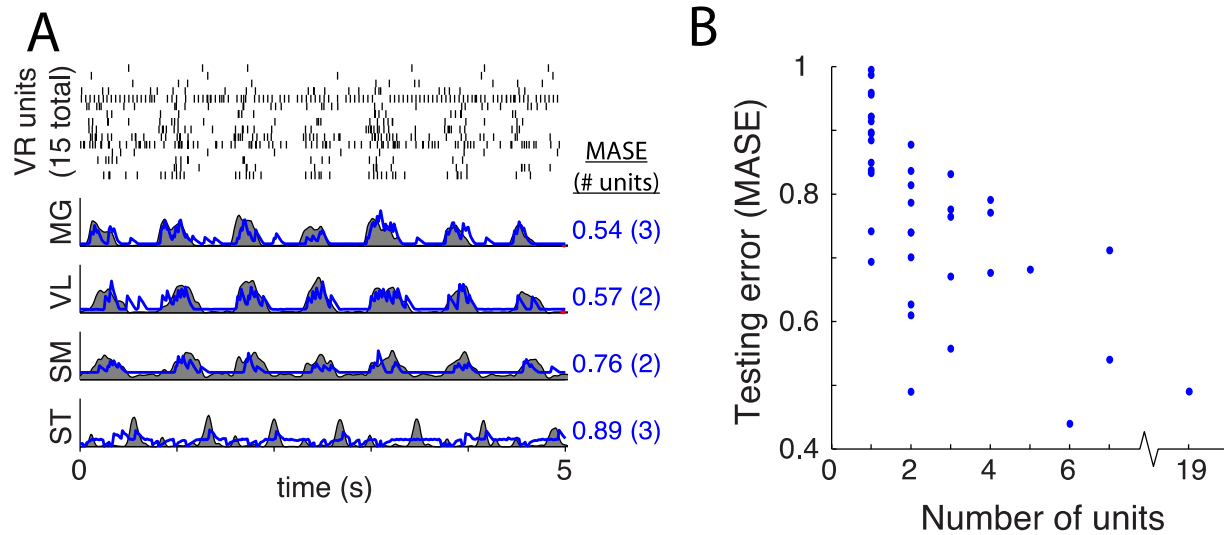


**Figure 14.** Accuracy of EMG estimations, example and summary. A) Example spike raster and four representative EMG envelopes for subject L. Each row of the spike raster is an isolated VR unit. In solid gray is the actual EMG activity during the testing period, with the estimated activation from the neural models in blue. The majority of the units modulated with the gait phase, and most were active during stance. As such, the models performed better on extensor muscles that were active during stance. Each muscle is annotated by its mean absolute scaled error (MASE; lower is better) and the number of units in the model. The selected EMGs include both the most (VL) and the least (ST) accurate models. B) Summary of average scaled model errors across all muscles and subjects, arranged by the number of units in the model. A value near one signifies that the model performed no better than a constant output based on the mean of the training set.

### 4.3.2 Kinematic estimation

The kinematic state of each subject's step cycle was determined by the movements and relative positions of the kinematic markers. Both the EMG envelopes and all units were used as inputs to multinomial logistic models to estimate the state. Across all subjects and input sources, the models were able to estimate the kinematic state with significantly better accuracy than constant output could achieve ( $p < 0.01$ , two-sided t-test with Dunn-Šidák correction). In general, the muscle activity was a better predictor of the kinematic state than the ventral root activity, and significantly so in 4 of the subjects ( $p < 0.01$ ).

While the simple classifier had no inherent knowledge of the state transitions, almost all of the state transitions were between consecutive states in the step cycle in both the EMG and VR models. Across all subjects, 91% of the estimated state transitions were between consecutive states in the step cycle with EMGs as the predictor, and 86% with the VR models. Both sets of models displayed some noisiness at the state transition, oscillating between two states around the actual transition time, with an average of 1.7 and 2.5 estimated changes per actual change for the EMG and VR models, respectively. In general, the VR models were more variable at the state transitions than the EMG models, but this difference is largely an artifact of the simple one-sided causal kernel used for convolving the firing rates. Filtering the firing rates with a similar cutoff as the EMG data eliminates this difference in state transition jitteriness and has no significant impact on the actual prediction accuracy.

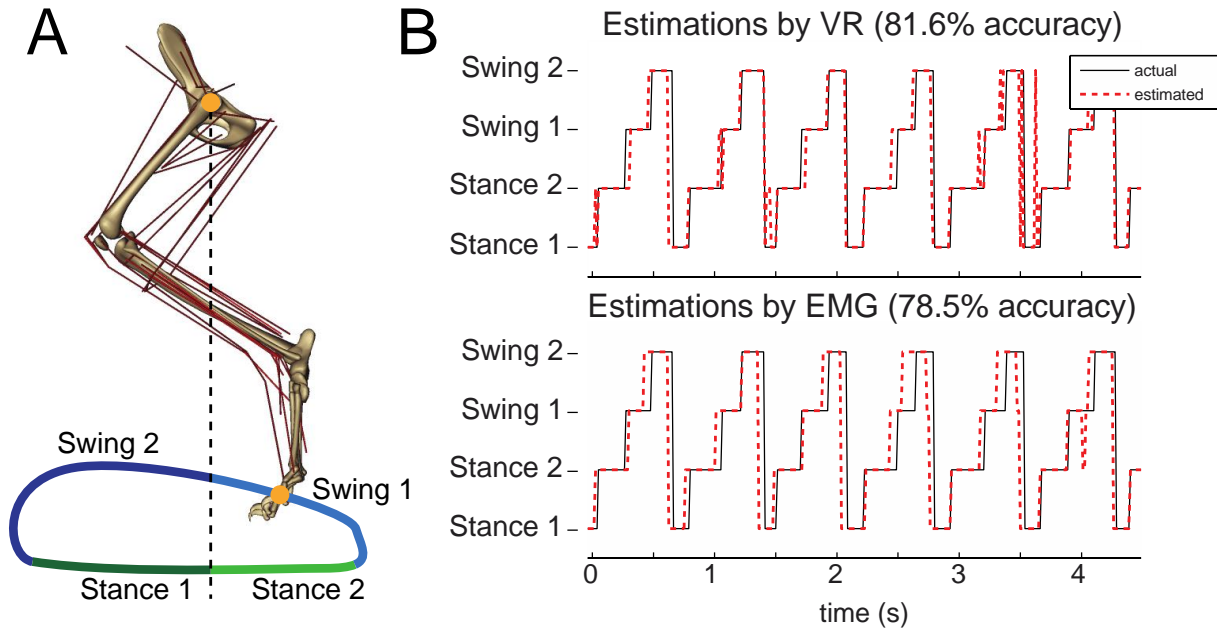


**Figure 15.** Example decoding of kinematic state. A) The step cycle was divided into four states, based upon the kinematic positions of the MTP and hip markers. B) A short snippet from the test set estimations for subject M. The solid black line represents the actual step state, with the estimations in dashed red. Both VR and EMG sources do quite well, with the VR data demonstrating a tendency to oscillate around the state transitions.

In both sets of models, the estimated timing of stance onset slightly led the actual event as marked by the kinematic step cycle detection algorithm. Due to the aforementioned jittery transitions, the timing of the estimated state transition was defined by the midpoint between the first transition and the last transition. On average, both VR and EMG models accurately detected stance onset, with a median time offset of 0 milliseconds. The VR models had slightly more variance, with interquartile ranges spanning from -28 to 42ms about the actual stance onset, whereas the EMG interquartile ranges were symmetrical about 14ms.

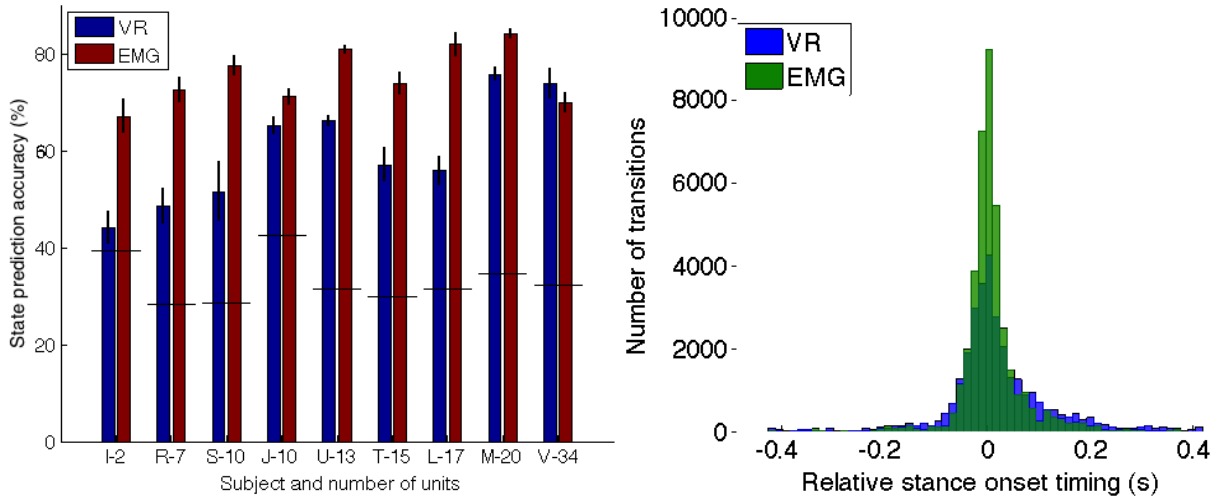


**Figure 16.** State prediction accuracy and relative timing of the estimated stance onset. A) The accuracy of the state prediction models across all subjects, arranged by the number of ventral root units. The horizontal line marks the chance level for each subject. B) A histogram of the relative stance onset timing for both classifiers. In general, both classifiers estimated the stance onset very close to the actual event, with the EMG classifiers performing slightly more precisely.

#### 4.4 DISCUSSION

This study demonstrates using populations of single unit activity of motor nerves in the ventral roots of walking cats to estimate muscle activity and kinematics. Single unit firing rates covaried with the EMG activity of target muscles and allowed for direct estimation of EMG signals during treadmill walking across gait speeds ranging from 0.4-1.0 m/s. Furthermore, pattern classification of the motor unit population activity demonstrated accurate discrimination of four phases of the step cycle, comparable to gait phase classification using EMG from the whole leg. Collectively, these results demonstrate that motor unit recordings in ventral roots could be used to provide direct

neural control of a lower limb prosthesis. The results from this study offer new opportunities for control; the ability to estimate EMG speaks to the generalizability of such an approach, whereas the gait phase estimation is a more immediate solution to state estimation difficulties in traditional powered prostheses. However, technical challenges associated with targeting and establishing a reliable interface with ventral root nerves remain major limiting factors.

A major difficulty in this study was obtaining sufficient yield for accurate control. The number of units had a very large effect on the accuracy of both the state-based and continuous decoders. The challenges in maintaining chronic recordings (Appendix A) limited the number of available recordings; each subject was limited to their best recording day to ensure a homogenous analysis across subjects.

A further limitation was in the motor unit identification process. This algorithm is designed with the goal of removing all signals that do not conform to a typical motor unit, using both interspike interval distributions and anesthetized activity to accomplish this goal. It is perhaps too conservative, and it's not unlikely that some motor units are erroneously excluded from analysis. Motor reflexes or spurious activity may occur even under sedation, or a noisy or multi-unit recording may obscure the true firing rate such that they get excluded. Conversely, some sensory afferents may have had limited receptive fields or sufficiently high thresholds such that they were not activated under anesthesia and also happen to have a firing rate distribution that is similar to a motor unit; these afferents would wrongly be included. We estimated an upper bound on the number of false-positive identifications by examine the firing rates of the units that were eliminated by anesthetized activity. Approximately 18% of those units eliminated had motor-like firing rates and therefore would have been identified as ventral root efferents if they had not been activated during the anesthetized session. Indeed, some of those may indeed be motor units that

were not completely suppressed by the anesthetic. Therefore, it's possible that some high-threshold sensory afferents were included in this analysis, but they would have been a small fraction of the total number of units.

Estimations of the EMG envelopes were limited by two sampling effects: not all hindlimb muscles were instrumented and each neuron only represents a small window into a muscle's recruitment. If, for example, we recorded from a motor unit that innervated a non-instrumented muscle, that unit may get miss-identified as innervating a correlated muscle, negatively impacting the generalizability of the model. Similarly, if we only happened to record from high-threshold motor units, the linear models would effectively be blind to lower force output. Finally, the very rudimentary targeting algorithm that may have misidentified co-contractors with correlated muscles. Therefore, while the estimations of EMG demonstrate feasibility in replacing recordings from transected muscles, they do not paint a complete picture.

The kinematic classifications were hampered by the kinematic definition of the gait cycle. Instead of using a more physiological definition with the loading of the knee, we were limited by the optical markers and tracking such that the gait phase transitions were imprecise and somewhat arbitrary. While stance and swing are very relevant and well-defined, the separation of each of those states into two parts was simply defined by the relative location of the MTP. A more rigorous definition to include loading at the knee would perhaps improve performance across the board. Indeed, simply limiting the classifier to the stance and swing states recovers up to 49% of the errors committed (mean 22% across all subjects). Oscillations about the state transitions also negatively impacted performance, but these could be easily remedied with a more advanced controller that enforced state transitions akin to existing work on lower limb prostheses (Varol, Sup, and Goldfarb 2010).

Other groups have previously demonstrated improvements in context awareness and state switching by augmenting powered lower limb prostheses with residual neural control. For example, Hargrove et al. demonstrated that they could completely eliminate critical state decoding errors (those that may lead to a fall) from their lower limb prosthesis by augmenting its sensors with surface EMG from a combination of residual proximal muscles and targeted muscle reinnervation from nerve transfers (Hargrove et al. 2013). The additional bandwidth provided by the reinnervated muscles was essential to achieve this excellent performance; the residual proximal muscles alone were not sufficient. This study presents a potential alternative to targeted muscle reinnervation, demonstrating the ability to decode both muscle activity and kinematic state from recordings in the ventral root. This could be critically important for patients with more proximal transections that do not afford space for nerve transfers. Additionally, there is promise for a minimally invasive surgical technique to provide access to the spinal roots that would dramatically reduce complications and surgical trauma as compare to denervation and nerve transfers. Closing the loop in a real-time control system would allow for compensation by the subject to improve performance (Chase, Schwartz, and Kass 2009). Indeed, subjects have demonstrated control of single motor unit efferents under closed-loop control (Kudina and Andreeva 2010).

## **4.5 CONCLUSION**

This study demonstrates the ability to use population recordings from the ventral roots for neuroprosthetic control. This open-loop estimation and classification of muscle activity and gait

phase in an intact animal promisingly demonstrate that recordings from the ventral roots are feasible and sufficient for neural control of a lower limb. Implementations in a closed loop system have promise to do even better.

Much remains, however, in order for neural implants in the ventral roots to become a viable clinical procedure. Yield is critically important for high bandwidth control, and yet targeting of this structure is a major challenge. We attempted to mitigate that with both intraoperative targeting and post-operative analysis techniques, but yield remained a challenge throughout. Even more crucially, chronic reliability was a challenge, as reported in Appendix A (Debnath et al. 2014). Further development is necessary for a neural interface at the ventral roots to become a reality, but this study presents evidence that such a device would have sufficient information to control a device for locomotion, and with a sufficient number of neurons its accuracy rivals the estimations from more distal recording sites—sites that may not be available to a patient with a proximal transection of the limb.

## **5.0 THE BEHAVIOR OF MOTOR UNITS AND FUTURE EXPERIMENTS**

### **5.1 INTRODUCTION**

In the course of developing the ventral root neuroprosthetic interface, we have collected a large corpus of unitary recordings from the spinal roots alongside muscle and kinematic recordings during both volitional and passive, anesthetized movements. Beyond simply validating the promise of a prosthetic interface, these recordings contain a wide range of motor unit behaviors and their associated actions. A closer look at these behaviors allows us to validate and further refine previous assumptions about the peripheral nervous system and look into possible future experiments, their challenges and possible results.

Recordings from the spinal roots have a distinct advantage in their interpretability over other locations simply by virtue of the anatomical location. At this point in the peripheral nervous system, each action potential represents a single action. The identification of these individuated actions and responses enables a more complete examination of how individual motor units participate in the peripheral nervous system as a whole.

Historically, spike-triggered or stimulus-triggered averaging has been used to identify the termination or effective action of a neuron as a form of reverse correlation. This process reveals target signals or actions that have temporally-linked activity at short time-scales with the neuron. With a chronically implanted array in the spinal roots, action potentials from motor units may be

used to trigger averages of muscle activity during volitional control, theoretically revealing the muscles that contain the units' innervated fibers as well as their conduction velocities. As compared to the lower latency correlations between smoothed firing rate and low-frequency smoothed EMG envelope as used in Chapter 4 for linear decoding, STA has been used to identify muscles directly innervated by motor units (Hoffer, Loeb, Marks, et al. 1987; McKiernan et al. 1998). A more conclusive identification of motor units' targets could help validate and verify the discrimination between motor and sensory units (Chapter 3), and it could further inform decoding strategies (Chapter 4).

In Hoffer and Loeb's previous work, they used STA to identify target muscles in the anterior thigh for 43 motor units out of 164 recorded axons in the L5 ventral root (Hoffer, Loeb, Marks, et al. 1987). This was achieved through a visual comparison of the recorded averages, looking for large deviations in the averaged EMG signal with a shape and latency consistent with a motor potential. Another 8 units were ambiguous, with multiple such responses across several muscles. This was attributed to a general spread in the volume conduction of the potential along with an incomplete common-mode rejection from the bipolar electrodes. With all instrumented muscles in the anterior thigh, the EMG electrodes were very close to one another and the muscles had similar behaviors.

The large corpus of simultaneous motor unit and muscle recordings examined in Chapters 3 and 4 provide improves our ability to examine the underlying physiology. The more diverse set of muscles instrumented in these subjects were farther apart and located throughout the hindlimb. Not only did this reduce the potential for common-mode inputs across electrodes, but it also

ensured the behaviors of the muscles were more varied. While locomotion is highly stereotyped task, examining both flexors and extensors reduces task-based correlations between some pairs of muscles

At the same time, scaling this analysis to investigate so many possible unit-muscle pairs requires very carefully constructed confidence intervals in order to ensure meaningful and accurate results. The highly correlated nature of locomotion and phasic activity of the motor units means that a high threshold unit will have large variances in its spike-triggered averages simply due to the many other nearby coactivated muscle fibers innervated by other units.

## 5.2 METHODS

This chapter provides a further examination into the recorded data from the subjects and experiments described in Chapters **Error! Reference source not found.** and 3. As noted in those chapters, all procedures were approved by the University of Pittsburgh Institutional Animal Care and Use Committee and the US Army Medical Department Animal Care and Use Review Office.

### 5.2.1 Identifying innervated muscles by spike-triggered averages

Whereas the analysis technique in Chapter 4 identified the muscles a given ventral root unit activated based upon correlative co-activations against low-pass filtered and rectified EMG envelopes, it is possible to further refine this identification with spike triggered averages over shorter timescales using higher frequency components of the EMG signals. This takes advantage of the fact that every recorded action potential from the ventral root propagates through the

peripheral nerve and results in a motor-evoked potential (MEP) in the tens to hundreds of fibers that it innervates, which may be recorded by an EMG electrode. By averaging many repeated activations, uncorrelated activity goes to zero while time-locked MEPs remain.

Just as in Chapter 4, the signals from the ventral roots (FMA electrodes) and muscles (EMG electrodes) were simultaneously recorded with a high channel count data acquisition system (Omniplex D, Plexon Inc., Dallas Texas) at 40kHz and 20kHz, respectively. The ventral root recordings were band-pass filtered (300-3000 Hz). Action potentials (spikes) were detected by threshold crossings, using a threshold level set to three standard deviations of the neural signals on each channel measured during a 10 second period with the animal at rest. The threshold spikes were manually sorted to identify well-isolated units using OfflineSorter (Plexon Inc.). The subjects walked freely on a treadmill (Bertec) at belt speeds ranging from 0.4 m/s to 1.2 m/s.

As kinematic data were not required for these analyses, the exclusionary criteria in Chapter 4 were widened to include all sorted units from all 15 subjects with at least 300 spikes from any awake walking trial. For every sorted neuron with over 300 recorded spikes, a spike-triggered average (STA) response was computed by averaging the spike-aligned EMG signal within a symmetric 24ms window. The net response for a given neuron-muscle pair was defined as difference between the root mean square (RMS) power within two 10 ms windows symmetric about the spike. The power preceding the spike within a window from 2 ms to 12 ms prior is used as a baseline and subtracted from the power in the symmetric window 2 ms to 12 ms following the spike. These windows were chosen assuming conduction velocities of  $\alpha$ -motor neurons between 50-100 m/s to destinations between 5-40 cm away and allowing for an EMG response duration of

2-4 ms (Cullheim 1978; Westbury 1982). In order to prevent a single noise burst from dominating the response, windows with the largest RMS values (top 5%) were dropped prior to averaging and computing the net response (Figure 17).

Similarly, a distribution of null responses was computed to characterize the muscle's response to random input (simulated spikes) and establish a threshold for significance. For a given neuron-muscle pair, each spike was replaced by a simulated spike, with its spike time drawn from a uniform 100ms window centered about the actual spike. The above algorithm computed the muscle's null response to these randomly simulated spikes. This process was repeated with different randomly simulated spikes for a total of 2000 times to build a distribution of null responses for that neuron-muscle pair (Figure 18).

This randomization scheme was carefully crafted to eliminate short-latency causal links (if any) exhibited in the real response while at the same time ensuring that the muscle activity remained within a time-period representative actual activity when the real neuron spiked. This is particularly important for phasically modulated neurons which match periods of higher or lower activity within a given muscle; in such cases a more naïve randomization scheme could significantly bias the variance in the distribution of null responses.

A neuron-muscle pair was determined to have a significant STA response (SSR) if its net RMS value exceeded the 99.9th percentile of the null distribution. By construction, therefore, we would expect that this method would lead to a 0.1% false-positive rate. This entire analysis was repeated with an initial set of completely random spikes uniformly distributed across a subset of the trials to validate that the number of false positives was within expected values.

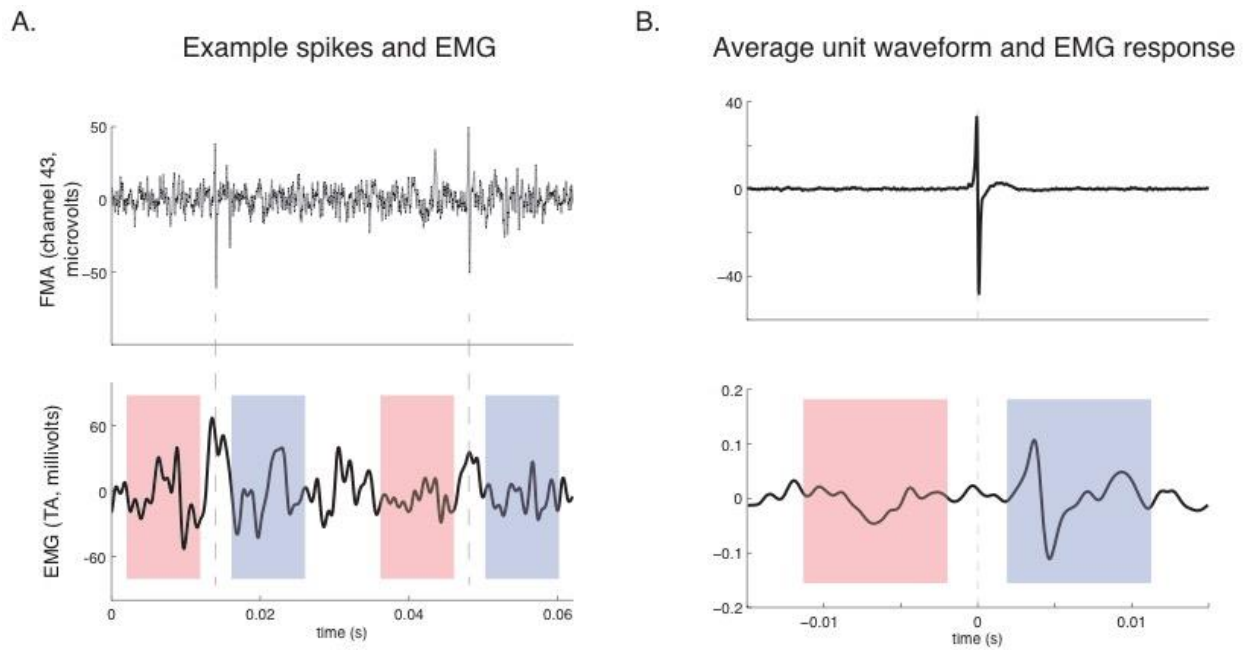


**Figure 17.** Example spike-triggered average of a spike and its response in EMG. A) Example continuous recordings from both an electrode on the FMA (top) and an EMG channel (TA, bottom). Two spikes are shown in this plot, marked by vertical dashed lines. The windows about each spike wherein the RMS power of the signal is evaluated is highlighted in blue and red, with the RMS power preceding the spike (in red) is subtracted from that following the spike (in blue). The 5% largest RMS values are discarded, with the remainder aligned and averaged. B) The average unit waveform and its EMG response. The STA response is defined as the RMS power in the red window subtracted from that in the blue window. In this case there was a significant response.

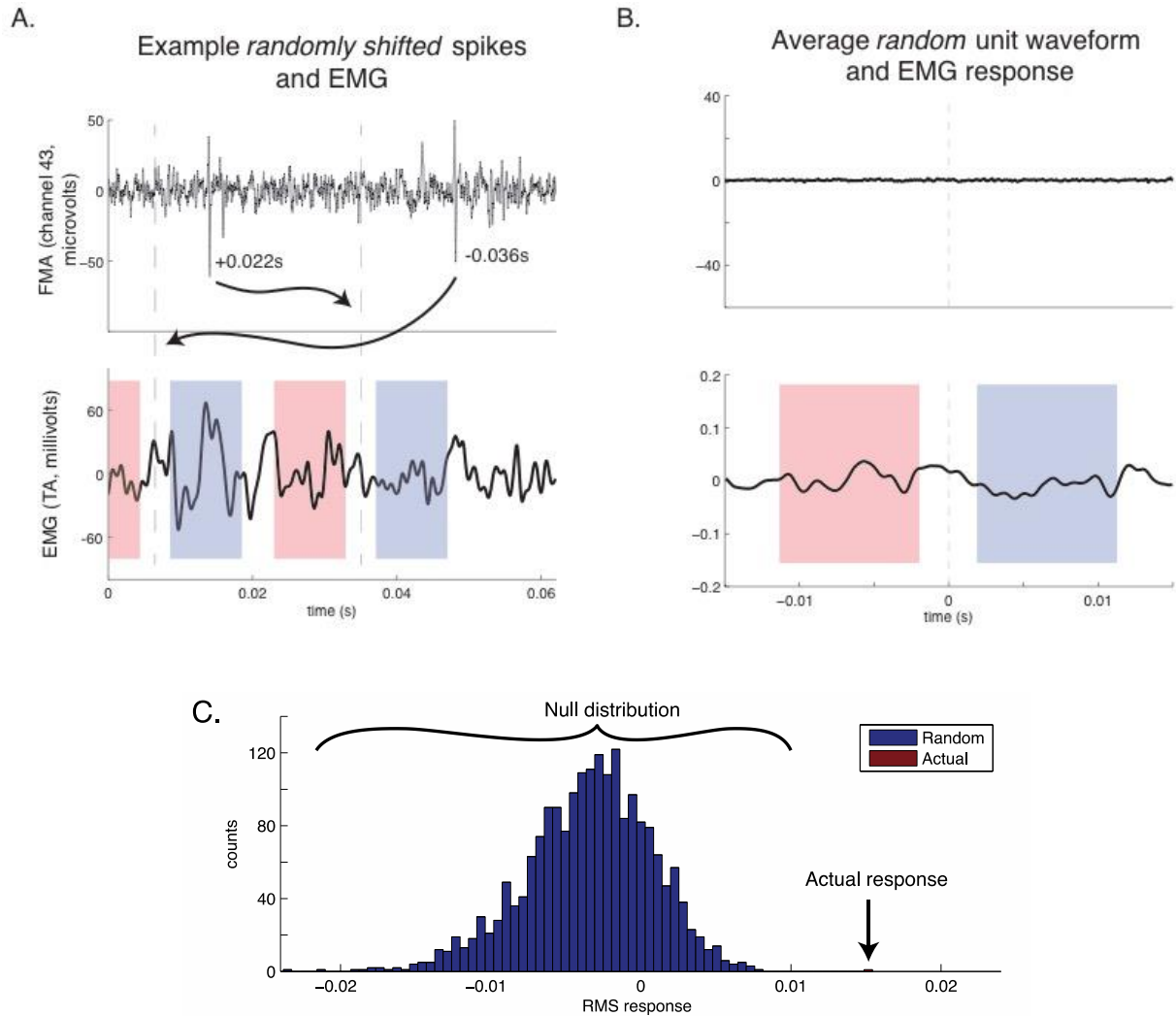


**Figure 18.** Example randomized spike-triggered average of a spike and its EMG response. **A)** Just as in Figure 17, example continuous recordings from the same the FMA electrode (top) and an EMG channel (TA, bottom) are shown, except the spike times used for all subsequent computations have been shifted by a random offset within  $\pm 50$  ms (uniformly distributed). **B)** These randomized spikes and their EMG responses are averaged, resulting in a null response. **C)** This is repeated 2000 times to form a null distribution and compared against the actual RMS response. In this case, the actual response well exceeded the 99.9th percentile of the null distribution, leading to a confirmed statistically significant response.

## 5.3 RESULTS

### 5.3.1 Detected muscle responses by spike-triggered averaging

Significant EMG STA responses were detected in 264 of the 1817 units (14.5%) identified as ventral root axons in Chapter 3. A priori, we expected that this technique would only detect the evoked EMG responses that were a direct result of the recorded axon's action potential, with each axon innervating just one muscle. Unexpectedly, 111 axons had significant responses across multiple muscles, and 65 of those had more than two SSRs (example, Figure 19). Also surprising was that so many of the units that had been excluded from consideration as motor units in Chapter 3 were revealed to have a statistically significant response in at least one muscle within the 12ms window following the spike. Of the 2744 excluded units, 253 (9.2%) had SSRs in at least one muscle and 96 of those had significant responses in two or more muscles (Figure 20).

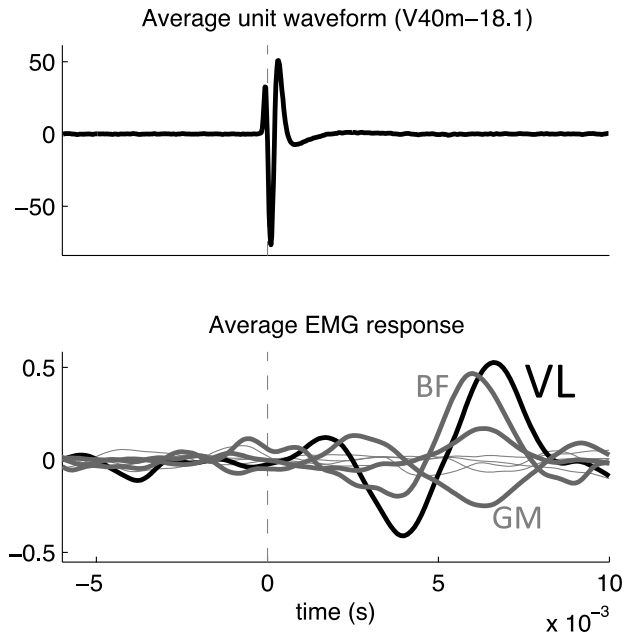


**Figure 19.** Example spike-triggered averages of unit with multiple significant EMG responses. The top panel shows the average unit waveform, with averages triggered on its threshold crossing, and the bottom panel shows the simultaneously triggered averages from all implanted EMG electrodes. Four averages were identified as significant: vastus lateralis (VL), biceps femoris (BF), gluteus maximus (GM), and sartorius.

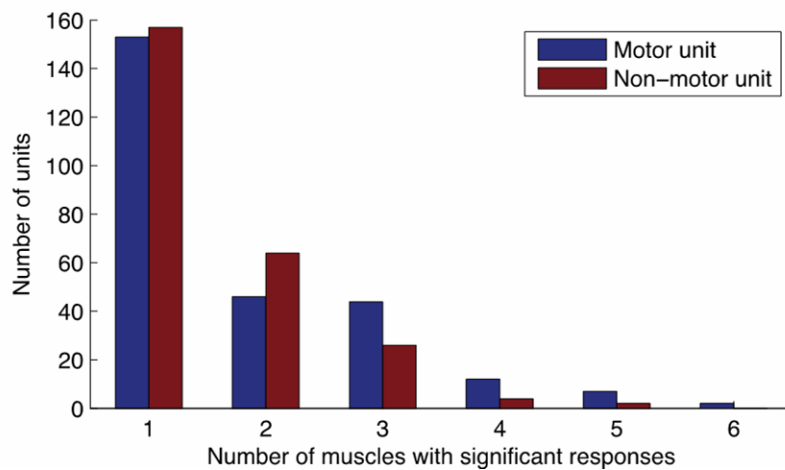


**Figure 20.** Number of units with statistically significant STA results. Both classifications from Chapter 3 had muscles identified with statistically significant post-spike facilitation, but such responses were relatively rarer among the non-VR units (9.2% of non-VR units had at least one muscle identified vs. 14.5% of VR-classified units).

Due to Hoffer and Loeb’s reasonable hypothesis that “ambiguous” STA results may be the result of volume conduction and poor isolation between two EMG electrodes, we undertook an analysis of the most frequent muscle pairs that co-occurred together as SSRs for a single axon. A total of 237 units had more than one statistically significant STA result, resulting in 536 pairs of muscles that co-occurred together. The most common 8 pairs of muscles and their frequency of occurrence is displayed in Figure 21. Note that two of the top eight pairs are actually separated by the knee. Indeed, overall, 232 out of the 536 total pairs (43.3%) are separated by the knee.

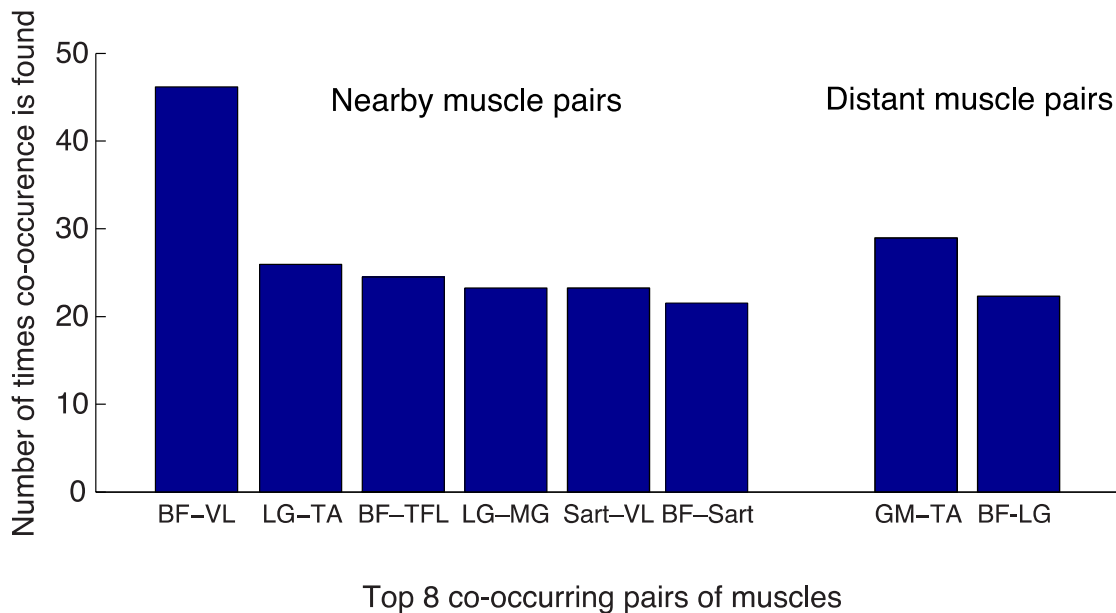


**Figure 21.** Most frequently co-occurring pairs of significant STA results. Note that both “nearby” muscle pairs (on the left) and distant muscle pairs (on the right) are represented. The distant muscle pairs are all separated by the knee.

## 5.4 DISCUSSION

The analyses here show a number of interesting and surprising results, most notably that there was such a high proportion of axons with simultaneous statistically significant spike-triggered averages across multiple muscles. The previous rationales do not adequately explain such a result; the distances between muscles with simultaneous responses are much greater than previously found, and there is no evidence of crosstalk at larger timescales. Further, Hoffer and Loeb's previous identifications were only established through qualitative metrics. Determining significance bounds, while challenging, allows a more careful analysis of a larger corpus.

We carefully constructed independent null distributions for each neuron-muscle pair to accurately reflect the behavior of the muscle around the time when the actual neuron is active. Since muscles are known to have phasic activation patterns with many correlating co-activations between muscles during locomotion, this aimed to preserve overall activity of the muscle for neurons with similarly phasic firing behaviors (Engberg and Lundberg 1969). Importantly, the simulated spikes were not chosen to be uniformly distributed across the entire duration of the trail. Instead, each actual spike time was replaced by a simulated time randomly drawn from a uniform distribution within a centered 100 ms window. The reasoning for this is perhaps most clear by considering the alternative for a neuron active during the stance phase of locomotion. If the random spikes for the null distribution were chosen uniformly over the entire trial, they would sample from periods of both activity and inactivity, thus the largest response in the null distribution would be smaller than expected for muscles contracting during the stance phase and larger than expected for swing phase muscles.

It's important to note an implicit assumption that is required to be true in order for STA to identify the target muscle of any given motor unit: no other unit may be synchronously and

consistently active within a short latency (likely less than 1ms). While seemingly unlikely, short-latency synchronization between both intra- and inter-muscular motor unit pairs have been observed in the human forearm (Huesler, Maier, and Hepp-Reymond 2000). Huesler and colleagues identified 14 out of 83 possible intra- and 24 out of 328 possible inter-muscular unit pairs with cross-correlograms that had significant synchronization peaks less than 2ms apart, although they included the caveat that their results were already demonstrating closer narrowing synchronization than had been previously reported.

It's also possible that what was thought to be a well-isolated neuron was actually multi-unit activity. In such a case, if both units participating in the multi-unit waveform have large and significant MEPs near or in an instrumented muscle, then it is highly likely that both muscles could persist through the null averages and yield a pair of significant results. Were this commonly occurring, however, I would expect to see a higher proportion of multiple SSRs within the discarded, non-VR units as the ISI criterion helped gate multiunit activity.

One of the most plausible explanations here is actually that common mode input to many motor units is dramatically increasing the variance in multiple muscles at once, without strong time-locked signals. While this wouldn't result in nice looking MEP action potentials in the averages, it can often be difficult for even a trained eye to discern the difference between noise and an action potential.

The spike-triggered average is a powerful technique, especially when coupled with carefully constructed confidence intervals that enable large-scale analysis of many units. Unfortunately, its limitations in conclusively identifying targeted actions remain a difficulty. Carefully constructed future experiments could work to detangle multiple significant responses. Identifying these neurons with multiple significant responses in distinct muscles online—in the

midst of conducting the experiment—would enable further validation via concrete unit identification. While challenging, dynamically altering the task to isolate just one of the two muscles could provide evidence that the multiple significant responses are possibly the result of multiple motor units.

## **6.0 SUMMARY OF RESULTS AND CONCLUSION**

### **6.1 SUMMARY OF RESULTS**

In addressing the first specific aim, Chapter 2 presented a thorough examination of the methods, techniques and tools that were required to make the subsequent chapters a reality. Perhaps the biggest success from this chapter was the development of the adapter board and one-connector interface. Not only did it simplify and facilitate the necessary connections for my thesis, but it was also valuable to other, parallel projects — including somatosensory stimulation through the dorsal root ganglia.

We developed an implant procedure and supporting hardware that enabled access to large populations of ventral root axons through a dorsal laminectomy, although targeting was and remained an ongoing challenge throughout the experiments. The blind approach and huge size imbalance between the dorsal and ventral structures led to a large over-sampling of sensory neurons. These sensory neurons posed a challenge in isolating only the motor units, and a large section in Chapter 3 was devoted to identifying and eliminating the confounding influence from sensory afferents. They were simply discarded for much of the remainder of this work. Chapter 3 and accompanying Appendix A also examined the ability to record high-SNR well-isolated ventral root units and reinforced the importance of a well-placed array.

Chapter 4 tackles the challenge of the second aim: decoding limb state and kinematics from the identified ventral root units. A simple linear decoder is up to the task, even with the limited yields from the ventral root. The open-loop nature of the preparation simplifies the experiment design but likely leaves accuracy on the table. Both muscle activations and kinematic states are identified and estimated with the ventral root activity. While the distal muscles were able to consistently perform well in estimating the kinematic state, the ventral roots required a relatively large sample size in order to challenge their performance. Even so, we were able to demonstrate a wide diversity in the targeted actions of the motor units and recorded activity. In that vein, Chapter 5 takes a speculative look at the difficulty in using spike-triggered averages to perform such an identification.

## 6.2 CONCLUSION

Patients living with loss of limb now have access to modern prosthetic devices with powered and individually articulated anthropomorphic joints and movements. These devices, however, require a rich and high bandwidth control interface in order to fully exercise the many independent degrees of freedom. In order to assess and validate the use of the ventral roots as a potential interface location, this work has developed and engineered methods, devices, and algorithms required to access, record, and identify motor efferents with a multielectrode array chronically implanted in the lumbar spinal roots through a dorsal laminectomy in an intact cat.

We demonstrated the ability to chronically record well-isolated signals from diverse populations of motor axons. We subsequently used these motor signals to estimate kinematics during locomotion, in some cases as accurately as estimations from simultaneously recorded

muscle activity in the intact limb, demonstrating that a ventral root prosthetic interface is possible for patients living with loss of limb. Finally, we take a brief examination into the difficulties and interesting questions posed by the challenge of achieving motor unit target information through spike-triggered averages.

Throughout this dissertation, I repeatedly stressed the unique anatomical location of the ventral roots and how the separation between the ventral and dorsal compartments enable distinct targeting of the two modalities. At the same time, we struggled in accurately targeting the ventral roots — so much so that we actually recorded and discarded more non-motor neurons than motor units. I believe the true power in this interface location lies in the joining together between somatosensory stimulation and ventral root recordings to construct a bidirectional interface. In such a scenario, you wouldn't design a device to just target the ventral roots or carelessly toss aside electrodes that landed outside the ventral root. With ongoing miniaturization and research into minimally invasive techniques, I believe the true success here will come from a single device that is able to interface with both aspects of the anatomy with a greater flexibility than was possible for my experiments.

## **APPENDIX A**

### **MICROELECTRODE ARRAY RECORDINGS FROM THE VENTRAL ROOTS IN CHRONICALLY IMPLANTED CATS**

This paper, as submitted to and published in *Frontiers in Neurology* (Debnath et al. 2014), examines the chronic recording quality over time as a function of the electrode properties.

The ventral spinal roots contain the axons of spinal motoneurons and provide the only location in the peripheral nervous system where recorded neural activity can be assured to be motor rather than sensory. This study demonstrates recordings of single unit activity from these ventral root axons using floating microelectrode arrays (FMAs). Ventral root recordings were characterized by examining single unit yield and signal-to-noise ratios (SNR) with 32-channel FMAs implanted chronically in the L6 and L7 spinal roots of 9 cats. Single unit recordings were performed for implant periods of up to 12 weeks. Motor units were identified based on active discharge during locomotion and inactivity under anesthesia. Motor unit yield and SNR were calculated for each electrode, and results were grouped by electrode site size, which were varied

systematically between 25-160  $\mu\text{m}$  to determine effects on signal quality. The unit yields and SNR did not differ significantly across this wide range of electrode sizes. Both SNR and yield decayed over time, but electrodes were able to record spikes with  $\text{SNR} > 2$  up to 12 weeks post-implant. These results demonstrate that it is feasible to record single unit activity from multiple isolated motor units with penetrating microelectrode arrays implanted chronically in the ventral spinal roots. This approach could be useful for creating a spinal nerve interface for advanced neural prostheses, and results of this study will be used to improve design of microelectrodes for chronic neural recording in the ventral spinal roots.

## **A.1 INTRODUCTION**

In 2005, nearly 2 million people in the United States were living with the loss of a limb, and it is projected that this number will double by 2050 (Ziegler-Graham et al. 2008) due to amputations following vascular disease, trauma, and cancer. In order to restore function to these individuals, neural interface technologies are being developed to enable intuitive control of robotic prostheses (Dhillon et al. 2004; Navarro et al. 2005; Schwartz et al. 2006; Hochberg et al. 2006; Kuiken et al. 2009; Schultz and Kuiken 2011; Collinger et al. 2013). These neural interfaces extract control signals from the nervous system by decoding motor intent from the signals recorded in the brain (Serruya et al. 2002; Schwartz et al. 2006; Hochberg et al. 2006; Schalk et al. 2008), peripheral nerves (Dhillon et al. 2004), or muscles (Englehart and Hudgins 2003; Kuiken et al. 2009).

The spinal nerves, and specifically the ventral roots, provide a potentially compelling target for a neural interface to extract motor control signals from the nervous system. Because of the unique organization of the spinal roots, a ventral root interface would have access to a large

numbers of motor nerve fibers, which are packed densely in the ventral roots and are physically isolated from sensory fibers located in the adjacent dorsal roots. Further, neural activity in the motor axons of the ventral root leads directly to muscle contraction and could therefore provide a source for motor control signals that are linked directly to normal musculoskeletal action, including force production and, ultimately, limb motion. Additionally, the vertebral bones surrounding the spinal nerves provide mechanical protection for the implanted electrodes and a degree of electrical isolation to reduce EMG interference. There are also well-established minimally invasive spine surgery procedures (American Association of Neurological Surgeons 2017) that could potentially be adapted for implantation of electrodes in the spinal roots.

In the 1980s, Hoffer, Loeb, and colleagues conducted a set of experiments, where they recorded simultaneously from up to 12 penetrating ‘hatpin’ microelectrodes implanted chronically in the L5 ventral roots of cats (Hoffer, Loeb, Marks, et al. 1987; Hoffer, Sugano, et al. 1987; Hoffer, Loeb, Sugano, et al. 1987; Loeb, Marks, and Hoffer 1987). These studies were performed to study motor unit recruitment physiology in locomoting cats and demonstrated initial feasibility for chronic ventral root recordings. While allowing the cats to move freely, individual units could be recorded for a whole day or longer, allowing recording to occur during a range of activities and over long periods of time. The studies found that the modulation of firing frequency closely resembled modulation in EMG amplitude recorded in individual leg muscles. Motor unit recordings were made in ventral root axons over several months, but the chronic stability of these recordings was never characterized.

The primary aim of this study was to characterize the motor unit recording performance of high-density microelectrode arrays implanted chronically in the ventral roots of awake behaving cats. Different electrode tip exposure lengths were tested with the hypothesis that larger electrode

tips would be more likely to record neural activity than smaller electrode tips. Signal-to-noise ratios, unit yield, and electrical impedance were measured for the duration of the implants. The primary outcome of this study was that high SNR motor unit signals were recorded in nearly all implants during treadmill locomotion, although there was significant variability between implants. Electrode tip exposure lengths (site sizes) had minimal impact on the ability to record single unit activity and electrode array positioning was the most important factor in achieving robust single unit neural recordings.

## **A.2 METHODS**

The objective of this study was to evaluate the neural recording capability of floating microelectrode arrays (FMAs) implanted chronically in the ventral roots of cats as assessed by motor unit yield and signal-to-noise ratios over time. All procedures were approved by the University of Pittsburgh Institutional Animal Care and Use Committee and the US Army Medical Department Animal Care and Use Review Office.

### **A.2.1 Electrode design and pre-operative testing**

The FMA (Microprobes for Life Science, Gaithersburg, MD, USA) is a direct descendant of the ‘hatpin’ electrode technology used by Hoffer, Loeb, and colleagues in their ventral root studies. The FMA is comprised of conventional ‘stiff’ platinum-iridium microelectrodes mounted into a ceramic substrate with a flexible set of gold lead wires, allowing the array to “float” within the neural tissue. Importantly for this study, the FMA allows user-defined electrode lengths,

facilitating a dorsal approach to ventral root electrode implantation, inserting the electrodes through the dorsal root ganglia (DRG) into the ventral root. The recording electrode lengths varied from 2.3 to 3.5 mm, which allowed them to fully penetrate the DRG and span the depth of the ventral root. The L7 arrays (2.8-3.5 mm) were longer than L6 arrays (2.3-3.0 mm). Each array included two reference and ground electrodes at the corners, which were 3.7 mm long.

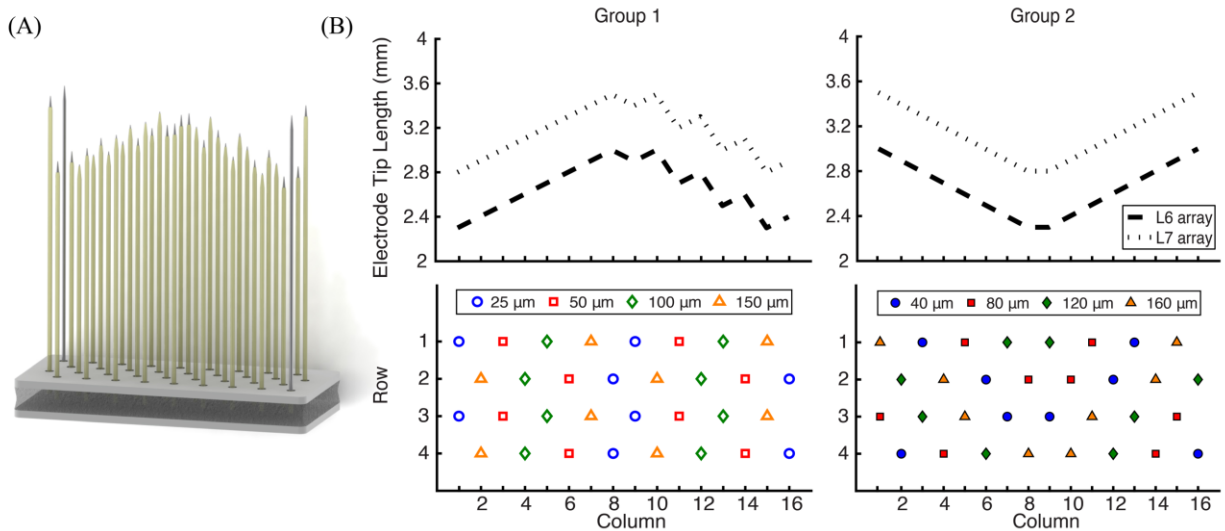


**Figure 22.** Floating microelectrode array geometry. (A) Rendering of a 32-channel FMA that was implanted in the L6 and L7 ventral roots of 9 cats. (B) Electrode length profile and site size layout. The electrode lengths were customized to reach the ventral root through the DRG. L7 arrays (2.8-3.5 mm) were longer than L6 arrays (2.3-3.0 mm), and the profile was updated for group 2 implants. Electrode recording site sizes varied from 25 to 150 µm for group 1 and 40 to 160 µm for group 2, for which the layout was also changed. Each array also included two ground and two reference electrodes at the corners.

It was hypothesized that the geometry of the exposed tip length (or site size) would have an impact on the quality and number of neurons recorded. For recordings from axons, these dimensions may be especially important since high SNR neural activity is most likely to be recorded near a node of Ranvier, where the current densities are highest. The 32 recording electrodes on each FMA (Figure 24) were spaced equidistantly at 400  $\mu\text{m}$  and had a variety of site sizes, which were different for each of two groups. Group 1 electrode arrays had site sizes of 25, 50, 100, and 150  $\mu\text{m}$ , while group 2 electrode arrays had site sizes of 40, 80, 120, and 160  $\mu\text{m}$ . Reference electrodes had exposures of 500  $\mu\text{m}$ , while ground electrodes were completely uninsulated.

Before implantation of the FMAs, each array was inspected through a microscope to check for bent or broken electrodes and to examine the integrity of the wire bundle. Additionally, the electrode connectivity was confirmed prior to implantation by measuring impedances of all electrodes before implantation. A multi-channel potentiostat (niPOD, NeuroNexus Technologies, Ann Arbor, MI, USA) was used to measure electrical impedances in vitro at 1k Hz with the electrode array in a normal saline solution (0.9% sodium chloride). To form a three-electrode system, a reference electrode (silver/silver chloride) was also placed in the solution with current supplied by a gold counter electrode.

### **A.2.2 Surgery and electrode placement**

Nine adult male cats (3-6 kg) were included in this study. Anesthesia was induced with ketamine (20 mg/kg, IM), followed by intubation and continuous administration of isoflurane (1-2.5%) for the duration of the implant surgery. Respiratory rate, expired CO<sub>2</sub>, O<sub>2</sub> saturation, blood pressure,

heart rate, and rectal temperature were monitored throughout the procedure and maintained within normal physiological ranges.

After revealing the spinal lamina by reflecting the paraspinous muscles overlying the L5-S1 vertebrae, a dorsal laminectomy was performed to expose the left L6 and L7 spinal roots. While direct access to the ventral root with flexible wire electrodes has been previously demonstrated without traversing the DRG (Hoffer, Loeb, and Pratt 1981), FMAs were too large to use this approach. Penetration of the DRG to reach the ventral root has also been reported (Hoffer, Loeb, Marks, et al. 1987) and lead to stable implants, and thus, in this study, the FMA was inserted through the DRG and into the ventral root. A custom vacuum holder attached to a micromanipulator was used to position the FMA over the DRG during visualization through a surgical microscope. A pneumatic-actuated inserter with 1.5 mm of travel (Blackrock Microsystems, Salt Lake City, UT, USA) was used to rapidly insert the FMAs through the epineurium by impacting the back end of the vacuum holder. High-speed insertion was required because the epineurium of the spinal roots cannot be penetrated using traditional slow, but continuous, insertion techniques used for cortical implantation of the FMAs. For chronic implantation, peeling back the epineurium was avoided. While it would have enabled slow insertion of the arrays, the process could have led to damage to the spinal roots themselves. After initial insertion, intraoperative electrophysiological recordings were performed to confirm the location in the ventral root. To successfully target the ventral root, the FMA must first travel through the DRG. Under surgical anesthesia, sensory afferents, but not motor efferents, within the spinal nerves remain active and responsive to hindlimb manipulation. To ensure that the electrode tips were located in the ventral root, the FMAs were advanced incrementally using the pneumatic

inserter until only the shortest electrodes recorded sensory activity, or evoked neural activity was absent on all electrode channels.

With the FMAs inserted, the wire bundles were secured to the dura with 8-0 silk suture. A stainless steel wire (AS 636, Cooner Wire Company, Chatsworth, CA, USA) was attached to a bone screw in the iliac crest to act as an additional ground electrode, and a recording reference wire (AS 632, Cooner Wire Company, Chatsworth, CA, USA) was placed in the epidural space near the spinal cord. All connectors and external wires were passed through a percutaneous port and gathered into a custom housing unit. This protective plastic backpack was mounted on percutaneous posts anchored to a baseplate attached subcutaneously to the iliac crests and dorsal fascia. After surgery, animals were typically walking within 6 to 12 hours and displayed essentially normal gain within 3 to 5 days.

### **A.2.3 Neural signal recording**

Before surgical implantation of the FMA, the cats were trained to walk on a treadmill at speeds ranging from 0.2 to 1.4 m/s. Cats were trained to walk continuously for 15 minutes, five days per week.

Neural signals from the microelectrode arrays were recorded with an OmniPlex D data acquisition system (Plexon Inc., Dallas, TX, USA) at 40 kHz and monitored constantly during all trials. Neural data were bandpass filtered between 300 Hz and 6 kHz. Awake trials consisted of three testing blocks. First, the cat would walk on the treadmill for up to five minutes at speeds ranging from 0.2 to 1.4 m/s (slower immediately after surgery but up to maximum speeds within a week). Second, the cat would stand quietly on all four legs. Third, the cat stood on its hindlimbs while leaning against a wall of the enclosure around the treadmill. The two standing conditions

were used to provide recording of relatively static activation of the muscles, compared to phasic muscular activity that occurs during walking. High speed walking and bipedal standing conditions were also used to generate high force activation of the hindlimb muscles in order to recruit higher threshold motor units that might not be activated during quiet standing. Awake trials were performed two to four times per week.

Anesthetized trials were completed one to three times per week and provided a method to classify recordings as either motor or sensory based on the knowledge that motor units are quiescent under anesthesia while sensory afferents remain modulated by limb movement. After completing all three awake blocks, the cat was lightly anesthetized with an injection of dexdomitor (40  $\mu\text{g}/\text{kg}$ , IM). First, a baseline trial lasting one minute was recorded without any stimulus or movement. Second, the implanted left leg was manipulated by alternately flexing and extending the entire leg at a moderate pace, pausing momentarily at each reversal point. The leg was continually maneuvered in this pattern for up to a minute while neural signals were recorded. Finally, neural activity was recorded while the leg was moved in a random pattern and manipulated in various motions, including flexing and extending different joints at different speeds and cycling rostrocaudally. Based on recordings during awake and anesthetized trials, units were classified as motor if they were active only during awake trials and sensory if they additionally responded during anesthetized movements.

#### **A.2.4 Electrode impedance measurements**

While the cat was anesthetized, electrical impedances were recorded for each of the 32 electrodes on each array. Impedances were measured at a frequency of 1k Hz. The array's reference and ground electrodes were employed as reference and ground points for in vivo impedance

measurements. The niPOD (NeuroNexus Technologies, Ann Arbor, MI, USA) was used for impedance measurements for the first 7 subjects, while other multi-channel potentiostat systems (Multi System, Metrohm Autolab, Utrecht, The Netherlands and CompactStat, Ivium Technologies, Eindhoven, The Netherlands) were used for trials in the last 2 subjects. All systems were compared with test electrodes in vitro and produced similar impedance results. Only functional electrodes with impedance less than 2 M $\Omega$  and greater than 10 k $\Omega$  were included for all analyses. Electrodes with impedances above 2 M $\Omega$  were considered to be broken as a likely result of mechanical damage to the lead wire or electrode tip, while electrodes with impedances below 10 k $\Omega$  were believed to have failed due to delaminated insulation or other factors. This criterion allowed the inclusion of the maximum number of functional electrodes at each post-implant time point while ensuring that failed electrodes did not confound the data analysis. A more stringent impedance criterion was tested where the upper bound was varied by site size (0.5 M $\Omega$ , 1 M $\Omega$ , 1.5 M $\Omega$ , 2 M $\Omega$  for largest to smallest electrodes), but no difference was seen the results, so a 2 M $\Omega$  upper limit was used for all electrode sizes.

The impedance data were not normally distributed, as confirmed by Chi-square goodness-of-fit test for a normal distribution. Therefore, a Kruskal-Wallis analysis of variance was performed to test effects of electrode site size and time on impedance measurements, followed by post-hoc testing by the Mann-Whitney U test. Resulting p-values less than 0.05 were treated as significant.

### **A.2.5 Neural signal processing and analysis**

Individual action potentials were extracted from the data stream by detecting amplitude threshold crossings. The threshold was set to -3.5 times the standard deviation ( $\sigma$ ) of the continuous data,

and a spike event was stored each time this threshold was crossed. Each spike event consisted of a time stamp and an 800  $\mu$ s snippet of voltage data before and after the threshold crossing.

All blocks (awake and anesthetized) for a single day were merged and sorted together using Offline Sorter (Plexon Inc., Dallas, TX, USA), as units typically remained on the same channel for all trials during one day. Cross channel artifacts were invalidated by removing spike events occurring on at least 25% of channels within a 75  $\mu$ s window. Spike sorting was performed using the first three principal components of the snippet waveforms along with the voltage traces. Many channels contained activity from multiple single units, and these clusters were verified by hand sorting. Units that exhibited modulated activity during anesthetized test recordings were classified as sensory units and eliminated from further analysis.

The signal amplitude for each sorted unit was defined as the average extremum of all the individual action potential waveforms. Because the action potential is polyphasic, the extremum value could occur at a positive or negative voltage. The noise amplitude was set to  $3\sigma$  of the filtered neural signal once all identified spikes were removed. Spiking activity was removed from the data signal prior to the noise amplitude estimation, as channels with highly active units could lead to overestimation of the noise. The SNR for a given unit was defined as the signal amplitude divided by the noise amplitude, which is an approach that has been used previously (Vetter et al. 2004).

Single unit yield was quantified as the number of individual neural signals on each electrode that were classified as exhibiting motor-related activity. Units only counted towards yield if they had an SNR greater 1.2, as units with a lower SNR were typically poorly isolated. It should be noted that these poorly isolated often exhibited activity that was clearly modulated during motor

tasks and could be useful for providing neural signals to control a prosthetic device. The SNR and single unit yield calculations for all testing blocks for all cats were aggregated by week, and median values are reported, unless otherwise specified.

A nearest-neighbor analysis was also conducted to examine the relationship between electrodes that successfully recorded single unit activity. With the dorsal implantation approach used in this study, the ability to record from motor axons requires electrodes to be precisely targeted within the ventral root, which is a significantly smaller target (~1 mm diameter) than the overlying DRG (~3 mm diameter) through which the electrode must pass. Well-positioned electrodes recording motor units were expected to be spatially clustered together on each array such that they were co-located within the ventral root. To assess the importance of electrode location on the ability to target and record from motor axons, the percentage of neighboring electrodes that recorded motor unit activity was computed for three groups of electrodes: those that recorded any single unit activity, those that specifically recorded motor unit activity, and those that did not record motor unit activity. An analysis of variance (ANOVA) was used to statistically compare these groups. Each electrode had up to six neighboring electrodes within 500  $\mu\text{m}$  (see Figure 24) with electrodes in the center of the array having 6 nearest neighbors and electrodes on the edge or in the corners having from 2 to 5 nearest neighbors.

### **A.3 RESULTS**

The ability to record action potentials from the axons of motor neurons in the ventral root was assessed by analyzing signal quality based on SNR and single unit yield over time. FMAs were implanted chronically in the left L6 and L7 ventral roots of nine cats. Neural recordings were

performed approximately weekly for 4 to 12 weeks, and signal quality metrics were compared over a variety of electrode site sizes. Electrodes were excluded from analyses at any time point when the impedances were less than 10 k $\Omega$  or greater than 2 M $\Omega$ .

### **A.3.1 SNR and unit yield over time**

Figure 23 shows an example of neural recordings during a treadmill locomotion trial. Figure 23A displays 5 seconds of raw voltage waveforms on 15 of 64 channels in cat V. All channels show neural spiking activity that was phasically modulated during the locomotor step cycle. Figure 23B shows the action potential waveforms extracted from two of the electrodes, along with their respective SNR values.

The number of single units with an SNR > 1.2 that were recorded on each array for each post-implant week is shown in Figure 24B. In the first post-implant week, there was a median of 13 units per array. Of the 12 recording weeks, the median number of units per array was greater than 10 for 6 weeks. Only 1, 2, and 7 motor units per array remained on the 3 implanted arrays that lasted to the end of the 12-week study.

While the goal of the study was to track signal quality of the implanted electrodes over three months, implant lifetimes were highly variable from subject to subject. Table 3 shows the implant durations for all electrode arrays and the reasons for termination of each experiment. Figure 24C shows the total number of functioning electrode arrays tested at each time point after implantation and included in the analysis. Only two cats reached the end of the planned 3-month implantation period.

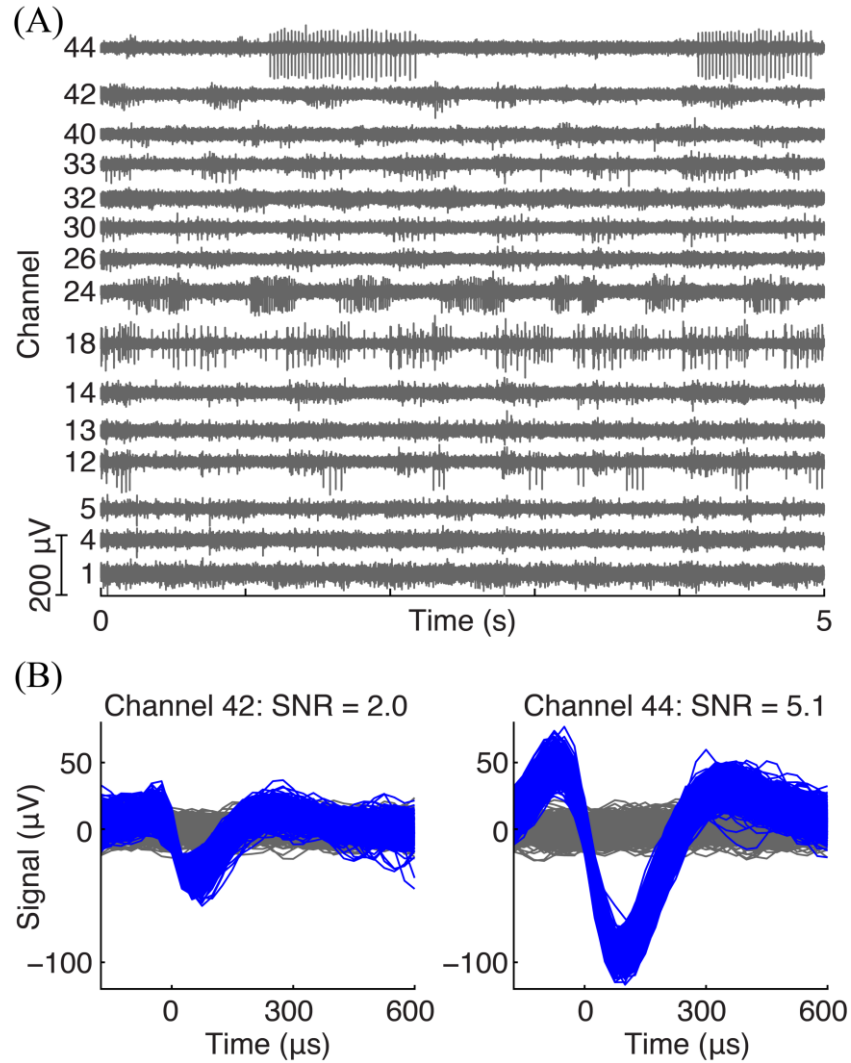


**Figure 23.** Example recordings. (A) Example of ventral root recordings during an awake trial. Phasically modulated spiking activity occurred on many channels during a treadmill locomotion trial. (B) Typical action potential waveforms recorded from motor axons in the ventral root with their respective SNRs. Figure 24 summarizes the SNR and single unit yield for all motor units recorded from all cats throughout the study. Of 2726 total single units recorded in the 9 cats, 1277 (46.8%) were classified as motor units, having exhibited activity only during awake trials. Figure 24A shows the stability of the SNR for all motor units over time. The median SNR (shown by the red line) remained at 2 or higher over the lifetime of all implants, out to a maximum post-implant time of 12 weeks. In the first four weeks after implantation, very high SNR values ( $> 5$ ) were frequently observed and are shown by the outliers denoted by red “+” signs.

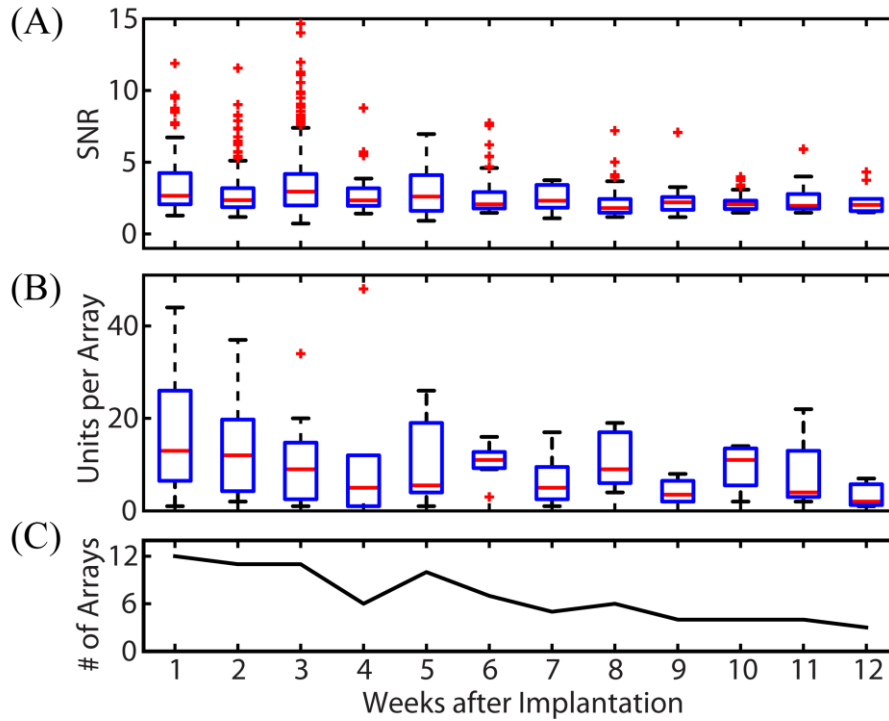


**Figure 24.** Summary of recording quality and quantity for the duration of all implants. (A) Summary of the SNR of all units over time. The median SNR (shown by the red line) remained at 2 or higher over the lifetime of all implants. Some single unit recordings with very high SNR values were observed in the first 4 weeks post-implantation. (B) Summary of motor unit yields over time. Single unit yield was calculated using units with an SNR greater than 1.2. The mean number of units per array was 17.3 in week 1 and remained between 10.5 and 13.5 through week 6. The total single unit yield decayed over the implant periods, resulting in a mean of 3.3 units per array at week 12. (C) Number of arrays recorded from per week. Because the total implant time in each animal and the number of recording session per week varied, only available arrays were included in unit yield and SNR calculations. These variations explain the increases in yield between weeks 5 and 6 (and other weeks), which reflects the elimination of failed implants from the pool of arrays being evaluated. In the boxplots of panels A and B, the red line represents the median values, the upper and lower limits of the boxes represent the 75<sup>th</sup> and 25<sup>th</sup> percentiles, and the whiskers extend to cover approximately 99.3% of the data. Red '+'s are data that fall outside of this range and are considered outliers.

**Table 3.** Summary of data, initial yield description, and reasons for terminating experiments.

	<b>Group</b>	<b>Implant Duration (weeks after implantation)</b>	<b>Initial Ventral Root Yield</b>	<b>Reason for termination</b>
Cat W	1	12	Good	End of study
Cat V	1	8	Good	Slow signal degradation
Cat U	1	5	Moderate	Broken leads
Cat T	1	6	Good	Hardware/conne ctor failure
Cat S	2	6	Moderate	Broken leads
Cat R	2	9	Good	Slow signal degradation
Cat Q	2	6	Poor	Immune reaction to surgery
Cat P	2	12	Moderate	End of study
Cat O	2	8	Poor	Slow signal degradation

### **A.3.2 Effects of nearest neighbor electrodes**

The ability to successfully target the ventral root and the importance of the relative location of individual electrodes with respect to one another was determined using a nearest neighbor analysis. Averaged across implanted arrays, 13% of an electrode's neighbors recorded motor activity during awake treadmill walking trials. However, given that an electrode itself recorded motor activity, 35% of its neighboring electrodes recorded motor activity, which was a significantly higher percentage ( $p < 0.01$ ). If an electrode did not record motor activity, the percentage of neighboring

electrodes recording motor activity was only 10%, which was significantly less than the previous two groups ( $p < 0.01$ ). These results suggest that if an electrode was successfully positioned in the ventral root and recorded motor activity, its neighbors also frequently recorded motor activity. This behavior was observed for 15 of the 18 implanted arrays.

### **A.3.3 Effect of site size on SNR and unit yield**

The effects of site size on SNR and unit yield are shown in Figure 25. Because SNR data were not normally distributed (Chi-square goodness-of-fit test), Kruskal-Wallis analysis was used to show that there was no significant effect of site size upon SNR ( $p = 0.56$ ), and all site sizes recorded units with median SNR values between 2 and 4, as shown in Figure 25. The number of units with an SNR  $> 15$  is shown by the red number above each box for each site size.

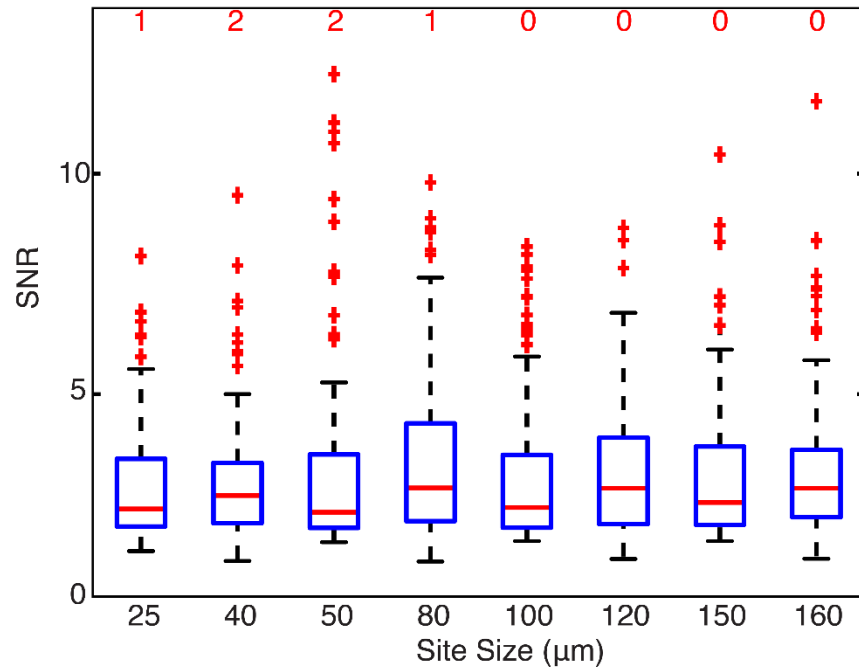


**Figure 25.** Signal to noise ratio by site size. The red line represents the median values, the upper and lower limits of the boxes represent the 75<sup>th</sup> and 25<sup>th</sup> percentiles, and the whiskers extend to cover approximately 99.3% of the data. Red '+'s are data that fall outside of this range and are considered outliers. All site sizes recorded units with median SNR between 2 and 4. The number of high SNR units (SNR > 15) is shown by the red number above each box for each site size. By statistical testing, there was no effect of site size on SNR ( $p = 0.56$ ).

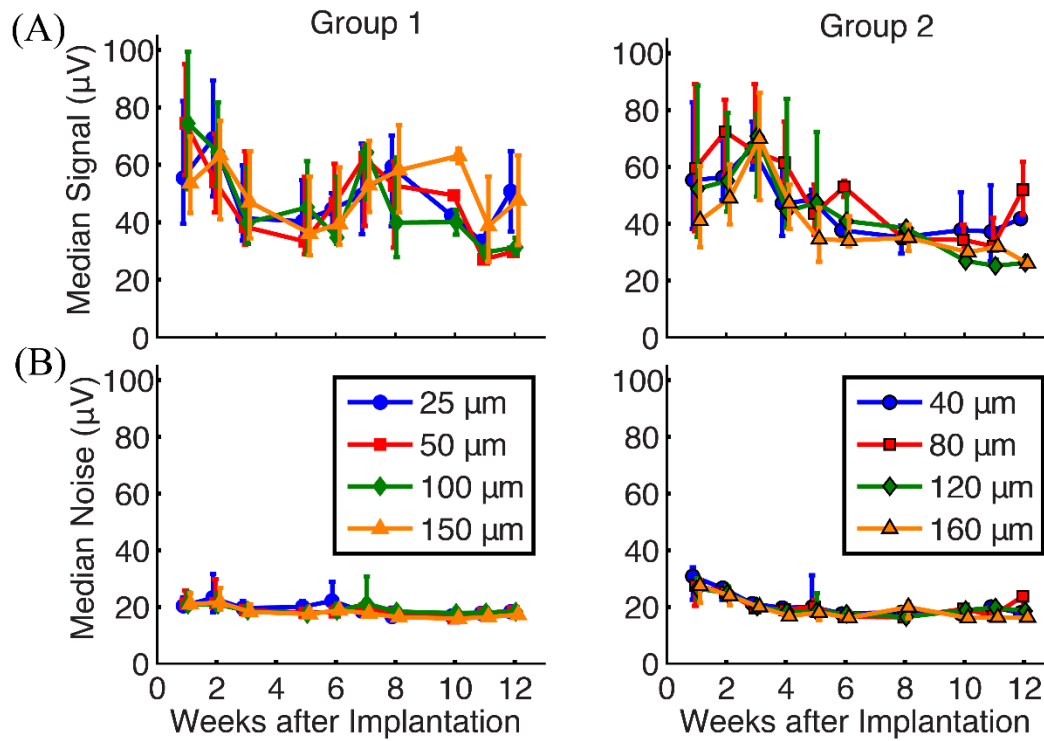


**Figure 26.** Signal to noise ratio over time. (A) Signal calculated over time for each site size. Median signal amplitude decreased over time for all site sizes, and site size was not significant factor upon signal amplitude ( $p = 0.47$  and  $0.45$  for groups 1 and 2, respectively). (B) Noise calculated over time for each site size. Median noise remained at approximately  $20 \mu\text{V}$  for the duration of the implants, and site size did contribute to noise in group 1 electrodes ( $p < 0.01$ ), but not group 2 electrodes ( $p = 0.17$ ).

The effects of site size on signal and noise were also examined separately. The median signal amplitude (Figure 26A) decreased over time for all site sizes, while the median noise (Figure 26B) remained constant near 20  $\mu\text{V}$  for the lifetime of the implants. Signal and noise data were not normally distributed (Chi-square goodness-of-fit test) and statistical testing using a Kruskal-Wallis analysis showed that site size was not a significant factor upon signal amplitude in both groups of electrodes ( $p = 0.47$  and  $0.45$  for groups 1 and 2, respectively). Site size had a significant effect on the noise levels for group 1 ( $p < 0.01$ ) but not for group 2 ( $p = 0.17$ ) electrodes. Post-hoc testing using the Mann-Whitney U test confirmed that noise levels were larger for smaller site sizes in group 1. Signal and noise measurements were also examined in a restricted time window (2-3 weeks post-implant) when signal quality was best and few electrode arrays had failed. Even in this time period, linear regressions between signal amplitude and site size were not significant for group 1 ( $p = 0.47$ ) or group 2 ( $p = 0.69$ ) electrodes. Linear regression between noise and site size was not significant for group 2 electrodes ( $p = 0.51$ ) but was significant for group 1 electrodes ( $p = 0.04$ ), mirroring the statistical analysis described above.

Figure 27 shows the percentage of electrodes for each site size that were able to record 1, 2, or 3 or more single units. Each bar represents the total percentage of electrodes on an implanted array that recorded at least one unit. Statistical testing using an ANOVA showed that site size was not a significant factor on the number of units recorded per electrode ( $p = 0.45$ ). An average of 37.1% and 25.8% of the electrodes in group 1 and 2 arrays, respectively, recorded at least one motor unit, while an average of 16.2% and 9.2% of the electrodes in group 1 and 2 arrays, respectively, recorded two or more motor units.

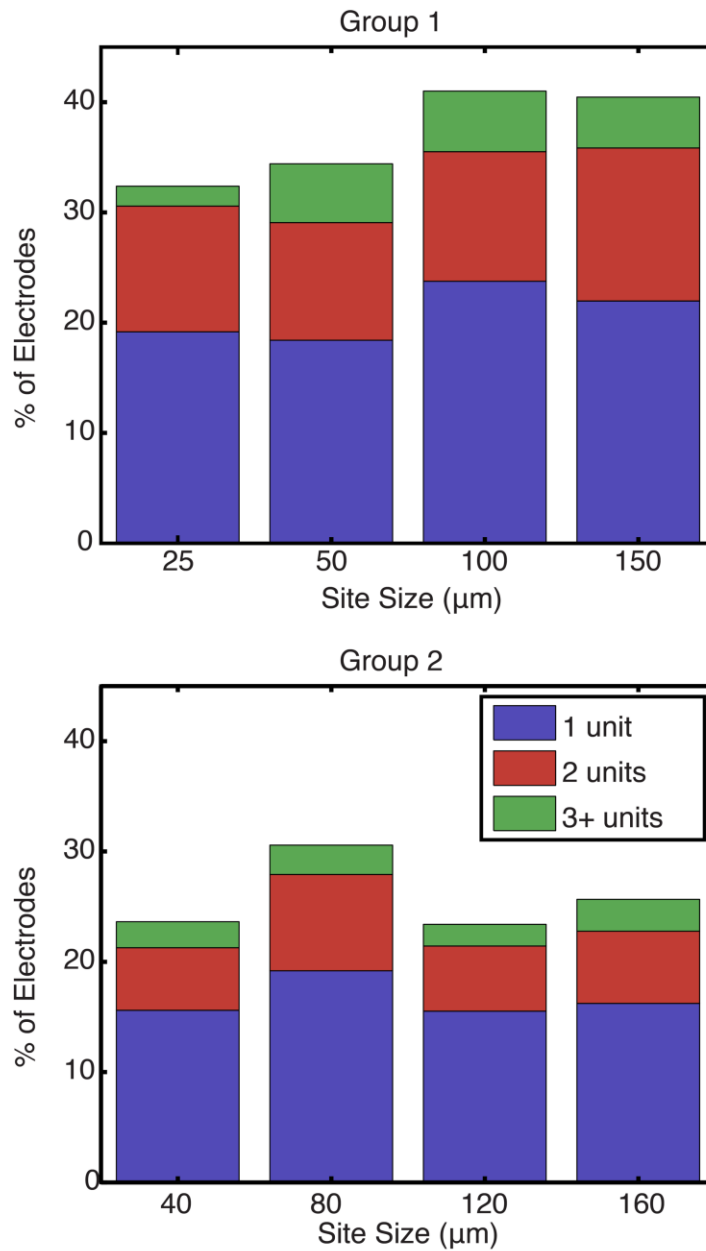


**Figure 27.** Percentage of electrodes recording at least one unit by site size. For each site size, each bar represents the total percentage of electrodes that recorded at least one unit, while the stacks represent the percentage of functional electrodes that were able to record 1, 2, or more than 3 units in blue, red, and green, respectively. Site size was not found to be a significant factor on the number of units recorded per electrode ( $p = 0.45$ ).

#### **A.3.4 Effect of site size on chronic electrode impedances**

Figure 28A shows a summary of chronic impedance measurements of all electrodes in all animals over the lifetime of the implants. Out of 32 electrodes on each array, there were 8 electrodes of each site size. The line plot shows the median impedance of the electrodes of a particular site size while the error bars express the upper and lower quartiles of the data. As time progressed, the number of functioning electrodes decreased (Figure 28B). Neural recordings on electrodes with impedances greater than 2 M $\Omega$  or less than 10 k $\Omega$  were extremely noisy and considered to be broken, and therefore were not included in chronic impedance data.

Electrical impedances, as expected, were inversely correlated with site size. The results of a Kruskal-Wallis analysis of variance showed that site size had a significant effect on electrical impedance ( $p < 0.01$  in both groups of electrodes). Post-hoc testing using the Mann-Whitney U test confirmed that impedance measurements were larger for smaller site sizes, as shown in both groups. Impedances were not significantly related to post-implant time ( $p = 0.86$  and  $0.35$  for groups 1 and 2, respectively), and overall, the impedances remained stable within a range of 50 to 500 k $\Omega$  while implanted.

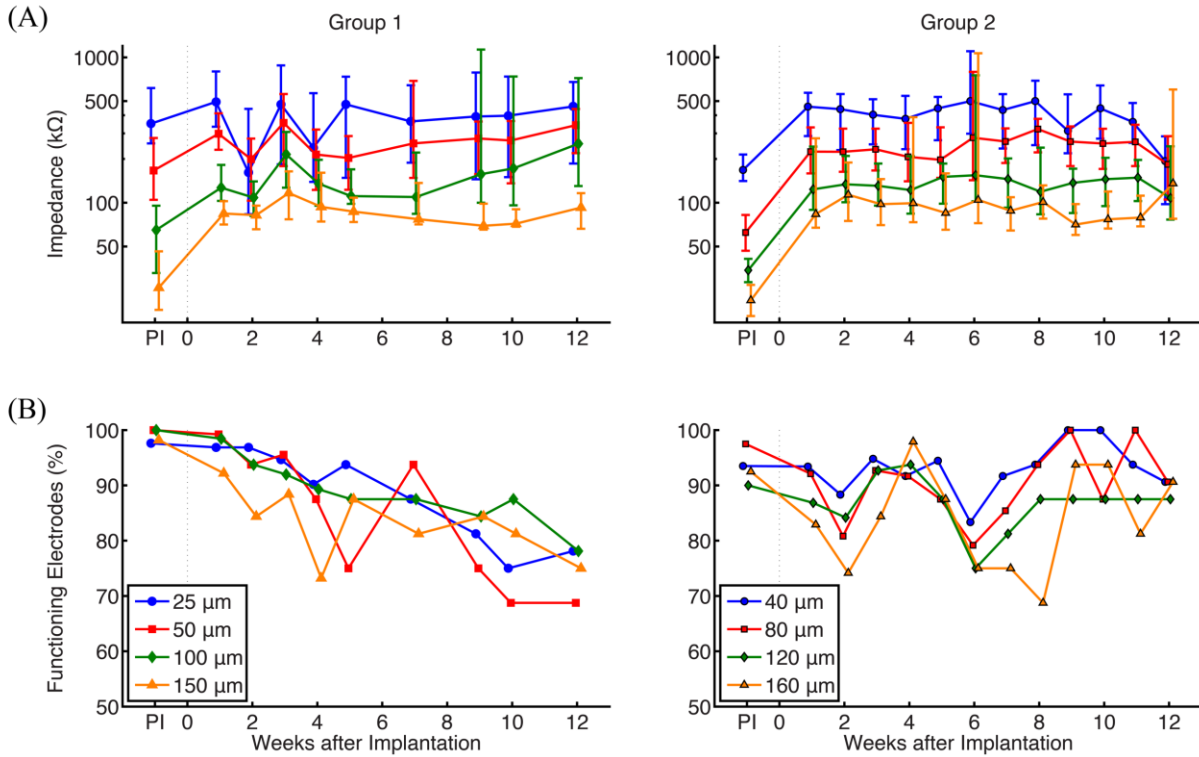


**Figure 28.** Electrode impedances and fraction functional over time. (A) Summary of chronic impedance measurements of all arrays. The line plots show the median impedance of the 8 different electrode site sizes, with error bars representing the 75th and 25th percentiles of the data. The pre-implant (PI) impedance values, measured immediately before preparation for surgical implantation, are also shown. Electrodes with impedance greater than 2 MΩ or less than 10 kΩ were considered non-functional and were not included in these graphs. Impedances were inversely correlated with site size and median impedances of functioning electrodes remained stable within a range of 50 to 500 kΩ while implanted. Results of a Kruskal-Wallis test showed that site size was statistically significant ( $p < 0.01$ ) in both groups, while the effect of time was not significant ( $p = 0.86$  and  $0.35$  for groups 1 and 2, respectively.) (B) Percentage of implanted electrodes with impedances less than 2 MΩ and greater than 10 kΩ. Each time point represents all implanted electrodes at each week, while electrodes from FMAs that suffered catastrophic failures were not included. Around 70% to 80% of group 1 and 90% of group 2 electrodes that remained implanted were functional at 12 weeks.

As described earlier, increased electrical impedance was used to diagnose broken electrodes (impedances  $> 2 \text{ M}\Omega$  or impedance  $< 10 \text{ k}\Omega$ ). Figure 28B shows the percentage of implanted electrodes that were considered functional as time progressed, separated by group and site size. Each time point represents all implanted electrodes at each week. While nearly 100% of electrodes were functional immediately after implant, this value decreased over time. Instances where complete failure of an array occurred due to broken lead wires were removed from this dataset. In group 1 electrodes, the percentage of functional electrodes slowly dropped to between 70% and 80% for all site sizes, while group 2 electrodes remained stable at 90% after 12 weeks. The large variation in the impedance measurements for some weeks may be attributed to a faulty connection within the adapter chain between the implanted electrode array and potentiostat, such as an electrical short (e.g. group 1, week 2) or broken lead (e.g. group 2, week 5).

#### **A.4 DISCUSSION**

The primary goal of this work was to assess the ability to record extracellular action potentials from populations of motor axons in the ventral roots using penetrating microelectrode arrays implanted chronically in lumbar spinal roots of adult cats. Because of notable differences in implant location, animal model, spike sorting techniques, and measurements of signal quality, it is difficult to compare this work with the performance of other types of implantable microelectrodes (e.g., (Rousche and Normann 1999; Nicolelis et al. 2003; Kane et al. 2011; Prasad and Sanchez 2012; Collinger et al. 2013)). Nonetheless, based on the results of this study, it is clear that it was possible to record single unit activity from populations of motor units in the ventral root for up to 12 weeks after implantation.

When successfully placed, many electrodes recorded activity from motor axons. However, accurate placement of electrodes in the ventral root was challenging to achieve, even using intraoperative recordings to guide placement. In post-operative testing, all of the implanted arrays contained at least one electrode that demonstrated activity during anesthetized recordings, suggesting that they were recording sensory activity from neurons in the dorsal root. Optimal placement of the arrays was difficult to achieve, but at least 20 motor units per array were recorded in 7 of 9 implanted animals. In addition, these well-targeted electrodes tended to be clustered together. Electrodes that recorded motor activity were statistically more likely to be neighbors of other electrodes that also recorded motor activity than those that did not.

The specifications for electrode design were also investigated to examine whether there was a relationship between an electrode's site size and recording signal quality. It was originally expected that the larger electrodes would be more likely to record neural activity from multiple single units, since the probability of being near signal sources would be higher, albeit with lower SNR. On the other hand, it was expected that small electrodes would provide better unit isolation leading to high SNR recordings. The hypothesis was formulated upon the idea that larger site sizes would offer a higher likelihood of being positioned close to nodes of Ranvier where extracellular current densities are high, while smaller site sizes would have fewer nodes of Ranvier close to their electrode tip. However, in this study, there was no significant relationship between SNR and site size, as has been previously reported (Vetter et al., 2004). In another study of the effects of site size on recording quality in the cortex (Nordhausen et al., 1994), it was reported that the SNR increased with decreasing electrode tip length, but concluded that the optimum range for single unit recordings was 30 to 220  $\mu\text{m}$ , without providing statistical comparisons of site sizes within

that range. Finally, the single unit yields were also compared across all site sizes. Ultimately, it was found that site size was not a statistically significant factor for the number of units recorded and that all site sizes recorded units with similar SNR values.

While no statistically significant relationship between site size and SNR was found, there were reasons to expect that signal amplitudes and noise levels might vary with site size independently. Based solely on the higher impedances associated with smaller electrodes, it would be expected that smaller electrodes would have higher noise levels. Meanwhile, it was unclear whether the spatial averaging effects that should occur with larger electrodes along with their increased probability of being near a node of Ranvier would dominate the recorded signal amplitude. Interestingly, site size did not have a significant effect on noise levels in group 2 electrodes, nor did they influence signal amplitudes in either group. In group 2 electrodes, the noise levels did not follow impedance trends, suggesting that the source of the noise was predominantly background neuronal activity, not electrode thermal noise (Cogan, 2008; Ward et al. 2009). The somewhat larger site sizes associated with group 2 electrodes could have also contributed to these findings.

Electrical impedances were measured over time for all implanted electrodes to diagnose electrode integrity. Electrodes with impedances greater than 2 M $\Omega$  or less than 10 k $\Omega$  were considered to be broken, as neural recordings on these channels were always extremely noisy, no single unit's neural activity was ever detected, and the impedance levels were significantly higher than the original manufactured specifications. Electrode impedance may increase for a number of biotic (e.g. encapsulation (Turner et al., 1999; Szarowski et al., 2003; Polikov et al., 2005), immune response to foreign body (Polikov et al., 2005; Winslow and Tresco, 2009)) and abiotic (e.g. broken electrode tips (Sanchez et al., 2006), insulation damage (Patrick et al., 2011), breaks in

wire bundle) failure modes. It was hypothesized that smaller site sizes would be more quickly affected by encapsulation, and therefore would demonstrate earlier biotic failure than larger recording sites. Since the mechanical structure of all electrodes and leads were similar, the chance of abiotic failure modes was hypothesized to be the same for all implanted electrodes.

For all site sizes, the electrical impedances remained stable during the post-implantation period, with the smaller sites have a higher value, similar to previous studies that examined the relationship between recording site size and impedance (Vetter et al., 2004). This was consistent for all cats and implanted arrays. Statistical analysis showed that site size was statistically significant factor ( $p < 0.01$ ), while post-implant time was not. While microstimulation studies have revealed a pattern of a sharp increase in impedance within the first two to three weeks post-implantation followed by a decay to some baseline (Rousche and Normann, 1999; Parker et al., 2011; Koivuniemi et al., 2011; Prasad and Sanchez, 2012), the findings here follow impedance patterns shown in long-term implantation studies applying microelectrode arrays solely for neural recording (Vetter et al., 2004; Kane et al., 2011).

This study tracked the percentage of functional electrodes over time based on electrical impedances and found that the rates of failure for all site sizes were not statistically different. While electrodes did break in many animals and only 2 cats completed the planned 12-week implant time, the percentage of implanted electrodes that remained functional stayed relatively stable, suggesting that solving technical issues related to lead failure could allow a large number of neural recordings. In the two animals that completed the planned 12-week implants, 80% of the implanted electrode remained viable.

This study demonstrated the feasibility of achieving chronic recordings from motor axons in the ventral root. However, some limitations still remain. Implanting FMAs through intact

epineurium proved to be difficult and required high-speed insertion methods. In part, because of this difficulty, consistent electrode targeting has remained a challenge. Observations of perfused spinal nerve tissue have shown that electrodes can pass through the ventral surface of the ventral root and that these electrode shafts can bend, presumably as a result of mechanical contact with the spinal canal. These results suggest that other approaches to implantation or other approaches of implantation, such as targeting the ventral root from the lateral or ventral side, may be more appropriate for accessing the ventral root.

Despite these limitations, this study presents the first chronic neural recordings from multichannel microelectrode arrays in the ventral roots. These results show that it is possible to record from motor axons in the ventral root, and that the neural signals can be detected by variety of electrode site sizes. These findings suggest that the ventral root is a potentially feasible site for a peripheral motor interface.

Further work with these devices will focus on improving the approach to the ventral root such that proper and accurate targeting can be achieved more consistently. Additionally, a detailed analysis of histological data will be performed to identify any biotic causes to changes in the unit yield observed over the course of the study. Future studies will focus on the development of methods to decode the motor commands associated with ventral root recordings in order to attain useful control signals for devices such as prosthetic limbs and orthoses.

## **A.5 ACKNOWLEDGEMENTS**

This work was sponsored by the Defense Advanced Research Projects Agency (DARPA) Microsystems Technology Office under the auspices of Dr. Jack Judy (jack.judy@darpa.mil) through the Space and Naval Warfare Systems Center, Pacific Grant No. N66001-11-C-4171.

## BIBLIOGRAPHY

- American Association of Neurological Surgeons. 2017. “Minimally Invasive Spine Surgery.” *Aans.org*. Accessed November 11. <https://www.aans.org/en/Patients/Neurosurgical-Conditions-and-Treatments/Minimally-Invasive-Spine-Surgery>.
- Amputee Coalition. 2015. “Limb Loss Statistics.” *Amputee-Coalition.org*. Accessed February 20. <http://www.amputee-coalition.org/limb-loss-resource-center/resources-by-topic/limb-loss-statistics/limb-loss-statistics/>.
- Basmajian, J V. 1963. “Control and Training of Individual Motor Units.” *Science* 141 (3579): 440–41.
- Bauman, Matthew J, Tim M Bruns, Joost B Wagenaar, Robert A Gaunt, and Douglas J Weber. 2011. “Online Feedback Control of Functional Electrical Stimulation Using Dorsal Root Ganglia Recordings.” In, 2011:7246–49. Boston, MA. doi:10.1109/IEMBS.2011.6091831.
- Bessou, P, F Emonet-Dénand, and Y Laporte. 1965. “Motor Fibres Innervating Extrafusal and Intrafusal Muscle Fibres in the Cat.” *Journal of Physiology* 180 (3): 649–72. doi:10.1113/jphysiol.1965.sp007722.
- Birdwell, J Alexander, Levi J Hargrove, Richard F ff Weir, and Todd A Kuiken. 2015. “Extrinsic Finger and Thumb Muscles Command a Virtual Hand to Allow Individual Finger and Grasp Control.” *IEEE Transactions on Biomedical Engineering* 62 (1): 218–26. doi:10.1109/TBME.2014.2344854.
- Bourbeau, Dennis Joseph. 2011. “Ventral Root or Dorsal Root Ganglion Microstimulation to Evoke Hindlimb Motor Responses.” Pittsburgh, PA: University of Pittsburgh.

- Brooke, M H, and K K Kaiser. 1970. "Muscle Fiber Types: How Many and What Kind?." *Archives of Neurology*. 23, no. 4 (1970): 369-379.
- Bruns, Tim M, Joost B Wagenaar, Matthew J Bauman, Robert A Gaunt, and Douglas J Weber. 2013. "Real-Time Control of Hind Limb Functional Electrical Stimulation Using Feedback From Dorsal Root Ganglia Recordings." *Journal of Neural Engineering* 10 (2): 026020. doi:10.1088/1741-2560/10/2/026020.
- Burke, R E, W Z Rymer, and J V Walsh Jr. 1973. "Functional Specialization in the Motor Unit Population of Cat Medial Gastrocnemius Muscle." In *Control of Posture and Locomotion*, edited by R B Stein, K G Pearson, R S Smith, and J B Redford. New York: Plenum Press.
- Chase, Steven M, Andrew B Schwartz, and Robert E Kass. 2009. "Bias, Optimal Linear Estimation, and the Differences Between Open-Loop Simulation and Closed-Loop Performance of Spiking-Based Brain-Computer Interface Algorithms." *Neural Networks* 22 (9). NIH Public Access: 1203-13. doi:10.1016/j.neunet.2009.05.005.
- Clark, Gregory A, Suzanne Wendelken, David M Page, Tyler Davis, Heather A C Wark, Richard A Normann, David J Warren, and Douglas T Hutchinson. 2014. "Using Multiple High-Count Electrode Arrays in Human Median and Ulnar Nerves to Restore Sensorimotor Function After Previous Transradial Amputation of the Hand." *Conference Proceedings : ... Annual International Conference of the IEEE Engineering in Medicine and Biology Society. IEEE Engineering in Medicine and Biology Society. Annual Conference 2014 (August): 1977-80*. doi:10.1109/EMBC.2014.6944001.
- Coggeshall, R E. 1980. "Law of Separation of Function of the Spinal Roots." *Physiological Reviews* 60 (3). American Physiological Society: 716-55.
- Collinger, Jennifer L, Brian Wodlinger, John E Downey, Wei Wang, Elizabeth C Tyler-Kabara, Douglas J Weber, Angus J C McMorland, Meel Velliste, Michael L Boninger, and Andrew B Schwartz. 2013. "High-Performance Neuroprosthetic Control by an Individual with Tetraplegia." *Lancet* 381 (9866): 557-64. doi:10.1016/S0140-6736(12)61816-9.
- Collins, S H, and A Ruina. 2005. "A Bipedal Walking Robot with Efficient and Human-Like Gait." *Robotics and Automation, 2005. ICRA 2005. Proceedings of the 2005 IEEE International Conference on*, pp. 1983-1988. IEEE, 2005..

- Creutzfeldt, O D. 1977. "Generality of the Functional Structure of the Neocortex." *Die Naturwissenschaften* 64 (10): 507–17. doi:10.1007/BF00483547.
- Cullheim, Staffan. 1978. "Relations Between Cell Body Size, Axon Diameter and Axon Conduction Velocity of Cat Sciatic A-Motoneurons Stained with Horseradish Peroxidase." *Neuroscience Letters* 8 (1): 17–20. doi:10.1016/0304-3940(78)90090-3.
- Davis, T S, H A C Wark, D T Hutchinson, D J Warren, K O'Neill, T Scheinblum, G A Clark, R A Normann, and B Greger. 2016. "Restoring Motor Control and Sensory Feedback in People with Upper Extremity Amputations Using Arrays of 96 Microelectrodes Implanted in the Median and Ulnar Nerves." *Journal of Neural Engineering* 13 (3): 036001. doi:10.1088/1741-2560/13/3/036001.
- Debnath, Shubham, Matthew J Bauman, Lee E Fisher, Douglas J Weber, and Robert A Gaunt. 2014. "Microelectrode Array Recordings From the Ventral Roots in Chronically Implanted Cats." *Frontiers in Neurology* 5: 104. doi:10.3389/fneur.2014.00104.
- del Valle, Jaume, and Xavier Navarro. 2013. "Interfaces with the Peripheral Nerve for the Control of Neuroprostheses." *International Review of Neurobiology* 109: 63–83. doi:10.1016/B978-0-12-420045-6.00002-X.
- Denslow, J S. 1948. "Double Discharges in Human Motor Units." *Journal of Neurophysiology* 11 (3): 209–15.
- Dhillon, Gurpreet S, Stephen M Lawrence, Douglas T Hutchinson, and Kenneth W Horch. 2004. "Residual Function in Peripheral Nerve Stumps of Amputees: Implications for Neural Control of Artificial Limbs." *The Journal of Hand Surgery* 29 (4): 605–15. doi:10.1016/j.jhsa.2004.02.006.
- Di Pino, G, E Guglielmelli, and P M Rossini. 2009. "Neuroplasticity in Amputees: Main Implications on Bidirectional Interfacing of Cybernetic Hand Prostheses." *Progress in Neurobiology* 88 (2): 114–26. doi:10.1016/j.pneurobio.2009.03.001.
- Dollar, A M, and H Herr. 2007. "Active Orthoses for the Lower-Limbs: Challenges and State of the Art." *Rehabilitation Robotics, 2007. ICORR 2007. 2007 IEEE 10th International Conference on ...*, pp. 968-977. IEEE, 2007.

- Durand, Dominique M, Brian Wodlinger, and Hyunjoo Park. 2013. "Neural Interfacing with the Peripheral Nervous System: a FINE Approach." In *Neural Engineering*, edited by Bin He, 2nd ed., 657–83. New York: Springer.
- Eccles, J C, and C S Sherrington. 1930. "Numbers and Contraction-Values of Individual Motor-Units Examined in Some Muscles of the Limb." *Proc. R. Soc. Lond. B* 106, no. 745: 326-357..
- Edell, David J. 1986. "A Peripheral Nerve Information Transducer for Amputees: Long-Term Multichannel Recordings From Rabbit Peripheral Nerves." *IEEE Transactions on Biomedical Engineering* BME-33 (2). IEEE: 203–14. doi:10.1109/TBME.1986.325892.
- Emonet-Dénand, F, and Y Laporte. 1975. "Proportion of Muscles Spindles Supplied by Skeletofusimotor Axons (Beta-Axons) in Peroneus Brevis Muscle of the Cat." *Journal of Neurophysiology* 38 (6): 1390–94. doi:10.1152/jn.1975.38.6.1390.
- Engberg, I, and A Lundberg. 1969. "An Electromyographic Analysis of Muscular Activity in the Hindlimb of the Cat During Unrestrained Locomotion." *Acta Physiologica Scandinavica*.
- Englehart, K, and B Hudgins. 2003. "A Robust, Real-Time Control Scheme for Multifunction Myoelectric Control." *IEEE Transactions on Biomedical Engineering* 50 (7): 848–54. doi:10.1109/TBME.2003.813539.
- Erim, Z, C J De Luca, K Mineo, and T Aoki. 1996. "Rank-Ordered Regulation of Motor Units." *Muscle & Nerve* 19 (5): 563–73. doi:10.1002/(SICI)1097-4598(199605)19:5<563::AID-MUS3>3.0.CO;2-9.
- Ethier, Christian, E R Oby, Matthew J Bauman, and L E Miller. 2012. "Restoration of Grasp Following Paralysis Through Brain-Controlled Stimulation of Muscles." *Nature* 485 (7398): 368–71. doi:10.1038/nature10987.
- Farber, Neil E, Karl A Poterack, and William T Schmeling. 1997. "Dexmedetomidine and Halothane Produce Similar Alterations in Electroencephalographic and Electromyographic Activity in Cats." *Brain Research* 774 (1-2): 131–41. doi:10.1016/S0006-8993(97)81696-4.
- Feindel, W, J R Hinshaw, and G Weddell. 1952. "The Pattern of Motor Innervation in Mammalian Striated Muscle." *Journal of Anatomy* 86 (1): 35–48.

- Fisher, Lee E, Christopher A Ayers, Mattia Ciollaro, Valérie Ventura, Douglas J Weber, and Robert A Gaunt. 2014. “Chronic Recruitment of Primary Afferent Neurons by Microstimulation in the Feline Dorsal Root Ganglia.” *Journal of Neural Engineering* 11 (3): 036007. doi:10.1088/1741-2560/11/3/036007.
- Fite, K, J Mitchell, F Sup, and Michael Goldfarb. 2007. “Design and Control of an Electrically Powered Knee Prosthesis.” In, 10:902–5. Noordwijk, The Netherlands. doi:10.1109/ICORR.2007.4428531.
- Gandevia, S C, V G Macefield, D Burke, and D K McKenzie. 1990. “Voluntary Activation of Human Motor Axons in the Absence of Muscle Afferent Feedback.” *Brain* 113, no. 5: 1563-1581.
- Garde, Kshitija, Edward Keefer, Barry Botterman, Pedro Galvan, and Mario I Romero. 2009. “Early Interfaced Neural Activity From Chronic Amputated Nerves.” *Frontiers in Neuroengineering* 2: 5. doi:10.3389/neuro.16.005.2009.
- Goodall, E V, T M Lefurge, and K W Horch. 1991. “Information Contained in Sensory Nerve Recordings Made with Intrafascicular Electrodes.” *IEEE Transactions on Biomedical Engineering* 38 (9): 846–50. doi:10.1109/10.83604.
- Gordon, T, and M C Pattullo. 1993. “Plasticity of Muscle Fiber and Motor Unit Types.” *Exercise and Sport Sciences Reviews* 21: 331–62.
- Granit, Ragnar. 1975. “The Functional Role of the Muscle Spindles—Facts and Hypotheses.” *Brain* 98 (4): 531–56. doi:10.1093/brain/98.4.531.
- Griffin, Darcy M, Donna S Hoffman, and Peter L Strick. 2015. “Corticomotoneuronal Cells Are ‘Functionally Tuned’.” *Science*. June 11. doi:10.1126/science.aaa8035.
- Hargrove, Levi J, Ann M Simon, Aaron J Young, Robert D Lipschutz, Suzanne B Finucane, Douglas G Smith, and Todd A Kuiken. 2013. “Robotic Leg Control with EMG Decoding in an Amputee with Nerve Transfers.” *The New England Journal of Medicine* 369 (13): 1237–42. doi:10.1056/NEJMoa1300126.
- Henneman, E, and G Somjen. 1965. “Functional Significance of Cell Size in Spinal Motoneurons.” *Journal of neurophysiology* 28, no. 3: 560-580.

- Hochberg, Leigh R, Mijail D Serruya, Gerhard M Friehs, Jon A Mukand, Maryam Saleh, Abraham H Caplan, Almut Branner, David Chen, Richard D Penn, and John P Donoghue. 2006. "Neuronal Ensemble Control of Prosthetic Devices by a Human with Tetraplegia." *Nature* 442 (7099). Nature Publishing Group: 164–71. doi:10.1212/WNL.58.5.794.
- Hoffer, J A, and G E Loeb. 1980. "Implantable Electrical and Mechanical Interfaces with Nerve and Muscle." *Annals of Biomedical Engineering* 8 (4-6). Kluwer Academic Publishers: 351–60. doi:10.1007/BF02363438.
- Hoffer, J A, G E Loeb, and C A Pratt. 1981. "Single Unit Conduction Velocities From Averaged Nerve Cuff Electrode Records in Freely Moving Cats." *Journal of Neuroscience Methods* 4 (3): 211–25. doi:10.1016/0165-0270(81)90033-9.
- Hoffer, J A, G E Loeb, N Sugano, W B Marks, M J O'Donovan, and C A Pratt. 1987. "Cat Hindlimb Motoneurons During Locomotion. III. Functional Segregation in Sartorius." *Journal of Neurophysiology* 57 (2): 554–62.
- Hoffer, J A, G E Loeb, W B Marks, M J O'Donovan, C A Pratt, and N Sugano. 1987. "Cat Hindlimb Motoneurons During Locomotion. I. Destination, Axonal Conduction Velocity, and Recruitment Threshold." *Journal of Neurophysiology* 57 (2): 510–29.
- Hoffer, J A, N Sugano, G E Loeb, W B Marks, M J O'Donovan, and C A Pratt. 1987. "Cat Hindlimb Motoneurons During Locomotion. II. Normal Activity Patterns." *Journal of Neurophysiology* 57 (2): 530–53.
- Holinski, B J, D G Everaert, V K Mushahwar, and R B Stein. 2013. "Real-Time Control of Walking Using Recordings From Dorsal Root Ganglia." *Journal of Neural Engineering* 10 (5): 056008. doi:10.1088/1741-2560/10/5/056008.
- Huesler, Erhard J, Marc A Maier, and Marie-Claude Hepp-Reymond. 2000. "EMG Activation Patterns During Force Production in Precision Grip. III. Synchronisation of Single Motor Units." *Experimental Brain Research. Experimentelle Hirnforschung. Expérimentation Cérébrale* 134 (4): 441–55. doi:10.1007/s002210000484.
- Hunt, C C, and S W Kuffler. 1954. "Motor Innervation of Skeletal Muscle: Multiple Innervation of Individual Muscle Fibres and Motor Unit Function." *Journal of Physiology* 126 (2): 293–303.

- Hunt, Carlton C. 1951. "The Reflex Activity of Mammalian Small-Nerve Fibres." *Journal of Physiology* 115 (4). Wiley/Blackwell (10.1111): 456–69.  
doi:10.1113/jphysiol.1951.sp004681.
- Hyndman, R J, and A B Koehler. 2006. "Another Look at Measures of Forecast Accuracy." *International Journal of Forecasting*.
- Johannes, Matthew S, John D Bigelow, James M Burck, Stuart D Harshbarger, Matthew V Kozlowski, and Thomas Van Doren. 2011. "An Overview of the Developmental Process for the Modular Prosthetic Limb." *Johns Hopkins APL Technical Digest* 30 (3). JHU/APL: 207–16.
- Kane, S R, S F Cogan, J Ehrlich, T D Plante, and D B McCreery. 2011. "Electrical Performance of Penetrating Microelectrodes Chronically Implanted in Cat Cortex." In, 5416–19. IEEE.  
doi:10.1109/IEMBS.2011.6091339.
- Kudina, Lydia P, and Regina E Andreeva. 2010. "Repetitive Doublet Firing of Motor Units: Evidence for Plateau Potentials in Human Motoneurons?." *Experimental Brain Research. Experimentelle Hirnforschung. Expérimentation Cérébrale* 204 (1): 79–90.  
doi:10.1007/s00221-010-2298-z.
- Kuiken, Todd A, Guanglin Li, Blair A Lock, Robert D Lipschutz, Laura A Miller, Kathy A Stubblefield, and Kevin B Englehart. 2009. "Targeted Muscle Reinnervation for Real-Time Myoelectric Control of Multifunction Artificial Arms." *Jama* 301 (6). American Medical Association: 619–28. doi:10.1001/jama.2009.116.
- Lefurge, T, E Goodall, K Horch, L Stensaas, and A Schoenberg. 1991. "Chronically Implanted Intrafascicular Recording Electrodes." *Annals of Biomedical Engineering* 19 (2): 197–207.
- Liu, X, D B McCreery, R R Carter, L A Bullara, T G Yuen, and W F Agnew. 1999. "Stability of the Interface Between Neural Tissue and Chronically Implanted Intracortical Microelectrodes." *IEEE Transactions on Rehabilitation Engineering : a Publication of the IEEE Engineering in Medicine and Biology Society* 7 (3): 315–26.
- Loeb, G E, W B Marks, and J A Hoffer. 1987. "Cat Hindlimb Motoneurons During Locomotion. IV. Participation in Cutaneous Reflexes." *Journal of Neurophysiology* 57 (2): 563–73.

- Lotfi, Parisa, Kshitija Garde, Amit K Chouhan, Ebrahim Bengali, and Mario I Romero-Ortega. 2011. "Modality-Specific Axonal Regeneration: Toward Selective Regenerative Neural Interfaces." *Frontiers in Neuroengineering* 4: 11. doi:10.3389/fneng.2011.00011.
- MacKenzie, Ellen J, Renan C Castillo, Alison Snow Jones, Michael J Bosse, James F Kellam, Andrew N Pollak, Lawrence X Webb, et al. 2007. "Health-Care Costs Associated with Amputation or Reconstruction of a Limb-Threatening Injury." *The Journal of Bone & Joint Surgery* 89 (8). The Journal of Bone and Joint Surgery: 1685–92. doi:10.2106/JBJS.F.01350.
- Marks, A F. 1969. "Bullfrog Nerve Regeneration Into Porous Implants." *The Anatomical Record* 163 (2). Wiley-Liss Div John Wiley & Sons Inc, 605 Third Ave, New York, NY 10158-0012: 226.
- McFarland, Lynne V, Sandra L Hubbard Winkler, Allen W Heinemann, Melissa Jones, and Alberto Esquenazi. 2010. "Unilateral Upper-Limb Loss: Satisfaction and Prosthetic-Device Use in Veterans and Servicemembers From Vietnam and OIF/OEF Conflicts." *Journal of Rehabilitation Research and Development* 47 (4): 299. doi:10.1682/JRRD.2009.03.0027.
- McKiernan, Brian J, Joanne K Marcario, Jennifer Hill Karrer, and Paul D Cheney. 1998. "Corticomotoneuronal Postspike Effects in Shoulder, Elbow, Wrist, Digit, and Intrinsic Hand Muscles During a Reach and Prehension Task." *Journal of Neurophysiology* 80 (4). American Physiological Society: 1961–80.
- Milner-Brown, H S, R B Stein, and R Yemm. 1973. "The Orderly Recruitment of Human Motor Units During Voluntary Isometric Contractions." *Journal of Physiology* 230 (2): 359–70.
- Mrówczyński, Włodzimierz, Jan Celichowski, Rositsa Raikova, and Piotr Krutki. 2015. "Physiological Consequences of Doublet Discharges on Motoneuronal Firing and Motor Unit Force." *Frontiers in Cellular Neuroscience* 9. Frontiers. doi:10.3389/fncel.2015.00081.
- Navarro, Xavier, Thilo B Krueger, Natalia Lago, Silvestro Micera, Thomas Stieglitz, and Paolo Dario. 2005. "A Critical Review of Interfaces with the Peripheral Nervous System for the Control of Neuroprostheses and Hybrid Bionic Systems." *Journal of the Peripheral Nervous System* 10 (3): 229–58. doi:10.1111/j.1085-9489.2005.10303.x.

- Nicolelis, Miguel A L, Dragan Dimitrov, Jose M Carmena, Roy Crist, Gary Lehew, Jerald D Kralik, and Steven P Wise. 2003. "Chronic, Multisite, Multielectrode Recordings in Macaque Monkeys." *Proceedings of the National Academy of Sciences of the United States of America* 100 (19): 11041–46. doi:10.1073/pnas.1934665100.
- Normann, Richard A, Patrick K Campbell, and Kelly E Jones. 1991. "Micromachined, Silicon Based Electrode Arrays for Electrical Stimulation of or Recording From Cerebral Cortex." *IEEE*, 247–52.
- Novak, Christine B, Hossein Mehdian, and Herbert P von Schroeder. 2012. "Laxity of the Ulnar Nerve During Elbow Flexion and Extension." *The Journal of Hand Surgery* 37 (6): 1163–67. doi:10.1016/j.jhsa.2012.03.016.
- Park, Hyun-Joo, and Dominique M Durand. 2015. "Motion Control of the Rabbit Ankle Joint with a Flat Interface Nerve Electrode." *Muscle & Nerve* 52 (6). Wiley-Blackwell: 1088–95. doi:10.1016/j.apmr.2014.04.027.
- Patel, V V, F P Heidenreich, and R R Bindra. 1998. "Morphologic Changes in the Ulnar Nerve at the Elbow with Flexion and Extension: a Magnetic Resonance Imaging Study with 3-Dimensional Reconstruction." *Journal of Shoulder and ...*
- Prasad, Abhishek, and Justin C Sanchez. 2012. "Quantifying Long-Term Microelectrode Array Functionality Using Chronic in Vivo Impedance Testing." *Journal of Neural Engineering* 9 (2): 026028. doi:10.1088/1741-2560/9/2/026028.
- Rathelot, J A, and P L Strick. 2009. "Subdivisions of Primary Motor Cortex Based on Cortico-Motoneuronal Cells." *Proceedings of the National Academy of Sciences* 106 (3): 918–23. doi:10.1177/26.1.413864.
- Ren, Jian, Daniel J Chew, Suzanne Biers, and Nikesh Thiruchelvam. 2015. "Electrical Nerve Stimulation to Promote Micturition in Spinal Cord Injury Patients: a Review of Current Attempts." *Neurology and Urodynamics* 35 (3): 365–70. doi:10.1126/scitranslmed.3007186.
- Romanes, George J. 1951. "The Motor Cell Columns of the Lumbo-Sacral Spinal Cord of the Cat." *Journal of Comparative Neurology* 94 (2). The Wistar Institute of Anatomy and Biology: 313–63. doi:10.1001/archneurpsyc.1941.02280230025003.

- Rousche, P J, and R A Normann. 1999. "Chronic Intracortical Microstimulation (ICMS) of Cat Sensory Cortex Using the Utah Intracortical Electrode Array." *IEEE Transactions on Rehabilitation Engineering* 7 (1): 56–68. doi:10.1109/86.750552.
- Rousche, Patrick J, and Richard A Normann. 1992. "A Method for Pneumatically Inserting an Array of Penetrating Electrodes Into Cortical Tissue." *Annals of Biomedical Engineering* 20 (4): 413–22. doi:10.1007/BF02368133.
- Schalk, G, K J Miller, N R Anderson, J A Wilson, M D Smyth, J G Ojemann, D W Moran, J R Wolpaw, and E C Leuthardt. 2008. "Two-Dimensional Movement Control Using Electrocorticographic Signals in Humans." *Journal of Neural Engineering* 5 (1). IOP Publishing: 75. doi:10.1088/1741-2560/5/1/008.
- Schultz, Aimee E, and Todd A Kuiken. 2011. "Neural Interfaces for Control of Upper Limb Prostheses: the State of the Art and Future Possibilities." *PM & R : the Journal of Injury, Function, and Rehabilitation* 3 (1): 55–67. doi:10.1016/j.pmrj.2010.06.016.
- Schwartz, Andrew B, X Tracy Cui, Douglas J Weber, and Daniel W Moran. 2006. "Brain-Controlled Interfaces: Movement Restoration with Neural Prosthetics." *Neuron* 52 (1): 205–20. doi:10.1016/j.neuron.2006.09.019.
- Scott, W, J Stevens, and S A Binder-Macleod. 2001. "Human Skeletal Muscle Fiber Type Classifications." *Physical Therapy* 81, no. 11: 1810-1816.
- Serruya, Mijail D, Nicholas G Hatsopoulos, Liam Paninski, Matthew R Fellows, and John P Donoghue. 2002. "Brain-Machine Interface: Instant Neural Control of a Movement Signal." *Nature* 416 (6877): 141–42. doi:10.1097/00001756-199806010-00007.
- Shenoy, Krishna V, and Jose M Carmena. 2014. "Combining Decoder Design and Neural Adaptation in Brain-Machine Interfaces." *Neuron* 84 (4): 665–80. doi:10.1016/j.neuron.2014.08.038.
- Sherrington, C S. 1906. "Observations on the Scratch-Reflex in the Spinal Dog." *Journal of Physiology* 34, no. 1-2: 1-50.

- Shoffstall, Andrew J, Suraj Srinivasan, Mitchell Willis, Allison M Stiller, Melanie Ecker, Walter E Voit, Joseph J Pancrazio, and Jeffrey R Capadona. 2018. "A Mosquito Inspired Strategy to Implant Microprobes Into the Brain." *Scientific Reports* 8 (1): 122. doi:10.1038/s41598-017-18522-4.
- Smith, Lauren H, Todd A Kuiken, and Levi J Hargrove. 2014. "Real-Time Simultaneous and Proportional Myoelectric Control Using Intramuscular EMG." *Journal of Neural Engineering* 11 (6): 066013. doi:10.1088/1741-2560/11/6/066013.
- Stansbury, Lynn G, Steven J Lalliss, Joanna G Branstetter, Mark R Bagg, and John B Holcomb. 2008. "Amputations in US Military Personnel in the Current Conflicts in Afghanistan and Iraq." *Journal of Orthopaedic Trauma* 22 (1). LWW: 43–46.
- Sturman, D J. 1992. "Whole-Hand Input." PhD diss., Massachusetts Institute of Technology.
- Towe, A L, and G W Harding. 1970. "Extracellular Microelectrode Sampling Bias." *Experimental Neurology* 29 (2): 366–81. doi:10.1016/0014-4886(70)90065-8.
- VanderHorst, V G, and G Holstege. 1997. "Organization of Lumbosacral Motoneuronal Cell Groups Innervating Hindlimb, Pelvic Floor, and Axial Muscles in the Cat." *The Journal of Comparative Neurology* 382 (1): 46–76.
- Varol, H A, F Sup, and M Goldfarb. 2010. "Multiclass Real-Time Intent Recognition of a Powered Lower Limb Prosthesis." *IEEE Transactions on Biomedical Engineering* 57, no. 3: 542-551..
- Vetter, R J, J C Williams, J F Hetke, E A Nunamaker, and D R Kipke. 2004. "Chronic Neural Recording Using Silicon-Substrate Microelectrode Arrays Implanted in Cerebral Cortex." *IEEE Transactions on Biomedical Engineering* 51 (6): 896–904. doi:10.1109/TBME.2004.826680.
- Vidal, Jacques J. 1977. "Real-Time Detection of Brain Events in EEG." *Proceedings of the IEEE* 65 (5). IEEE: 633–41.
- Wagenaar, Joost B. 2011. "Using Primary Afferent Neural Activity for Predicting Limb Kinematics in Cat." Edited by Douglas J Weber. University of Pittsburgh.

- Westbury, D R. 1982. "A Comparison of the Structures of A-and  $\Gamma$ -Spinal Motoneurons of the Cat." *Journal of Physiology* 325, no. 1: 79-91..
- Wodlinger, B, J E Downey, E C Tyler-Kabara, A B Schwartz, M L Boninger, and J L Collinger. 2014. "Ten-Dimensional Anthropomorphic Arm Control in a Human Brain-Machine Interface: Difficulties, Solutions, and Limitations." *Journal of Neural Engineering* 12 (1): 016011. doi:10.1088/1741-2560/12/1/016011.
- Wodlinger, Brian, and Dominique M Durand. 2009. "Localization and Recovery of Peripheral Neural Sources with Beamforming Algorithms." *IEEE Transactions on Neural Systems and Rehabilitation Engineering : a Publication of the IEEE Engineering in Medicine and Biology Society* 17 (5): 461–68. doi:10.1109/TNSRE.2009.2034072.
- Woo, S L, M G Urbanchek, P S Cederna, and Nicholas B Langhals. 2014. "Revisiting Nonvascularized Partial Muscle Grafts: a Novel Use for Prosthetic Control." *Plastic and Reconstructive Surgery* 134 (2): 344e–346e.
- Yakovenko, Sergiy, Vivian Mushahwar, Veronique VanderHorst, Gert Holstege, and Arthur Prochazka. 2002. "Spatiotemporal Activation of Lumbosacral Motoneurons in the Locomotor Step Cycle." *Journal of Neurophysiology* 87 (3): 1542–53.
- Ziegler-Graham, Kathryn, Ellen J MacKenzie, Patti L Ephraim, Thomas G Travison, and Ron Brookmeyer. 2008. "Estimating the Prevalence of Limb Loss in the United States: 2005 to 2050." *Archives of Physical Medicine and Rehabilitation* 89 (3): 422–29. doi:10.1016/j.apmr.2007.11.005.